Filtered Mass Density Function for Design Simulation of High Speed Airbreathing Propulsion Systems

by

P. Givi, C.K. Madnia, L.Y.M. Gicquel,
M.R.H. Sheikhi and T.G. Drozda

Department of Mechanical and Aerospace Engineering
State University of New York at Buffalo
Buffalo, NY 14260-4400

Final Report to
The NASA Langley Research Center

Grant NAG 1-2238

for the Period

September 1, 1999 - August 31, 2002

Contents

Filtered Mass Density Function for Design Simulation of High Speed Airbreathing Propulsion Systems

P. Givi, C.K. Madnia, L.Y.M. Gicquel, M.R.H. Sheikhi and T.G. Drozda
Department of Mechanical and Aerospace Engineering
State University of New York at Buffalo
Buffalo, NY 14260-4400

Abstract

The objective of this research is to improve and implement the filtered mass density function (FDF) methodology for large eddy simulation (LES) of high-speed reacting turbulent flows. We have just completed three years of this research. This is the Final Report on our activities during the period: September 1, 1999 through August 31, 2002.

Dr. J. Philip Drummond (Hypersonic Propulsion Branch, NASA LaRC, Mail Stop 197, Tel: 757-864-2298) is the Technical Monitor of this Grant.

1 Introduction

An issue of current interest to NASA is associated with design of various components involved in air-breathing propulsion systems such as the scramjet [1]. A successful design needs the resolution of numerous issues such as fuel injector design and optimization, flame holding associated with the injection, critical design studies of certain areas (not the whole integrated engine), *etc.* Resolving these issues is of crucial importance to achieve the final goal of producing a more optimum aerospace propulsion system for hypersonic vehicles. To achieve this goal, however, there is a demand for development of robust tools that can aid in the design procedure. This is due to the fact that the physics of high-speed reactive flows is rich with many complexities. Few

examples of the physical issues of current interest are the questions associated with the chemical and thermodynamical non-equilibrium effects, the cause and effect of turbulence, the interaction of turbulence and chemistry, the real gas effects at high temperatures, *etc.*

The need for advanced computational methods for the analysis of high speed propulsion systems is obvious [1]. Within the past three decades the NASA Langley Research Center (LaRC) has been at the forefront in making use of advanced computational methods for investigations of such systems. Large eddy simulation (LES) is regarded as one the most promising means of simulating turbulent reacting flows [2,3]. Amongst the various LES strategies, the approach based on the probability density function (PDF) has proven particularly effective [4–19]. The formal means of conducting such LES is by consideration of the "filtered density function" (FDF) which is essentially the filtered fine-grained PDF of the transport quantities [20]. Colucci *et al.* [8] developed a transport equation for the FDF in constant density turbulent reacting flows. Jaberi *et al.* [9] extended the methodology for LES of variable density flows by consideration of the "filtered mass density function" (FMDF) which is the mass weighted FDF. The fundamental property of the PDF methods is exhibited by the closed form nature of the chemical source term appearing in the transport equation governing the FDF (FMDF). This property is very important as evidenced in several applications of FDF for LES of a variety of turbulent reacting flows [8–12, 16].

2 Accomplishments

The goal of this research was to improve the capabilities of the FDF method and to implement it for LES of chemically reacting turbulent flows. We feel that we have been very successful in achieving the specific objectives of this work. These objectives were:

1. Development and implementation of the velocity filtered density function (VFDF) for LES.
2. Development and implementation of the joint velocity-scalar filtered density function (VSFDF) for LES.
3. Implementation of the FDF for LES of hydrocarbon diffusion flames and comparison with experimental data.

The efforts pertaining to the first two objectives are completed and are fully described in journal articles (included here as Appendix I and Appendix II). The work pertaining to the third objective is premature for publication. Also, during the work on this project, the PI was invited to deliver a Keynote Lecture at the Third AFOSR International Conference on DNS and LES (Arlington, TX, August 5-9, 2001). A copy of the review article on this tutorial lecture is given in Appendix III. The efforts pertaining to each of these objectives are summarized in the next three subsections.

2.1 Velocity Filtered Density Function for Large Eddy Simulation of Turbulent Flows

In this part of our work, a methodology termed the "velocity filtered density function" (VFDF) is developed and implemented for large eddy simulation (LES) of turbulent flows. In this methodology, the effects of the unresolved subgrid scales (SGS) are taken into account by considering the joint probability density function (PDF) of all of the components of the velocity vector. An exact transport equation is derived for the VFDF in which the effects of the SGS convection appear in closed form. The unclosed terms in this transport equation are modeled. A system of stochastic differential equations (SDEs) which yields statistically equivalent results to the modeled VFDF transport equation is constructed. These SDEs are solved numerically by a Lagrangian Monte Carlo procedure in which the Itô-Gikhman character of the SDEs is preserved. The consistency of the proposed SDEs and the convergence of the Monte Carlo solution are assessed by comparison with results obtained by an Eulerian LES procedure in which the corresponding transport equations for the first two SGS moments are solved. The VFDF results are compared with those obtained via several existing SGS closures. These results are also analyzed via *a priori* and *a posteriori* comparisons with results obtained by direct numerical simulation (DNS) of an incompressible, three-dimensional (3D), temporally developing mixing layer.

This work is fully described in Appendix II.

2.2 Velocity-Scalar Filtered Density Function for Large Eddy Simulation of Turbulent Flows

In this part of our work, a methodology termed the "velocity-scalar filtered density function" (VSFDF) is developed and implemented for large eddy simulation (LES) of turbulent flows. In this methodology, the effects of the unresolved subgrid scales (SGS) are taken into account by considering the joint probability density function (PDF) of the velocity-scalar field. An exact transport equation is derived for the VSFDF in which the effects of the SGS convection and chemical reaction are closed. The unclosed terms in this equation are modeled. A system of stochastic differential equations (SDEs) which yields statistically equivalent results to the modeled VSFDF transport equation is constructed. These SDEs are solved numerically by a Lagrangian Monte Carlo procedure in which the Itô-Gikhman character of the SDEs is preserved. The consistency of the proposed SDEs and the convergence of the Monte Carlo solution are assessed by comparison with results obtained by a finite difference LES procedure in which the corresponding transport equations for the first two SGS moments are solved. The VSFDF results are compared with those obtained via other SGS closures, and all the results are assessed via comparison with data obtained by direct numerical simulation (DNS) of a temporally developing mixing layer involving transport of a passive scalar. It is shown that the values of both the SGS and the resolved components of all second order moments including the scalar fluxes are predicted well by VSFDF. The sensitivity of the model's (empirical) constants are assessed and it is shown that the magnitudes of these constants are in the same range as that typically employed in PDF methods.

This work is fully described in Appendix II.

2.3 Scalar Filtered Density Function for Large Eddy Simulation of a Diffusion Flame

We have started work on the use of the filtered density function (FDF) method for large eddy simulation (LES) of the piloted jet flame configuration as considered in the experiments of the Combustion Research Facility at the Sandia National Laboratory [21–25]. This flame has been the subject of broad investigations by other computational/modeling methodologies [24]. In the experiments, three basic flames

are considered, identified by Flames D, E, and F. The geometrical configuration in these flames is the same, but the jet inlet velocity is varied. In Flame D, the fuel jet velocity is the lowest and the flame is close to equilibrium. The jet velocity increases from flames D to E to F, with noticeable non-equilibrium effects in the latter two.

Some preliminary work has already been completed in which the LES/SFDF is used for predictions for the Sandia piloted jet flame. In these simulations, combustion is modeled via two chemistry models: (1) an equilibrium model via realistic kinetics, (2) a finite rate, single-step model for non-equilibrium flames. In (1), the LES/SFDF is employed in conjunction with equilibrium methane-oxidation model. This model is enacted via "flamelet" simulations which consider a laminar counterflow (opposed jet) flame configuration [26–29]. The full methane oxidation mechanism of the Gas Research Institute (GRI) [30, 31] accounting for 53 species and 325 elementary reactions is employed. At low strain rates, the flame is close to equilibrium. Thus, the thermo-chemical variables are determined completely by the "mixture fraction." This flamelet library is coupled with our LES/SFDF solver in which transport of the mixture fraction is considered. It is useful to emphasize here that the PDF of the mixture fraction is NOT "assumed" *a priori* (as done in almost all other flamelet based LES [32–42]); rather, it is calculated explicitly via the SFDF. In (2), the methane oxidation is modeled via a finite-rate, single-step kinetics model [43]. The system of nonlinear ordinary different equations representing reactant conversion is solved via LES/SFDF for all of the scalar variables (mass fractions and enthalpy). With this, some aspects of non-equilibrium chemistry are taken into account, albeit in an idealized manner.

With the equilibrium chemistry model, the results obtained by LES/SFDF/flamelet are compared with Sandia's experimental data [21–25]. Up to now, we have only simulated Flame D and we have observed good agreements. But more work is required to ensure the accuracy of our results. Simulations of flames E and F have not been yet attempted.

In closure of this section, we would like to state that since our early work on FDF, this methodology has been used by several other investigators (*e.g.* Refs. [12,16,19]). Please see Appendix III for a recent review of current state of progress in LES/FDF.

3 Enhancement of Technology and Education

With completion of this research, we feel that we have been able to contribute to maintain U.S. leadership in a technology which is of significant importance to NASA. This is a very important matter, particularly when considering the extent of ongoing concentrated efforts in Europe and Asia in the efforts proposed here. To appreciate the seriousness of the competition, we indicate that the number of European researchers who are currently involved in mathematical & computational modeling of turbulent reacting flows is significantly larger than that in the U.S. In fact, considering only England, France and Germany, the number of senior investigators (not including graduate students) who are working on the *specific* research field of "LES of turbulent combustion" in these three countries is larger than that in the whole U.S.! This indicates the wide recognition of the importance of this research field in other countries. We feel that the approach proposed here is very promising in dealing with this challenging problem in addition to enhancing the current state of knowledge in turbulent combustion.

In order to demonstrate our visibility in this research, here we shall list all the awards and some of noticeable achievements of the personnel involved in this program.

3.1 Graduate Students

Involvement of students in research is an issue which is taken very seriously at our University We are committed to recruiting excellent quality students and involving them in high caliber research. During the past three years, the following students have been supported under this Grant.

1. Dr. Laurent Y.M. Gicquel (Ph.D. 2001). Currently: Research Scientist, CERFACS, Toulouse, France. NASA's support is acknowledged in Ph.D. Disseration [44].

2. Mr. Tomasz G. Drozda (M.S. 2002). Currently: Ph.D. candidate at the University of Pittsburgh. NASA's support is acknowledged in M.S. Thesis [45]

3. Mr. M. Reza H. Sheikhi (M.S. 2002). Currently: Ph.D. candidate at the University of Pittsburgh.

3.2 Awards and Honors

1. Peyman Givi: Promoted to University at Buffalo Distinguished Professor (2002).

2. Peyman Givi: Received Professor of the Year Award, Tau Beta Pi Engineering Honor Society, New York Nu Chapter (2001-2002).

3. Tomasz G. Drozda: Second Prize winner at the Graduate Technical Paper Competition of AIAA Northeast Regional Student Conference, Rensselaer Polytechnic Institute, Troy, NY. Title of paper: "A Hybrid Stochastic-Deterministic Methodology for Large Eddy Simulation of Scalar Mixing and Reaction in Turbulent Flows," April, 2002.

4. Profile Featured in:

- *Reporter*: 13 named UB Distinguished Professor **33** (28), p. 1, May 9, 2002.
- *The Buffalo News*: Rolls-Royce using UB technique to refine its engines, p. E4, March 19, 2002.
- *SEAS News*: LES results equal more expensive supercomputer simulations, **VIII**(1), p. 6, Spring (2002).
- *Reporter:* New method produces "super" results. **33**(21), p. 1, March 14, 2002.
- *Reporter*: Graduates bringing recognition to lab, **32**(20), p. 4, February 15, 2001.
- *ASEE Recruitment Video*, the NASA Langley Research Center, Office of Education, Hampton, VA, 1999-2000.

3.3 Publications

In all of the following publications, the support from NASA Langley is greatfully acknowledged:

Invited Review Articles:

1. P. Givi, "A Review of Modern Developments in Large Eddy Simulation of Turbulent Reactive Flows," Chapter in *DNS/LES: Progress and Challenges*, pp. 81-92, Editors: C. Liu, L. Sakell and T. Beutner, Greyden Press, Columbus, OH, 2001.

2. F.A. Jaberi, F. Mashayek, C.K. Madnia, D.B. Taulbee and P. Givi, "Advances in Analytical Description of Turbulent Reacting Flows," Chapter 9 in *Advances in Chemical Propulsion*, pp. 149-164, Editor: Gabriel, D. Roy, CRC Press LLC, Boca Raton, FL, 2002.

Refereed Papers:

1. M.R.H. Sheikhi, T.G. Drozda, P. Givi, and S.B. Pope, "Velocity-Scalar Filtered Density Function for Large Eddy Simulation of Turbulent Flows," submitted to *Physics of Fluids* (2002).

2. L.Y.M. Gicquel, P. Givi, F.A. Jaberi, and S.B. Pope, "Velocity Filtered Density Function for Large Eddy Simulation of Turbulent Flows," *Physics of Fluids*, **14**(3), 1196-1213, 2002.

3. L.Y.M. Gicquel, P. Givi, F.A. Jaberi, and S.B. Pope, "Velocity Filtered Density Function for Large Eddy Simulation of a Turbulent Mixing Layer, in *DNS/LES: Progress and Challenges*, pp. 327-334, Editors: C. Liu, L. Sakell and T. Beutner, Greyden Press, Columbus, OH, 2001.

Conference Papers:

1. M.R.H. Sheikhi, T.G. Drozda, P. Givi, and S.B. Pope, "Velocity-Scalar Filtered Density Function for Large Eddy Simulation of Turbulent Flows," submitted for presentation at the 55th Annual Meeting of the Division of Fluid Dynamics of the American Physical Society, Dallas, TX, November 2002.

2. P. Givi, L.Y.M. Gicquel, F.A. Jaberi and S.B. Pope, "PDF Methods for Large Eddy Simulation of Turbulent Reactive Flows," Proceedings of IUTAM Symposium on Turbulent Mixing and Combustion, pp. 96-97, Kingston, Ontario, Canada, June 2-6, 2001.

3. L.Y.M. Gicquel, P. Givi, F.A. Jaberi and S.B. Pope, "Velocity Filtered Density Function for Large Eddy Simulation of Turbulent Flows," *Bulletin of the American Physical Society*, **45**(9), p. 129, 53rd Annual Meeting of the Division of Fluid Dynamics of the American Physical Society, Washington, DC, Nov. 19-21, 2000.

4. F.A. Jaberi, S. James and P. Givi, "Large Eddy Simulations of Methane Jet Flames," *Bulletin of the American Physical Society*, **45**(9), p. 72, 53rd Annual Meeting of the Division of Fluid Dynamics of the American Physical Society, Washington, DC, Nov. 19-21, 2000.

5. S.C. Garrick, F.A. Jaberi and P. Givi, "Large Eddy Simulation of Turbulent Reacting Round Jets," *Bulletin of the American Physical Society*, **44**(8), p. 44, 52nd Annual Meeting of the Division of Fluid Dynamics of the American Physical Society, New Orleans, LA, November 21-23, 1999.

References

[1] Drummond, J. P., Supersonic Reacting Internal Flow Fields, in Oran, E. S. and Boris, J. P., editors, *Numerical Approaches to Combustion Modeling*, *Progress in Astronautics and Aeronautics*, Vol. 135, chapter 12, pp. 365–420, AIAA Publishing Co., Washington, D.C., 1991.

[2] Bilger, R. W., Future Progress in Turbulent Combustion Research, *Prog. Energy Combust. Sci.*, **26**(4-6):367–380 (2000).

[3] Peters, N., *Turbulent Combustion*, Cambridge University Press, Cambridge, UK, 2000.

[4] Givi, P., Model Free Simulations of Turbulent Reactive Flows, *Prog. Energy Combust. Sci.*, **15**:1–107 (1989).

[5] Madnia, C. K. and Givi, P., Direct Numerical Simulation and Large Eddy Simulation of Reacting Homogeneous Turbulence, in Galperin, B. and Orszag, S. A., editors, *Large Eddy Simulations of Complex Engineering and Geophysical Flows*, chapter 15, pp. 315–346, Cambridge University Press, Cambridge, England, 1993.

[6] Frankel, S. H., Adumitroaie, V., Madnia, C. K., and Givi, P., Large Eddy Simulations of Turbulent Reacting Flows by Assumed PDF Methods, in Ragab, S. A. and Piomelli, U., editors, *Engineering Applications of Large Eddy Simulations*, pp. 81–101, ASME, FED-Vol. 162, New York, NY, 1993.

[7] Givi, P., Spectral and Random Vortex Methods in Turbulent Reacting Flows, in Libby, P. A. and Williams, F. A., editors, *Turbulent Reacting Flows*, chapter 8, pp. 475–572, Academic Press, London, England, 1994.

[8] Colucci, P. J., Jaberi, F. A., Givi, P., and Pope, S. B., Filtered Density Function for Large Eddy Simulation of Turbulent Reacting Flows, *Phys. Fluids*, **10**(2):499–515 (1998).

[9] Jaberi, F. A., Colucci, P. J., James, S., Givi, P., and Pope, S. B., Filtered Mass Density Function for Large Eddy Simulation of Turbulent Reacting Flows, *J. Fluid Mech.*, **401**:85–121 (1999).

[10] Garrick, S. C., Jaberi, F. A., and Givi, P., Large Eddy Simulation of Scalar Transport in a Turbulent Jet Flow, in Knight, D. and Sakell, L., editors, *Recent Advances in DNS and LES, Fluid Mechanics and its Applications*, Vol. 54, pp. 155–166, Kluwer Academic Publishers, The Netherlands, 1999.

[11] James, S. and Jaberi, F. A., Large Scale Simulations of Two-Dimensional Non-premixed Methane Jet Flames, *Combust. Flame*, **123**:465–487 (2000).

[12] Réveillon, J. and Vervisch, L., Subgrid-Scale Turbulent Micromixing: Dynamic Approach, *AIAA J.*, **36**(3):336–341 (1998).

[13] Gao, F. and O'Brien, E. E., A Large-Eddy Simulation Scheme for Turbulent Reacting Flows, *Phys. Fluids A*, **5**(6):1282–1284 (1993).

[14] Cook, A. W. and Riley, J. J., A Subgrid Model for Equilibrium Chemistry in Turbulent Flows, *Phys. Fluids*, **6**(8):2868–2870 (1994).

[15] Pope, S. B., *Turbulent Flows*, Cambridge University Press, Cambridge, UK, 2000.

[16] Zhou, X. Y. and Pereira, J. C. F., Large Eddy Simulation (2D) of a Reacting Plan Mixing Layer Using Filtered Density Function, *Flow, Turbulence and Combustion*, **64**:279–300 (2000).

[17] Luo, K. H., DNS and LES of Turbulence-Combustion Interactions, in Geurts, B. J., editor, *Modern Simulation Strategies for Turbulent Flow*, chapter 14, pp. 263–293, R. T. Edwards, Inc., Philadelphia, PA, 2001.

[18] Poinsot, T. and Veynante, D., *Theoretical and Numerical Combustion*, R. T. Edwards, Inc., Philadelphia, PA, 2001.

[19] Tong, C., Measurements of Conserved Scalar Filtered Density Function in a Turbulent Jet, *Phys. Fluids*, **13**(10):2923–2937 (2001).

[20] Pope, S. B., Computations of Turbulent Combustion: Progress and Challenges, *Proc. Combust. Inst.*, **23**:591–612 (1990).

[21] Barlow, R. S. and Frank, J. I., Effects of Turbulence on Species Mass Fractions in Methane/Air Jet Flames, *Proc. Combust. Inst.*, **27**:1087–1095 (1998).

[22] Meier, W., Barlow, R. S., Chen, Y. L., and Chen, J. Y., Raman/Reyleigh/LIF Measurements in a Turbulent $CH_4/H_2/N_2$ Jet Diffusion Flame: Experimental Techniques and Turbulence-Chemistry Interaction, *Combustion and Flame*, **123**(3):326–343 (2000).

[23] Nooren, P. A., Versiuis, M., Van der Meer, T. H., Barlow, R. S., and Frank, J. H., Raman-Rayleigh-LIF Measurements of Temperature and Species Concentrations in the Delft Piloted Turbulent Jet Diffusion Flame, *Applied Physics*, **B71**(95) (2000).

[24] Barlow, R. S., Sandia National Laboratories, TNF Workshop website, `http://www.ca.sandia.gov/tdf/Workshop.html`, 2002.

[25] Sandia National Laboratory, Combustion Research Facility website, `http://www.ca.sandia.gov/tdf/`, 2002.

[26] Peters, N., Local Quenching Due to Flame Stretch and Non-Premixed Turbulent Combustion, *Combust. Sci. and Tech.*, **30**:1–17 (1983).

[27] Spalding, S. B., Theory of Mixing and Chemical Reaction in the Opposed-Jet Diffusion Flame, *Journal of the American Rocket Society*, **31**:763–771 (1961).

[28] Liñán, A., The Asymptotic Structure of Counterflow Diffusion Flames for Large Activation Energies, *Acta Astronautica*, **1**:1007–1039 (1974).

[29] Maruta, K., Yoshida, M., Guo, H., Ju, Y., and Niioka, T., Extinction of Low-Stretched Diffusion Flame in Microgravity, *Combust. and Flame*, **112**:181–187 (1998).

[30] Smith, G. P., Golden, D. M., Frenklach, M., Moriarty, N. W., Eiteneer, B., Goldenberg, M., Bowman, C. T., Hanson, R., Song, S., Gardiner, W. C., Lissianski, V., and Qin, Z., `http://www.me.berkeley.edu/gri-mech`

[31] Bowman, C. T., Hanson, R. K., Gardiner, W. C., Lissianski, V., Frenklach, M., Goldenberg, M., Smith, G. P., Crosley, D. R., and Golden, D. M., GRI-Mech 2.11–An Optimized Detailed Chemical Reaction Mechanism for Methane Combustion and NO Formation and Reburning, Report GRI-97/0020, Gas Research Institute, Chicago, IL, 1997.

[32] Cook, A. W., Riley, J. J., and Kosály, G., A Laminar Flamelet Approach to Subgrid-Scale Chemistry in Turbulent Flows, *Combust. Flame*, **109**:332–341 (1997).

[33] Cook, A. W. and Riley, J. J., Subgrid Scale Modeling for Turbulent Reacting Flows, *Combust. Flame*, **112**:593–606 (1998).

[34] De Bruyn Kops, S. M., Riley, J. J., Kosály, G., and Cook, A. W., Investigation of Modeling for Non-Premixed Turbulent Combustion, *Combust. Flame*, **60**:105–122 (1998).

[35] DesJardin, P. E. and Frankel, S. H., Large Eddy Simulation of a Turbulent Nonpremixed Reacting Jet: Application and Assessment of Subgrid-Scale Combustion Models, *Phys. Fluids*, **10**(9):2298–2314 (1998).

[36] DesJardin, P. E. and Frankel, S. H., Two-Dimensional Large Eddy Simulation of Soot Formation in the Near-Field of a Strongly Radiating Nonpremixed Acetylene-Air Turbulent Jet Flame, *Combust. Flame*, **119**:121–132 (1999).

[37] Pitsch, H. and Steiner, H., Large Eddy Simulation of a Turbulent Piloted Methane/Air Diffusion Flame (Sandia Flame D), *Phys. Fluids*, **12**(10):2541–2554 (2000).

[38] Ladeinde, F., Cai, X., Sekar, B., and Kiel, B., Application of Combined LES and Flamelet Modeling to Methane, Propane, and Jet-A Combustion, AIAA Paper 2001-0634, 2001.

[39] Jiménez, J., Liñán, A., Rogers, M. M., and Higuera, F. J., *A Priori* Testing of Subgrid Models for Chemically Reacting Non-Premixed Turbulent Flows, *J. Fluid Mech.*, **349**:149–171 (1997).

[40] Mathey, F. and Chollet, J. P., Large Eddy Simulation of Turbulent Reactive Flows, in *Proceedings of the Eleventh Symposium on Turbulent Shear Flows*, pp. 16.19–16.24, Grenoble, France, 1997.

[41] Forkel, H. and Janicka, J., Large-Eddy Simulation of a Turbulent Hydrogen Diffusion Flame, *Flow, Turbulence and Combustion*, **65**(2):163–175 (2000).

[42] Kempf, A., Forkel, H., Chen, J. Y., Sadiki, A., and Janicka, J., Large-Eddy Simulation of a Counterflow Configuration With and Without Combustion, *Proc. Combust. Inst.*, **28**:35–40 (2000).

[43] Bhui-Pham, M. N., Studies in Structures of Laminar Hydrocarbon Flames, Ph.D. Thesis, University of California, San Diego, San Diego, CA, 1992.

[44] Gicquel, L. Y. M., Velocity Filtered Density Function for Large Eddy Simulation of Turbulent Flows., Ph.D. Dissertation, Department of Mechanical and Aerospace Engineering, University at Buffalo, State University of New York, Buffalo, NY, 2001.

[45] Drozda, T. G., Consistency Assessment of Velocity-Scalar Filtered Density Function for Large Eddy Simulation of Turbulent Flows, M.S. Thesis, Department of Mechanical and Aerospace Engineering, University at Buffalo, State University of New York, Buffalo, NY, 2002.

[46] Gicquel, L. Y. M., Givi, P., Jaberi, F. A., and Pope, S. B., Velocity Filtered Density Function for Large Eddy Simulation of Turbulent Flows, *Phys. Fluids*, **14**(3):1196–1213 (2002).

[47] Gicquel, L. Y. M., Givi, P., Jaberi, F. A., and Pope, S. B., Velocity Filtered Density Function for Large Eddy Simulation of a Turbulent Mixing Layer, in Liu, C., Sakell, L., and Herklotz, R., editors, *DNS/LES-Progress and Challenges*, pp. 327–334, Greyden Press, Columbus, OH, 2001.

[48] Givi, P., A Review of Modern Developments in Large Eddy Simulation of Turbulent Reacting Flows, in Liu, C., Sakell, L., and Herklotz, R., editors, *DNS/LES-Progress and Challenges*, pp. 81–92, Greyden Press, Columbus, OH, 2001.

Appendix I

This Appendix is published as Ref. [46] and a part of it is published in Ref. [47].

Velocity Filtered Density Function for Large Eddy Simulation of Turbulent Flows

L.Y.M. Gicquel, P. Givi
Department of Mechanical and Aerospace Engineering
University at Buffalo, SUNY
Buffalo, NY 14260-4400

F.A. Jaberi
Department of Mechanical Engineering
Michigan State University
East Lansing, MI 48824-1226

S.B. Pope
Sibley School of Mechanical and Aerospace Engineering
Cornell University
Ithaca, NY 14853-1301

Abstract

A methodology termed the "velocity filtered density function" (VFDF) is developed and implemented for large eddy simulation (LES) of turbulent flows. In this methodology, the effects of the unresolved subgrid scales (SGS) are taken into account by considering the joint probability density function (PDF) of all of the components of the velocity vector. An exact transport equation is derived for the VFDF in which the effects of the SGS convection appear in closed form. The unclosed terms in this

transport equation are modeled. A system of stochastic differential equations (SDEs) which yields statistically equivalent results to the modeled VFDF transport equation is constructed. These SDEs are solved numerically by a Lagrangian Monte Carlo procedure in which the Itô-Gikhman character of the SDEs is preserved. The consistency of the proposed SDEs and the convergence of the Monte Carlo solution are assessed by comparison with results obtained by an Eulerian LES procedure in which the corresponding transport equations for the first two SGS moments are solved. The VFDF results are compared with those obtained via several existing SGS closures. These results are also analyzed via a priori and a posteriori comparisons with results obtained by direct numerical simulation (DNS) of an incompressible, three-dimensional (3D), temporally developing mixing layer.

Corresponding Author: Peyman Givi, Tel: (716) 645-2593 (x. 2320). Fax: 716-645-3875. E-mail: givieng.buffalo.edu.

1 INTRODUCTION

The probability density function (PDF) approach has proven useful for large eddy simulation (LES) of turbulent reacting flows.[1–15] The formal means of conducting such LES is by consideration of the "filtered density function" (FDF) which is essentially the filtered fine-grained PDF of the transport quantities. In all previous contributions, the FDF of the "scalar" quantities is considered: Gao and O'Brien,[3] Colucci et al.,[6] Réveillon and Vervisch[7] and Zhou and Pereira[12] developed a transport equation for the FDF in constant density turbulent reacting flows. Jaberi et al.[8] extended the methodology for LES of variable density flows by consideration of the "filtered mass density function" (FMDF), which is essentially the mass weighted FDF. The fundamental property of the PDF methods is exhibited by the closed form nature of the chemical source term appearing in the transport equation governing the FDF (FMDF). This property is very important as evidenced in several applications of FDF for LES of a variety of turbulent reacting flows.[6–10,12] However, since the FDF of only the scalar quantities are considered, all of the "hydrodynamic" effects are modeled. In all previous LES/FDF simulations, these effects have been modeled via "non-FDF" methods.

The objective of the present work is to extend the FDF methodology to also include the subgrid scale (SGS) velocity vector. This is facilitated by consideration of the joint "velocity filtered density function" (VFDF). With the definition of the VFDF, the mathematical framework for its implementation in LES is established. A transport

equation is developed for the VFDF in which the effects of SGS convection are shown to appear in closed form. The unclosed terms in this equation are modeled in a fashion similar to those in the Reynolds-averaged simulation (RAS) procedures. A Lagrangian Monte Carlo procedure is developed and implemented for numerical simulation of the modeled VFDF transport equation. The consistency of this procedure is assessed by comparing the first two moments of the VFDF with those obtained by the Eulerian finite difference solutions of the same moments transport equations. The results of the VFDF simulations are compared with those predicted by the Smagorinsky[16] closure, and the "dynamic" Smagorinsky model.[17–19] The VFDF results are also assessed via comparisons with direct numerical simulation (DNS) data of a three-dimensional (3D) temporally developing mixing layer in a context similar to that of Vreman et al.[20]

This work deals with LES of the velocity field in a constant density, non-reacting flow. Consideration of the joint velocity-scalar FDF (or FMDF) in variable density, chemically reacting flows will be the subject of future work. It is in this context that the approach has its principal advantage: convective transport (of momentum and species) is in closed form.

2 FORMULATION

In the mathematical description of incompressible (unit density) turbulent flows, the primary transport variables are the velocity vector, $u_i(\mathbf{x}, t)$ $(i = 1, 2, 3)$, and the

pressure, $p(\mathbf{x},t)$, field. The equations which govern transport of these variables in space (x_i) and time (t) are

$$\begin{aligned} \frac{\partial u_i}{\partial x_i} &= 0, \\ \frac{\partial u_j}{\partial t} + \frac{\partial u_i u_j}{\partial x_i} &= -\frac{\partial p}{\partial x_j} + \frac{\partial \sigma_{ij}}{\partial x_i}. \end{aligned} \tag{1}$$

For a Newtonian fluid, the viscous stress tensor σ_{ij} is represented by

$$\sigma_{ij} = \nu \left(\frac{\partial u_i}{\partial x_j} + \frac{\partial u_j}{\partial x_i} \right), \tag{2}$$

where ν is the kinematic viscosity and is assumed constant.

Large eddy simulation involves the spatial filtering operation[21-23]

$$\langle f(\mathbf{x},t) \rangle_L = \int_{-\infty}^{+\infty} f(\mathbf{x}',t) \mathcal{G}(\mathbf{x}',\mathbf{x}) d\mathbf{x}', \tag{3}$$

where $\mathcal{G}$ denotes the filter function, $\langle f(\mathbf{x},t) \rangle_L$ represents the filtered value of the transport variable $f(\mathbf{x},t)$, and $f' = f - \langle f \rangle_L$ denotes the fluctuations of f from the filtered value. We consider spatially and temporally invariant and localized filter functions, thus $\mathcal{G}(\mathbf{x}',\mathbf{x}) \equiv G(\mathbf{x}' - \mathbf{x})$ with the properties,[21] $G(\mathbf{x}) = G(-\mathbf{x})$, and $\int_{-\infty}^{\infty} G(\mathbf{x}) d\mathbf{x} = 1$. Moreover, we only consider "positive" filter functions[24] for which all the moments $\int_{-\infty}^{\infty} x^m G(x) dx$ exist for $m \geq 0$. The application of the filtering

operation to the instantaneous transport equations yields

$$\begin{aligned} \frac{\partial \langle u_i \rangle_L}{\partial x_i} &= 0, \\ \frac{\partial \langle u_j \rangle_L}{\partial t} + \frac{\partial \langle u_i \rangle_L \langle u_j \rangle_L}{\partial x_i} &= -\frac{\partial \langle p \rangle_L}{\partial x_j} + \frac{\partial \langle \sigma_{ij} \rangle_L}{\partial x_i} - \frac{\partial \tau_L(u_i, u_j)}{\partial x_i}, \end{aligned} \tag{4}$$

where $\tau_L(u_i, u_j) = \langle u_i u_j \rangle_L - \langle u_i \rangle_L \langle u_j \rangle_L$ denotes the "generalized SGS stresses".[18] These stresses satisfy[18]

$$\frac{\partial}{\partial t}\left[\tau_L(u_i, u_j)\right] + \frac{\partial}{\partial x_k}\left[\langle u_k \rangle_L \tau_L(u_i, u_j)\right] = -\frac{\partial T_{ijk}}{\partial x_k} - \Pi_{ij} + P_{ij} - \varepsilon_{ij}. \tag{5}$$

In this equation, $T_{ijk} = \tau_L(u_i, u_j, u_k) - \nu \frac{\partial}{\partial x_k}\left[\tau_L(u_i, u_j)\right]$ is the SGS turbulent transport tensor where $\tau_L(u_i, u_j, u_k) = \langle u_i u_j u_k \rangle_L - \langle u_i \rangle_L \tau_L(u_j, u_k) - \langle u_j \rangle_L \tau_L(u_i, u_k) - \langle u_k \rangle_L \tau_L(u_i, u_j) - \langle u_i \rangle_L \langle u_j \rangle_L \langle u_K \rangle_L$.[18] The other terms are the SGS pressure-velocity scrambling tensor, $\Pi_{ij} = \tau_L(u_i, \frac{\partial p}{\partial x_j}) + \tau_L(u_j, \frac{\partial p}{\partial x_i})$, the SGS production rate tensor, $P_{ij} = -\tau_L(u_i, u_k)\frac{\partial \langle u_j \rangle_L}{\partial x_k} - \tau_L(u_j, u_k)\frac{\partial \langle u_i \rangle_L}{\partial x_k}$, and the SGS dissipation rate tensor, $\varepsilon_{ij} = 2\nu\tau_L(\frac{\partial u_i}{\partial x_k}, \frac{\partial u_j}{\partial x_k})$.

3 VELOCITY FILTERED DENSITY FUNCTION (VFDF)

A Definitions

The "velocity filtered density function" (VFDF), denoted by P_L, is formally defined as

$$\begin{aligned} P_L(\boldsymbol{v};\mathbf{x},t) &\equiv \int_{-\infty}^{+\infty} \varrho\left[\boldsymbol{v},\boldsymbol{u}(\mathbf{x}',t)\right] G(\mathbf{x}'-\mathbf{x})d\mathbf{x}', \\ \varrho\left[\boldsymbol{v},\boldsymbol{u}(\mathbf{x},t)\right] &= \delta[\boldsymbol{v}-\boldsymbol{u}(\mathbf{x},t)] \equiv \prod_{i=1}^{3} \delta[v_i - u_i(\mathbf{x},t)] \end{aligned} \tag{6}$$

where δ denotes the delta function and $\boldsymbol{v}$ is the velocity state vector. The term $\varrho[\boldsymbol{v},\boldsymbol{u}(\mathbf{x},t)]$ is the "fine-grained" density,[25,26,11] and Eq. (6) defines the VFDF as the spatially filtered value of the fine-grained density. With the condition of a positive filter kernel,[24] P_L has all the properties of the PDF.[26] For further developments, it is useful to define the "conditional filtered value" of the variable $Q(\mathbf{x},t)$ by

$$\langle Q(\mathbf{x},t)|\boldsymbol{u}(\mathbf{x},t)=\boldsymbol{v}\rangle_L \equiv \langle Q|\boldsymbol{v}\rangle_L = \frac{\int_{-\infty}^{+\infty} Q(\mathbf{x}',t)\varrho\left[\boldsymbol{v},\boldsymbol{u}(\mathbf{x}',t)\right] G(\mathbf{x}'-\mathbf{x})d\mathbf{x}',}{P_L(\boldsymbol{v};\mathbf{x},t)} \tag{7}$$

where $\langle\alpha|\beta\rangle_L$ denotes the filtered value of α conditioned on β. Equation (7) implies

$$
\begin{aligned}
&(i) \qquad \text{For } Q(\mathbf{x},t) = c, && \langle Q(\mathbf{x},t)|\boldsymbol{v}\rangle_L = c, \\
&(ii) \qquad \text{For } Q(\mathbf{x},t) \equiv \widehat{Q}(\boldsymbol{u}(\mathbf{x},t)), && \langle Q(\mathbf{x},t)|\boldsymbol{v}\rangle_L = \widehat{Q}(\boldsymbol{v}), \\
&(iii) \qquad \text{Integral property :} && \langle Q(\mathbf{x},t)\rangle_L = \int_{-\infty}^{+\infty} \langle Q(\mathbf{x},t)|\boldsymbol{v}\rangle_L P_L(\boldsymbol{v};\mathbf{x},t)d\boldsymbol{v},
\end{aligned}
\tag{8}
$$

where c is a constant, and $Q(\mathbf{x},t) \equiv \widehat{Q}(\boldsymbol{u}(\mathbf{x},t))$ denotes the case where the variable Q is completely described by the variable $\boldsymbol{u}(\mathbf{x},t)$. From these properties it follows that the filtered value of any function of the velocity variable is obtained by integration over the velocity space

$$
\langle Q(\mathbf{x},t)\rangle_L = \int_{-\infty}^{+\infty} \widehat{Q}(\boldsymbol{v}) P_L(\boldsymbol{v};\mathbf{x},t)d\boldsymbol{v}. \tag{9}
$$

B VFDF Transport Equation

The exact transport equation for the VFDF is derived in this section. Two forms of this equation are considered similar to those previously developed in PDF methods.[27-31] The starting point is to consider the time-derivative of Eq. (6),

$$
\begin{aligned}
\frac{\partial P_L(\boldsymbol{v};\mathbf{x},t)}{\partial t} &= -\int_{-\infty}^{\infty} \frac{\partial u_i(\mathbf{x}',t)}{\partial t} \frac{\partial \varrho\left[\boldsymbol{v},\boldsymbol{u}(\mathbf{x}',t)\right]}{\partial v_i} G(\mathbf{x}'-\mathbf{x})\, d\mathbf{x}' \\
&= -\frac{\partial}{\partial v_i} \int_{-\infty}^{\infty} \frac{\partial u_i(\mathbf{x}',t)}{\partial t} \varrho\left[\boldsymbol{v},\boldsymbol{u}(\mathbf{x}',t)\right] G(\mathbf{x}'-\mathbf{x})\, d\mathbf{x}'.
\end{aligned}
\tag{10}
$$

This combined with Eq. (7) yields

$$\frac{\partial P_L(\boldsymbol{v};\mathbf{x},t)}{\partial t} = -\frac{\partial}{\partial v_i}\left[\left\langle \frac{\partial u_i}{\partial t}|\boldsymbol{v}\right\rangle_L P_L(\boldsymbol{v};\mathbf{x},t)\right]. \tag{11}$$

Substituting Eq. (1) into Eq. (11) yields,

$$\frac{\partial P_L(\boldsymbol{v};\mathbf{x},t)}{\partial t} = -\frac{\partial}{\partial v_i}\left\{\left[-\left\langle \frac{\partial u_i u_k}{\partial x_k}|\boldsymbol{v}\right\rangle_L - \left\langle \frac{\partial p}{\partial x_i}|\boldsymbol{v}\right\rangle_L + \left\langle \frac{\partial \sigma_{ik}}{\partial x_k}|\boldsymbol{v}\right\rangle_L\right] P_L(\boldsymbol{v};\mathbf{x},t)\right\}. \tag{12}$$

With the relation

$$\frac{\partial}{\partial v_i}\left[\left\langle \frac{\partial u_i u_k}{\partial x_k}|\boldsymbol{v}\right\rangle_L P_L(\boldsymbol{v};\mathbf{x},t)\right] = -v_k\frac{\partial P_L(\boldsymbol{v};\mathbf{x},t)}{\partial x_k}, \tag{13}$$

and decompositions

$$\begin{aligned} v_k P_L &= \langle u_k\rangle_L P_L + [v_k - \langle u_k\rangle_L]P_L, \\ \left\langle \frac{\partial p}{\partial x_i}|\boldsymbol{v}\right\rangle_L P_L &= \frac{\partial\langle p\rangle_L}{\partial x_i}P_L + \left[\left\langle \frac{\partial p}{\partial x_i}|\boldsymbol{v}\right\rangle_L - \frac{\partial\langle p\rangle_L}{\partial x_i}\right]P_L, \\ \left\langle \frac{\partial \sigma_{ik}}{\partial x_k}|\boldsymbol{v}\right\rangle_L P_L &= \frac{\partial\langle \sigma_{ik}\rangle_L}{\partial x_k}P_L + \left[\left\langle \frac{\partial \sigma_{ik}}{\partial x_k}|\boldsymbol{v}\right\rangle_L - \frac{\partial\langle \sigma_{ik}\rangle_L}{\partial x_k}\right]P_L, \end{aligned} \tag{14}$$

the VFDF transport equation becomes,

$$\begin{aligned} \frac{DP_L}{Dt} &= -\frac{\partial}{\partial x_k}[(v_k - \langle u_k\rangle_L)P_L] + \frac{\partial\langle p\rangle_L}{\partial x_i}\frac{\partial P_L}{\partial v_i} - \frac{\partial\langle \sigma_{ik}\rangle_L}{\partial x_k}\frac{\partial P_L}{\partial v_i} \\ &+ \frac{\partial}{\partial v_i}\left[\left(\left\langle \frac{\partial p}{\partial x_i}|\boldsymbol{v}\right\rangle_L - \frac{\partial\langle p\rangle_L}{\partial x_i}\right)P_L\right] - \frac{\partial}{\partial v_i}\left[\left(\left\langle \frac{\partial \sigma_{ik}}{\partial x_k}|\boldsymbol{v}\right\rangle_L - \frac{\partial\langle \sigma_{ik}\rangle_L}{\partial x_k}\right)P_L\right], \end{aligned} \tag{15}$$

where $\frac{D}{Dt} = \frac{\partial}{\partial t} + \langle u_k \rangle_L \frac{\partial}{\partial x_k}$ denotes the "filtered" material derivative.

Equation (15) is an exact transport equation for the VFDF. The first term on the right hand side represents the SGS convection of the VFDF in physical space and is closed. The second and third terms (which are also in closed form) represent the convection in velocity space due to the resolved pressure gradient and molecular diffusion, respectively. The last two terms are unclosed and denote convective effects in the velocity space due to SGS pressure gradient and SGS diffusion.

Alternatively, the conditional diffusion term in Eq. (15) can be represented as:

$$-\frac{\partial}{\partial v_i}\left[\left\langle \frac{\partial \sigma_{ik}}{\partial x_k} | \boldsymbol{v} \right\rangle_L P_L(\boldsymbol{v}; \mathbf{x}, t)\right] = \nu \frac{\partial^2 P_L(\boldsymbol{v}; \mathbf{x}, t)}{\partial x_k \partial x_k} - \frac{\partial^2}{\partial v_i \partial v_j}\left[\left\langle \nu \frac{\partial u_i}{\partial x_k}\frac{\partial u_j}{\partial x_k} | \boldsymbol{v} \right\rangle_L P_L(\boldsymbol{v}; \mathbf{x}, t)\right], \tag{16}$$

in which the second term on the RHS involves the conditional expected dissipation. With this, the alternate form of the VFDF transport equation is:

$$\begin{aligned}\frac{DP_L}{Dt} = &-\frac{\partial}{\partial x_k}\left[(v_k - \langle u_k \rangle_L) P_L\right] + \frac{\partial \langle p \rangle_L}{\partial x_i}\frac{\partial P_L}{\partial v_i} + \nu \frac{\partial^2 P_L}{\partial x_k \partial x_k} \\ &+ \frac{\partial}{\partial v_i}\left[\left(\left\langle \frac{\partial p}{\partial x_i} | \boldsymbol{v} \right\rangle_L - \frac{\partial \langle p \rangle_L}{\partial x_i}\right) P_L\right] - \frac{\partial^2}{\partial v_i \partial v_j}\left[\left\langle \nu \frac{\partial u_i}{\partial x_k}\frac{\partial u_j}{\partial x_k} | \boldsymbol{v} \right\rangle_L P_L\right].\end{aligned} \tag{17}$$

Equation (17) is another exact transport equation for the VFDF. The first term on the right hand side represents the SGS convection of the VFDF in physical space and is closed. The second term corresponds to the convection in the velocity space due to the resolved pressure gradient. The third term represents molecular diffusion

of the VFDF in physical space. The closure problem is associated with the last two terms. These represent, respectively, convection in velocity space by the unresolved SGS pressure gradient, and diffusion in velocity space by SGS dissipation rate tensor.

C Modeled VFDF Transport Equations

The generalized Langevin model (GLM)[27,32] is employed for closure of the VFDF transport equation. Here we introduce two modeled VFDF equations, which are denoted by "VFDF1" and "VFDF2." These are presented in order. To close Eq. (17), VFDF1 is

$$\frac{\partial}{\partial v_i}\left[\left(\left\langle \frac{\partial p}{\partial x_i}|\boldsymbol{v}\right\rangle_L - \frac{\partial \langle p\rangle_L}{\partial x_i}\right) P_L\right] - \frac{\partial^2}{\partial v_i \partial v_j}\left[\left\langle \nu \frac{\partial u_i}{\partial x_k}\frac{\partial u_j}{\partial x_k}|\boldsymbol{v}\right\rangle_L P_L\right]$$
$$\approx -\frac{\partial}{\partial v_i}\left[\, G_{ij}\,(v_j - \langle u_j\rangle_L)\, P_L\,\right] + \frac{1}{2}\, C_0\, \varepsilon\, \frac{\partial^2 P_L}{\partial v_i \partial v_i}$$
$$+ \nu \frac{\partial \langle u_i\rangle_L}{\partial x_k}\frac{\partial \langle u_j\rangle_L}{\partial x_k}\frac{\partial^2 P_L}{\partial v_i \partial v_j} + 2\nu \frac{\partial \langle u_i\rangle_L}{\partial x_k}\frac{\partial^2 P_L}{\partial x_k \partial v_i}. \quad (18)$$

To close Eq. (15), VFDF2 is:

$$\frac{\partial}{\partial v_i}\left[\left(\left\langle \frac{\partial p}{\partial x_i}|\boldsymbol{v}\right\rangle_L - \frac{\partial \langle p\rangle_L}{\partial x_i} - \left\langle \frac{\partial \sigma_{ik}}{\partial x_k}|\boldsymbol{v}\right\rangle_L + \frac{\partial \langle \sigma_{ik}\rangle_L}{\partial x_k}\right) P_L\right]$$
$$\approx -\frac{\partial}{\partial v_i}\left[\, G_{ij}\,(v_j - \langle u_j\rangle_L)\, P_L\,\right] + \frac{1}{2}\, C_0\, \varepsilon\, \frac{\partial^2 P_L}{\partial v_i \partial v_i}. \quad (19)$$

Note that these models (i.e., the first two terms on the right hand sides of Eqs. (18) and (19) are the same, but that they model slightly different quantities. With this

closure, the two terms in G_{ij} and ε jointly represent the SGS pressure-strain and SGS dissipation. These are modeled as:[26,11]

$$G_{ij} = -\,\omega\,\left(\frac{1}{2}+\frac{3}{4}C_0\right)\,\delta_{ij},\;\; \varepsilon = C_\varepsilon\,k^{3/2}/\Delta_L,\;\; \omega = \varepsilon/k. \tag{20}$$

where ω is the SGS mixing frequency, Δ_L is the filter width, $k = \frac{1}{2}\tau_L(u_i,u_i)$ is the SGS kinetic energy, and $\varepsilon = \frac{1}{2}\varepsilon_{ii}$ is the SGS dissipation rate.

With the GLM, the two forms of the VFDF transport equation are,

$$\begin{aligned}\frac{DP_L}{Dt} = &-\frac{\partial}{\partial x_k}\left[\,(v_k-\langle u_k\rangle_L)\,P_L\,\right] + \frac{\partial\langle p\rangle_L}{\partial x_i}\frac{\partial P_L}{\partial v_i} + \nu\frac{\partial^2 P_L}{\partial x_k\partial x_k} + \nu\frac{\partial\langle u_i\rangle_L}{\partial x_k}\frac{\partial\langle u_j\rangle_L}{\partial x_k}\frac{\partial^2 P_L}{\partial v_i\partial v_j}\\ &+2\nu\frac{\partial\langle u_i\rangle_L}{\partial x_k}\frac{\partial^2 P_L}{\partial x_k\partial v_i} - \frac{\partial}{\partial v_i}\left[\,G_{ij}\,(v_j-\langle u_j\rangle_L)\,P_L\,\right] + \frac{1}{2}\,C_0\,\varepsilon\,\frac{\partial^2 P_L}{\partial v_i\partial v_i},\end{aligned} \tag{21}$$

for VFDF1, and

$$\begin{aligned}\frac{DP_L}{Dt} = &-\frac{\partial}{\partial x_k}\left[(v_k-\langle u_k\rangle_L)P_L\right] + \frac{\partial\langle p\rangle_L}{\partial x_i}\frac{\partial P_L}{\partial v_i} - \frac{\partial\langle\sigma_{ik}\rangle_L}{\partial x_k}\frac{\partial P_L}{\partial v_i}\\ &-\frac{\partial}{\partial v_i}\left[\,G_{ij}\,(v_j-\langle u_j\rangle_L)\,P_L\,\right] + \frac{1}{2}\,C_0\,\varepsilon\,\frac{\partial^2 P_L}{\partial v_i\partial v_i}.\end{aligned} \tag{22}$$

for VFDF2. Hereinafter, Eqs. (21) and (22) are referred to as "VFDF1" and "VFDF2," respectively. The difference between these two equations is in the different treatment of the closed viscous terms.

D Transport Equations for Moments

The zeroth, first and second moment equations corresponding to these two formulations are:

For VFDF1:

$$\begin{aligned} \frac{\partial \langle u_i \rangle_L}{\partial x_i} &= 0, \\ \frac{\partial \langle u_j \rangle_L}{\partial t} + \frac{\partial \langle u_i \rangle_L \langle u_j \rangle_L}{\partial x_i} &= -\frac{\partial \langle p \rangle_L}{\partial x_j} + \nu \frac{\partial^2 \langle u_j \rangle_L}{\partial x_i \partial x_i} - \frac{\partial \tau_L(u_i, u_j)}{\partial x_i}, \end{aligned} \tag{23}$$

$$\begin{aligned} &\frac{\partial}{\partial t}[\tau_L(u_i,u_j)] + \frac{\partial}{\partial x_k}[\langle u_k \rangle_L \tau_L(u_i,u_j)] = -\frac{\partial}{\partial x_k}[\tau_L(u_i,u_j,u_k) - \nu \frac{\partial}{\partial x_k}[\tau_L(u_i,u_j)]] \\ &+ G_{ik}\tau_L(u_j,u_k) + G_{jk}\tau_L(u_i,u_k) - \tau_L(u_i,u_k)\,\frac{\partial \langle u_j \rangle_L}{\partial x_k} - \tau_L(u_j,u_k)\,\frac{\partial \langle u_i \rangle_L}{\partial x_k} + C_0\,\varepsilon\,\delta_{ij}. \end{aligned} \tag{24}$$

For VFDF2:

$$\begin{aligned} \frac{\partial \langle u_i \rangle_L}{\partial x_i} &= 0, \\ \frac{\partial \langle u_j \rangle_L}{\partial t} + \frac{\partial \langle u_i \rangle_L \langle u_j \rangle_L}{\partial x_i} &= -\frac{\partial \langle p \rangle_L}{\partial x_j} + \nu \frac{\partial^2 \langle u_j \rangle_L}{\partial x_i \partial x_i} - \frac{\partial \tau_L(u_i, u_j)}{\partial x_i}, \end{aligned} \tag{25}$$

$$\frac{\partial}{\partial t}[\tau_L(u_i,u_j)] + \frac{\partial}{\partial x_k}[\langle u_k\rangle_L \tau_L(u_i,u_j)] = -\frac{\partial}{\partial x_k}[\tau_L(u_i,u_j,u_k)]$$
$$+ G_{ik}\tau_L(u_j,u_k) + G_{jk}\tau_L(u_i,u_k) - \tau_L(u_i,u_k)\,\frac{\partial\langle u_j\rangle_L}{\partial x_k} - \tau_L(u_j,u_k)\,\frac{\partial\langle u_i\rangle_L}{\partial x_k} + C_0\,\varepsilon\,\delta_{ij}. \tag{26}$$

It may be seen that the zeroth and first moment equations are identical (and exact); whereas the second central moment equations differ by the additional viscous term in VFDF1 (Eq. (24)). A comparison of these modeled equations with Eq. (5) shows that the GLM model implies:

$$-\Pi_{ij} - (\varepsilon_{ij} - \frac{2}{3}\,\varepsilon\,\delta_{ij}) = -\,C_1\,\omega\,\left[\tau_L(u_i,u_j) - \frac{2}{3}\,k\,\delta_{ij}\right], \quad C_1 = 1 + \frac{3}{2}C_0. \tag{27}$$

This is the same as the Rotta[33] model as shown by Pope.[34] There are two model constants in the VFDF equation. In RAS, typically[34,35] $C_\varepsilon \approx 1$, and $C_0 \approx 2.1 (C_1 = 4.15)$. As shown in Refs.,[34,27] boundedness of the GLM coefficients $C_0 > 0$ guarantees that the SGS stress is realizable.

4 EQUIVALENT STOCHASTIC SYSTEMS

The solution of the VFDF transport equation provides all the statistical information pertaining to the velocity vector. The most convenient means of solving this equation is via the Lagrangian Monte Carlo scheme. The basis of this scheme relies upon

the principle of equivalent systems.[26,32] Two systems with different instantaneous behaviors may have identical statistics and satisfy the same PDF transport equation. In this context, the general diffusion process is considered via the following system of stochastic differential equations (SDEs),[26,36,37,31]

$$\begin{aligned} d\mathcal{X}_i(t) &= D_i(\mathcal{X}(t),\mathcal{U}(t);t)\,dt + B(\mathcal{X}(t),\mathcal{U}(t);t)\,dW_i^x(t), \\ d\mathcal{U}_i(t) &= M_i(\mathcal{X}(t),\mathcal{U}(t);t)\,dt + E(\mathcal{X}(t),\mathcal{U}(t);t)\,dW_i^v(t) \\ &\quad + F_{ij}(\mathcal{X}(t),\mathcal{U}(t);t)\,dW_j^x(t), \end{aligned} \tag{28}$$

where $\mathcal{X}_i$ and $\mathcal{U}_i$ are probabilistic representations of the $\mathbf{x}$ and $\boldsymbol{u}$, respectively. The coefficients D_i and M_i are the "drift" in the phase space of position and velocity, respectively. The terms B and E are the "diffusion" coefficients for physical and velocity spaces, respectively; and W_i^x and W_i^v denote independent Wiener-Lévy processes.[38] The tensor F_{ij} represents the dependency between the velocity and physical spaces. This terms is needed to satisfy the Itô condition for $B \neq 0$. A comparison of the Fokker-Planck equation of Eq. (28) with the the modeled VFDF1 transport equation, Eq. (21) yields:

$$\begin{gathered} M_i \equiv -\frac{\partial\langle p\rangle_L}{\partial x_i} + 2\nu\frac{\partial^2\langle u_i\rangle_L}{\partial x_k\partial x_k} + G_{ij}\,(\mathcal{U}_j - \langle u_j\rangle_L), \quad D_i \equiv \mathcal{U}_i, \\ B \equiv \sqrt{2\nu}, \quad E \equiv \sqrt{C_0\varepsilon}, \quad F_{ij} \equiv \sqrt{2\nu}\,\frac{\partial\langle u_i\rangle_L}{\partial x_j}. \end{gathered} \tag{29}$$

Therefore, the proper SDEs which represent VFDF1 in the Lagrangian sense are:

$$
\begin{aligned}
d\mathcal{X}_i(t) &= \mathcal{U}_i(t)\, dt + \sqrt{2\nu}\, dW_i^x(t), \\
d\mathcal{U}_i(t) &= \left[-\frac{\partial \langle p \rangle_L}{\partial x_i} + 2\nu \frac{\partial^2 \langle u_i \rangle_L}{\partial x_k \partial x_k} + G_{ij} \left(\mathcal{U}_j(t) - \langle u_j \rangle_L \right) \right] dt + \sqrt{C_0 \varepsilon}\, dW_i^v(t) \\
&\quad + \sqrt{2\nu}\, \frac{\partial \langle u_i \rangle_L}{\partial x_j}\, dW_j^x(t).
\end{aligned} \tag{30}
$$

This stochastic system is the same as that developed by Dreeben and Pope[29–31] for RAS.

For VFDF2, due to the absence of diffusion in physical space we must have $B = 0$. Therefore, the corresponding SDEs are:

$$
\begin{aligned}
d\mathcal{X}_i(t) &= \mathcal{U}_i(t)\, dt \\
d\mathcal{U}_i(t) &= \left[-\frac{\partial \langle p \rangle_L}{\partial x_i} + \frac{\partial \langle \sigma_{ik} \rangle_L}{\partial x_k} + G_{ij} \left(\mathcal{U}_j(t) - \langle u_j \rangle_L \right) \right] dt + \sqrt{C_0 \varepsilon}\, dW_i^v(t).
\end{aligned} \tag{31}
$$

This system is the same as that suggested by Pope[26] and Haworth and Pope[27] for RAS.

The primary difference between the two formulations VFDF1 and VFDF2 is due to molecular effects in the spatial diffusion of the VFDF. This is explicitly included in the VFDF1 formulation and is also present in the corresponding second moment equation. This difference is expected to be important in flows where viscous effects are important; e.g. flow near solid boundaries.[29–31] Both of these formulation are considered in our numerical simulations as discussed below.

5 NUMERICAL SOLUTION PROCEDURE

Numerical solution of the modeled VFDF transport equation is obtained by a Lagrangian Monte Carlo procedure. The basis of this procedure is the same as that in RAS[39–41] and in previous LES/FDF.[6,8] But there are some subtle differences which are explained here. In the Lagrangian description, the VFDF is represented by an ensemble of N statistically identical Monte Carlo particles. Each of these particles carries information pertaining to its velocity $\mathbf{U}^{(n)}(t)$ and position $\mathbf{X}^{(n)}(t)$, $n = 1, 2, \ldots N$. This information is updated via temporal integration of Eq. (30). The simplest means of performing this integration is via the Euler-Maruyamma approximation[42]

$$\begin{aligned} X_i^n(t_{k+1}) &= X_i^n(t_k) + D_i^n(t_k)\Delta t + B^n(t_k)(\Delta t)^{1/2}\zeta_i^n(t_k), \\ U_i^n(t_{k+1}) &= U_i^n(t_k) + M_i^n(t_k)\Delta t + E^n(t_k)(\Delta t)^{1/2}\xi_i^n(t_k) \\ &\quad + F_{ij}^n(t_k)(\Delta t)^{1/2}\zeta_j^n(t_k), \end{aligned} \tag{32}$$

where $D_i^n(t_k) = D_i(\mathbf{X}^{(n)}(t_k), \mathbf{U}^{(n)}(t_k); t)$, $B^n(t_k) = B(\mathbf{X}^{(n)}(t_k), \mathbf{U}^{(n)}(t_k); t)$, ... and $\xi_i^n(t_k), \zeta_j^n(t_k)$ are independent standardized Gaussian random variables. This formulation preserves the Markovian character of the diffusion processes[43,44] and facilitates affordable computations. Higher order numerical schemes for solving Eq. (30) are available,[42] but one must be cautious in using them for LES.[6] Since the diffusion term in Eq. (28) strongly depends on the stochastic processes, the numerical scheme must be consistent with Itô-Gikhman[45,46] calculus. Equation (32) exhibits this prop-

erty.

The statistics are evaluated by consideration of the ensemble of particles in a "finite volume" centered at a spatial location. This ensemble provides "one-time" statistics. This finite volume is characterized by a cubic box of length Δ_E. This is necessary as, with probability one, no particle will coincide with the point as considered.[32] Here, a cubic box of size Δ_E is used to construct the ensemble mean, variances and covariances of the velocity vector. These values are used in the finite difference LES solver of Eq. (4) as described below.

The SGS dissipation rate and the SGS mixing frequency as required in the solution of the VFDF are evaluated on the finite difference grid points and interpolated to the particle's location. Ideally, for reliable Eulerian statistics and minimum numerical dispersion, it is desired to have the size of the sample domain infinitesimally small (i.e. $\Delta_E \to 0$) and the number of particles within this domain infinitely large. That is,

$$P_L(\boldsymbol{v};\mathbf{x},t) \xleftarrow[\substack{N_E\to\infty \\ \Delta_E\to 0}]{} \mathcal{P}_{N_E}(\boldsymbol{v};\mathbf{x},t) \equiv \frac{1}{N_E}\sum_{n\in\Delta_E}\delta(\boldsymbol{v}-\mathbf{U}^{(n)}), \tag{33}$$

where $\mathcal{P}_{N_E}$ is the Eulerian PDF constructed from the particle ensemble, $n \in \Delta_E$ denotes the particles contained in an ensemble box of length Δ_E centered at $\mathbf{x}$; and N_E is the total number of particles within the box. With a finite number of particles, obviously a larger Δ_E is needed. This compromise between the statistical accuracy

and dispersive accuracy implies that the optimum magnitude of Δ_E cannot, in general, be specified a priori.[26,11] This does not diminish the capability of the procedure, but exemplifies the importance of the parameters governing the statistics.

To provide an estimate of the proper Δ_E size, a "point estimator" procedure is considered. With this procedure, the mean values (the first moments of the VFDF) are evaluated by ensemble averaging, and spatial variations of these mean values within the box are ignored. With the discrete representation (Eq. (32)), the first two moments in this procedure are evaluated via:

$$\begin{aligned} \langle u_i \rangle_L &\xleftarrow[\substack{N_E \to \infty \\ \Delta_E \to 0}]{} \frac{1}{N_E} \sum_{n \in \Delta_E} U_i^{(n)} \equiv \langle U_i \rangle_E, \\ \tau_L(u_i, u_j) &\xleftarrow[\substack{N_E \to \infty \\ \Delta_E \to 0}]{} \frac{1}{N_E - 1} \sum_{n \in \Delta_E} (U_i^{(n)} - \langle U_i \rangle_E)\,(U_j^{(n)} - \langle U_j \rangle_E). \end{aligned} \tag{34}$$

The point estimator is obviously subject to both statistical errors and dispersive errors for $\Delta_E \neq 0$.

To determine the pressure field, the "mean field solver" is based on the "compact parameter" finite difference scheme of Carpenter.[47] This is a variant of the McCormack[48] scheme in which fourth-order compact differences are used to approximate the spatial derivatives, and a second order symmetric predictor-corrector sequence is employed for time discretization. The numerical algorithm is a hyperbolic solver which considers a fully compressible flow. Here, the simulations are conducted with a low Mach number ($M \leq 0.3$) to minimize compressibility effects. All the finite difference opera-

tions are conducted on fixed and equally sized grid points. The transfer of information from these points to the location of the Lagrangian particles is conducted via interpolation. A second-order (bilinear) interpolation scheme is used for this purpose. The results of previous work indicate no significant improvements with the use of higher order interpolation schemes.[6]

The mean-field solver also determines the filtered velocity field. That is, there is a "redundancy" in the determination of the first filtered moments as both the finite difference and the Monte Carlo procedures provides the solution of this field. This redundancy is actually very useful in monitoring the accuracy of the simulated results. Detailed discussions pertaining to this issue are provided in Refs.[8,39–41]

To establish the consistency of the VFDF solver, another LES is also conducted in which the modeled transport equations for the filtered velocity and the generalized SGS stresses are solved strictly via the finite difference scheme. These simulations are referred to as LES-FD and are only applied for the case corresponding to VFDF2. That is, Eqs. (25) and (26) are considered. Since the SGS transport terms $\tau_L(u_i, u_j, u_k)$ are unclosed in Eq. (26), the values corresponding to these terms are taken from the Monte Carlo solver and substituted in the SGS stress transport equations. The attributes of all of the scheme are summarized in Table 1, with further discussions in Refs.[6,39–41]

6 RESULTS

A Flows Simulated

Simulations are conducted of a two-dimensional (2D) planar jet, and a 3D temporally developing mixing layer. The jet flow simulations are conducted primarily for establishing the consistency of the Lagrangian Monte Carlo solver. For this purpose, 2D simulations are sufficient. To analyze the overall performance of the VFDF and to demonstrate its full capabilities and drawbacks, 3D simulations are required.

In the planar jet, a fluid issues from a jet of width D into a co-flowing stream with a lower velocity. The size of the domain in the streamwise (x) and cross-stream (y) directions are $0 \leq x \leq 14D$ and $-3.5D \leq y \leq 3.5D$. The ratio of the co-flowing stream velocity to that of the jet at the inlet is kept fixed at 0.5. A double-hyperbolic tangent profile is utilized to assign the velocity distribution at the inlet plane. The formation of the large scale coherent structures are expedited by imposing low amplitude perturbations at the inlet. In the finite difference simulations, the characteristic boundary condition procedure of Ref.[49] is used at the inlet, free-shear boundary conditions are used at the free-streams and the pressure boundary condition of Ref.[50] is used at the outflow.

The temporal mixing layer consists of two parallel streams traveling in opposite directions with the same speed.[51–53] A hyperbolic tangent profile is utilized to assign the velocity distribution at the initial time. The simulations are conducted for a cubic

box, $0 \leq x \leq L,\ -L/2 \leq y \leq L/2,\ 0 \leq z \leq L$, where x, y and z denote the streamwise, the cross-stream and the spanwise directions, respectively; and the length, L is specified such that $L = 2^{N_P}\lambda_u$, where N_P is the desired number of successive vortex pairings and λ_u is the wavelength of the most unstable mode corresponding to the mean streamwise velocity profile imposed at the initial time. The flowfield is parameterized in a procedure somewhat similar to that by Vreman et al.[20] The formation of the large scale structures are expedited through eigenfunction based initial perturbations.[54,55] This includes two-dimensional[52,20,56] and three-dimensional[52,57] perturbations with a random phase shift between the $3D$ modes. This results in the formation of two successive vortex pairings and strong three-dimensionality.

The flow variables are normalized with respect to selected reference quantities. In the jet flow, the jet exit velocity and the jet width are the reference scales. In the temporal mixing layer, the reference length is the half initial vorticity thickness, $L_r = \frac{\delta_v(t=0)}{2}$, ($\delta_v = \frac{\Delta U}{|\partial\overline{\langle u_1\rangle_L}/\partial y|_{max}}$, where $\overline{\langle u_1\rangle_L}$ is the Reynolds averaged value of the filtered streamwise velocity and ΔU is the velocity difference across the layer). The reference velocity is $U_r = \Delta U/2$.

B Numerical Specifications

All finite difference simulations are conducted on equally-spaced grid points with grid spacings $\Delta x = \Delta y = \Delta z(\text{for 3D}) = \Delta$. The resolution for LES of the planar jet consists of 201×101 grid points. This allows simulations with a Reynolds number

$Re = \frac{U_r D}{\nu} = 14,000$. The simulations of the temporal mixing layer are conducted on 193^3 and 33^3 points for DNS and LES, respectively. This allows simulations with $Re = \frac{U_r L_r}{\nu} = 50$.

To filter the DNS data, a top-hat function[21] of the form below is used

$$G(\mathbf{x}' - \mathbf{x}) = \prod_{i=1}^{N_D} \widetilde{G}(x_i' - x_i)$$

$$\widetilde{G}(x_i' - x_i) = \begin{cases} \frac{1}{\Delta_L} & |x_i' - x_i| \leq \frac{\Delta_L}{2}, \\ 0 & |x_i' - x_i| > \frac{\Delta_L}{2}, \end{cases} \tag{35}$$

in which N_D denotes the number of dimensions, and $\Delta_L = 2\Delta$.[58] No attempt is made to investigate the sensitivity of the results to the filter function[24] or the size of the filter.[59]

For VFDF simulations of the temporal mixing layer, the Monte Carlo particles are initially distributed throughout the computational region. For the jet flow, the particles are supplied in the inlet region $-1.75D \leq y \leq 1.75D$. As the particles convect downstream, this zone distorts as it conforms to the flow as determined by the hydrodynamic field. The simulation results are monitored to ensure the particles fully encompass and extend well beyond regions of non-zero vorticity with an approximately uniform particle number density. All simulations are performed with a uniform "weight"[26] of the Monte Carlo particles. In the temporal mixing layer, due to flow periodicity in the streamwise and spanwise directions, if the particle leaves

the domain at one of these boundaries new particles are introduced at the other boundary with the same compositional values. In the cross-stream directions, the free-slip boundary condition is satisfied by the mirror-reflection of the particles leaving through these boundaries. In the planar jet, new particles are introduced through the inlet boundary at a rate proportional to the local flow velocity and with a velocity makeup dependent on the cross-stream direction only. When the particles leave the computational domain at the outflow, they are no longer tracked. The density of the Monte Carlo particles is determined by the average number of particles N_E within the ensemble domain of size $\Delta_E \times \Delta_E(\times\Delta_E)$. The effects of both of these parameters are assessed to ensure the consistency and the statistical accuracy of the VFDF simulations.

All results are analyzed both "instantaneously" and "statistically." In the former, the instantaneous contours (snap-shots) and scatter plots of the variables of interest are analyzed. In the latter, the "Reynolds-averaged" statistics constructed from the instantaneous data are considered. In the spatially developing flows this averaging procedure is conducted via sampling in time. In the temporal mixing layer, the statistics are constructed by spatial averaging over the $x - z$ plane of statistical homogeneity. All Reynolds averaged results are denoted by an overbar.

C Consistency and Convergence Assessments

The objective of this section is to demonstrate the consistency of the VFDF formulation and the convergence of its Monte Carlo simulation procedure. For this purpose, the results via VFDF and LES-FD are compared against each other. Since the accuracy of the finite difference procedure is well-established (at least for the first order filtered quantities), such a comparative assessment provides a good means of assessing the performance of the Monte Carlo solution of the VFDF. This assessment is done for 2D simulations and for VFDF2 as they are sufficient for establishing consistency and convergence. To do so, the statistical results obtained from the Monte Carlo simulations of Eq. (31) are compared with the finite difference solution of Eqs. (25) & (26). Also, no attempt is made to determine the appropriate values of the model constants; the values suggested in the literature are adopted[34] $C_0 = 2.1 (C_1 = 4.15)$ and $C_\epsilon = 1$.

In Fig. 1, the instantaneous contour plots of the vorticity are shown as determined by (a) VFDF2 and (b) LES-FD. This figure provides a simple visual demonstration of the consistency of the VFDF2. Scatter plots of $\langle u \rangle_L$ vs. $\langle v \rangle_L$ are presented in Fig. 2. The correlation and regression coefficients (denoted, respectively, by ρ and r on these figures) are insensitive to Δ_E. Figures 3 and 4 show the Reynolds averaged values of the streamwise velocity and several components of the SGS stress tensor for several values of Δ_E, with $N_E = 40$ kept fixed. It is observed that the first filtered moments as obtained by VFDF agree very well with those via LES-FD even for large Δ_E values.

However, smaller Δ_E values are required for convergence of the VFDF predicted SGS stresses to those by LES-FD. The relative difference between the L_2 norms of all of the components of the SGS tensor as a function of $(\Delta_E/\Delta)^2$ is presented in Fig. 5. Extrapolation to $\Delta_E = 0$ shows that the "error" goes to zero as $\Delta_E \to 0$.

The influence of N_E on the first two moments is shown in Figs. 6 and 7. It is observed that N_E does not have a significant influence on the first moments, but does slightly influence the second moments. In all the cases considered, $N_E \geq 40$ yields reliable predictions, consistent with previous consistency and convergence assessments of the scalar FDF.[6,8]

All the subsequent simulations are conducted with $\Delta_E = \Delta/2$ and $N_E = 40$.

D Comparative Assessments of the VFDF

The objective of this section is to analyze some of the characteristics of the VFDF via comparative assessments against DNS data. This assessment is done via both a priori and a posteriori analyses. In the former, the DNS results are used to determine the range of the empirical constants appearing in the VFDF sub-closures. In the latter, the final results as predicted by the VFDF are directly compared with those obtained by DNS. The procedure is similar to that in Ref.[20] and considers the 3D temporal mixing layer.

In addition to VFDF, three other LES are conducted with (1) no SGS model, (2) the

Smagorinsky[16,60] SGS closure, and (3) the dynamic Smagorinsky[17–19] model. In the case with no model, the contribution of the SGS is completely ignored, i.e. $\tau_L(u_i, u_j) = 0$. In this case, the numerical errors amount to an implied model. But as indicated in Ref.,[20] this case is included to provide a point of reference for the other closures. The Smagorinsky model is,[16,61]

$$\begin{aligned} \tau_L(u_i, u_j) - \frac{2}{3}\, k\, \delta_{ij} &= -2\, \nu_t\, S_{ij}, \\ S_{ij} &= \frac{1}{2}\left(\frac{\partial \langle u_i \rangle_L}{\partial x_j} + \frac{\partial \langle u_j \rangle_L}{\partial x_i}\right), \\ \nu_t &= C_\nu\, \Delta_L^2\, S. \end{aligned} \tag{36}$$

$C_\nu = \sqrt{2}\ \ 0.17^2 \approx 0.04$, $S = \sqrt{S_{ij} S_{ij}}$ and Δ_L is the characteristic length of the filter. This model considers the anisotropic part of the SGS stress tensor $a_{ij} = \tau_L(u_i, u_j) - 2/3\, k\, \delta_{ij}$. The isotropic components are absorbed in the pressure field. The dynamic version of the Smagorinsky model provides a means of approximating C_ν as suggested in Refs.[17–19] The procedure for the implementation of this model in the 3D temporal mixing layer LES is described by Vreman;[20] thus it is not repeated here. (See Refs.[11,23,62,63] for recent reviews on SGS closure strategy.)

In addition to the resolved velocity field, the primary integral statistical quantities considered for comparative assessments are:

$$E_f = \int \frac{1}{2} \langle u_i \rangle_L \langle u_i \rangle_L \, \mathbf{dx} \tag{37}$$

$$
\begin{aligned}
P_k &= \int p_k \, \mathbf{dx}, \quad \text{with} \quad p_k = -\tau_L(u_i, u_j)\frac{\partial \langle u_i \rangle_L}{\partial x_j}, \\
E_\nu &= \int \varepsilon_\nu \, \mathbf{dx}, \quad \text{with} \quad \varepsilon_\nu = \nu \frac{\partial \langle u_i \rangle_L}{\partial x_k}\left(\frac{\partial \langle u_i \rangle_L}{\partial x_k} + \frac{\partial \langle u_k \rangle_L}{\partial x_i}\right), \\
B_k &= \int min(0, p_k) \, \mathbf{dx}.
\end{aligned}
\tag{38}
$$

E_f is the kinetic energy of the resolved field, ϵ_ν represents the viscous molecular dissipation rate directly from the filtered field, P_k is the production rate of the SGS kinetic energy (or the rate of energy transfer from the resolved filtered motion to the SGS motion), and B_k is the total backscatter.[64-66] The resolved molecular dissipation rate is always positive (by definition), but the production rate of the SGS kinetic energy can be locally negative. This backscatter is not represented in the Smagorinsky model. The dynamic model is potentially capable of accounting for it, but at the expense of causing numerical instabilities. In the implementation of the dynamic model used here, backscatter is avoided by averaging the numerator and denominator of the expression determining C_ν (Refs.[19,20]) over the homogeneous directions. If negative values are still present, they are set equal to zero.[20,63] The "resolved" components of the Reynolds-averaged stress tensor are denoted by $\overline{R_{ij}}$ where $R_{ij} = (\langle U_i \rangle_L - \overline{\langle U_i \rangle_L})(\langle U_j \rangle_L - \overline{\langle U_j \rangle_L})$. The "total" Reynolds stresses are denoted by $\overline{r_{ij}}$ where $r_{ij} = (U_i - \overline{U_i})(U_j - \overline{U_j})$. These are approximated by $\overline{r_{ij}} \approx \overline{R_{ij}} + \overline{\tau_L(u_i, u_j)}$.[20,67,68] In DNS, the total stresses are evaluated directly and the results indicate that $\overline{R_{ij}} + \overline{\tau_L(u_i, u_j)}$ does indeed approximate $\overline{r_{ij}}$ with a maximum error of less than 10%

Figure 8 shows the distribution of the particle number density within the whole computational domain. Assuring an approximately uniform distribution, the values of the moments within local ensembles are compared with those of filtered DNS data. These DNS data are transposed from the original high resolution 193^3 points to the low resolution of 33^3 points, and then are compared with LES results on these coarse points.

The DNS data are also used to make a priori estimates of the model constants. The primary terms which require closure are the SGS dissipation and the velocity-pressure scrambling tensors. The model equation (Eq. (20)) involving C_ε is in a scalar form. For an estimate of C_1 (thus C_0), we consider the following norm of the corresponding closure (Eq. (27)):

$$\| - \Pi_{ij} - (\varepsilon_{ij} - \frac{2}{3}\,\varepsilon\,\delta_{ij})\| \approx C_1\,\omega\,\|\tau_L(u_i, u_j) - \frac{2}{3}\,k\,\delta_{ij}\|, \tag{39}$$

where $\|W_{ij}\| = \sqrt{W_{ji}W_{ij}}$. To estimate the coefficients, a linear regression is performed on all the data points at each computational time step. The optimized constants as obtained in this way are denoted by $\widetilde{C_\varepsilon}$ and $\widetilde{C_1}$. This procedure is also followed for the Reynolds averaged data, with the optimized models obtained in this way denoted by $\overline{C_\varepsilon}$ and $\overline{C_1}$. The temporal variations of these estimated values are shown in Fig. 9. The non-uniformity of the coefficients indicates the "non-universality" of the models.

This is expected as the flow evolves from an initially smooth laminar state to a strong three-dimensional state (at $t \approx 40$) before the action of the small scales becomes significant. The closures as adopted are not fully suitable for application in all of these flow regions. Nevertheless, Fig. 9 indicates that the values for these coefficients as suggested in RAS, i.e. $C_1 \approx 4.15$, $C_\varepsilon \approx 1$ are reasonable, at least within the turbulent regime. The influences of these parameters are further investigated via a posteriori analysis of the results as discussed below.

Figures 10 and 11 show the contours of the spanwise and the streamwise components of the vorticity field, respectively, at time $t = 80$. By this time, the flow has gone through several pairings and exhibits strong 3D effects. This is evident by the formation of large scale spanwise rollers with presence of counter-rotating streamwise vortex pairs in all the simulations. The results via the no-model indicate too many small-scale structures which clearly are not captured accurately on the coarse grid. The amount of SGS diffusion with the Smagorinsky model is very significant at initial times. Due to this dissipative characteristics of the model, the predicted results are too smooth and only contain the large scale structures. The vortical structures as depicted by the dynamic Smagorinsky and the VFDF are very similar and predict the DNS results better than the other two models. The results obtained by VFDF1 and VFDF2 are virtually indistinguishable from each other. This is expected, due to the lack of importance of molecular effects in this free shear flow.

The Reynolds averaged values of the streamwise velocity and the temporal variations

of the momentum thickness:

$$\delta_m(t) = \frac{1}{4}\int_{-L/2}^{L/2} \left(1 - \overline{\langle u \rangle_L} \right) \left(1 + \overline{\langle u \rangle_L} \right) dy, \tag{40}$$

are shown in in Figs. 12 and 13, respectively. In Fig. 12 the Reynolds averaged values of both filtered and unfiltered DNS data are considered and are shown to be essentially equivalent. Therefore, the latter are not shown in subsequent figures. The dissipative nature of the Smagorinsky model at initial times resulting in a slow growth of the layer is shown. Several values of the model parameters (C_0, C_ε) are considered in the VFDF simulations. It is observed that as the magnitude of C_ε decreases, the initial rate of the layer's spread is higher. With the exception of the case with $C_\varepsilon = 0.5$ and the Smagorinsky model, all the other VFDF cases, the dynamic Smagorinsky and the no-model yield a similar rate of layer's growth at late times.

The temporal variations of the resolved kinetic energy and all of the terms defined in Eq. (38) are shown in Fig. 14. The overall features displayed in this figure are similar to those reported by Vreman et al.[20] for the no model, the Smagorinsky model and the dynamic Smagorinsky model. The initial rate of decay of the resolved kinetic energy for the Smagorinsky model is the highest. This is due to the excessive production of the SGS kinetic energy by this model in the transitional region, and explains the reason for the lack of small scales in the vortical structures as discussed before. For all the other models the initial rate of decrease of the resolved kinetic energy is small and increases as the flow develops. The trend portrayed by DNS results is

best captured by the VFDF simulations. For the no model case the only means of dissipation of the resolved kinetic energy is through molecular action and numerical dissipation which become significant at later stages due to presence of a large amount of small scales. In this case, the amount of numerical dissipation is the highest. For all the other closures, the productions rate of the SGS kinetic energy is larger than the molecular dissipation as the flow develops. The dynamic Smagorinsky and the no-model simulations predict the same initial rate of decay for the resolved kinetic energy. This is due to low initial values of P_k predicted by the dynamic Smagorinsky model. After $t = 40$ the amount of P_k as predicted by the dynamic model is more than that of molecular dissipation by the no-model. Thus the rate of decay of the resolved kinetic energy becomes higher for the dynamic model and is closer to that obtained by DNS.

With the exception of the no-model case, all the simulations predict similar trends for the molecular dissipation. The magnitude of this dissipation as predicted by VFDF changes slightly with the variation of the model parameter. The production rate of the SGS kinetic energy depends more strongly on the model coefficients; as C_ε decreases, the peak magnitude of P_k is larger. The Smagorinsky model does not adequately predict P_k, and the dynamic model yields better predictions at long times. The overall trends are best predicted by VFDF. The same is true in capturing the backscatter phenomenon. By design, the backscatter is identically zero in the Smagorinsky and the dynamic Smagorinsky model. But VFDF is capable of capturing it, and its extent

is controlled by the model parameters. In this regard it is important to note that there are no numerical instability problems in the VFDF solver for negative B_k values. However, the amount of predicted backscatter is less than that of DNS and its relative magnitude is less than those of P_k and E_ν.

Several components of the planar averaged values of the SGS anisotropy tensor, $\overline{a_{ij}} = \overline{\tau_L(u_i, u_j)} - 2/3\ \overline{k}\ \delta_{ij}$ are presented in Figs. 15 & 16. Both the Smagorinsky and the dynamic model under-predict all of the components of this stress. The VFDF predictions are much more satisfactory. In this regard, the VFDF is expected to be more effective than the other closures for LES of reacting flows since the extent of SGS mixing is heavily influenced by SGS convection.[69,70] "Optimum" values for C_ε and C_0 cannot be suggested to predict all of the components of this tensor at all times, but it is obvious that there is too much SGS energy with $C_\varepsilon = 0.5$.

Several components of the resolved stress tensor $\overline{R_{ij}}$ are shown in Figs. 17 & 18. As expected, the performance of the Smagorinsky model is not very good as it does not predict the spread and the peak value of the resolved Reynolds stresses. None of the other models show a distinct superiority in predicting the DNS results. The no-model and the dynamic Smagorinsky model predict large peak values at the middle of the layer. The VFDF predicts both the spread and the peak values reasonably well. The results for small C_ε values are not shown since the amount of energy in the resolved scale decreases too much in favor of the increase of the SGS stress (as shown in Figs. 15 & 16). The cross-stream variations of the total Reynolds stress $\overline{r_{12}}$

are presented in Figs. 19. The peak values by the no-model simulations are again the highest. The dynamic model and VFDF perform similarly and capture the DNS trends equally well.

E Comparison with Previous Investigations

All of the results obtained here by DNS, and LES via the Smagorinsky and the dynamic Smagorinsky models agree very well with those of Vreman et al.[20] The slight differences are due to the non-identical flow initializations, and the different computational methodologies employed in the two simulations. To compare with results of other investigations, simulations are conducted of another temporally developing mixing layer with $Re = 500$ in a larger computational domain, $L_x = 120$. An initial forcing of the form $\mathcal{A}e^{-(y/2)^2}$ is used, where $\mathcal{A}$ is a uniformly distributed random number with an amplitude of 0.05. Rogers and Moser[60] perform DNS of a high Re number flow on $512 \times 210 \times 192$ spectral points. The results of these simulations are in excellent agreements with laboratory data of Bell and Mehta.[71] Here, LES is conducted of this flow via the dynamic Smagorinsky model.

The profiles of the mean streamwise velocity and several components of the resolved stresses at $t = 250$ are presented in Figs. 20 and 21, respectively. In these figures, $\xi = y/\delta_m(t)$ and the symbols denote the experimental data[71] at several streamwise locations. The good agreement with these data also indicates good agreement with DNS results of Rogers and Moser.[72]

F Computational Requirements

The total computational times associated with simulations of the 3D temporal mixing layer are shown in Table 2. Expectedly, the overhead associated with the VFDF simulation is extensive as compared to the other models; nevertheless this requirement is significantly less that of DNS. This overhead was tolerated in present simulations, but can be reduced with utilization of an optimum parallel simulation procedure. This has been discussed for use in PDF[73] and is recommended for future VFDF simulations.

7 SUMMARY AND CONCLUDING REMARKS

The filtered density function (FDF) methodology[1] has proven very effective for large eddy simulation (LES) of turbulent reacting flows.[3,6–11] In all of previous contributions, the LES/FDF of only the scalar quantities are considered. The objective of the present work is to develop the FDF methodology for LES of the velocity field. For this purpose, a methodology termed the velocity filtered density function (VFDF) is developed. The VFDF is basically the probability function (PDF) of the subgrid scale (SGS) velocity vector. The exact transport equation governing the evolution of the VFDF is derived. It is shown that the effects of SGS convection in this equation appears in a closed form. The unclosed terms in this transport equation are modeled via two formulations: VFDF1 and VFDF2. The primary difference between the two

models is the inclusion of the molecular diffusion in the spatial transport of the VFDF in the first formulation. The closure strategy in the formulation similar to that in PDF methods in Reynolds averaged simulation (RAS) procedures.[32] In this way, the VFDF formulation is at least equivalent to a second-order moment SGS closure.

The modeled VFDF transport equations are solved numerically via a Lagrangian Monte Carlo scheme in which the solutions of the equivalent stochastic differential equations (SDEs) are obtained. Two Monte Carlo procedures are considered. The schemes preserve the Itô-Gikhman nature of the SDEs and provide a reliable solution for the VFDF. The consistency of the VFDF formulation and the convergence of its Monte Carlo solutions are assessed. This is done via comparisons between the results obtained by the Monte Carlo procedure and the finite difference solution of the transport equations of the first two filtered moments of VFDF (LES-FD). With inclusion of the third moments from the VFDF into the LES-FD, the consistency and convergence of the Monte Carlo solution is demonstrated by good agreements of the first two SGS moments with those obtained by LES-FD.

The VFDF predictions are compared with those with LES results with no SGS model, with the Smagorinsky[16] SGS closure, and with the dynamic Smagorinsky[17–19] model. All of these results are also compared with direct numerical simulation (DNS) results of a three-dimensional, temporally developing mixing layer in a context similar to that conducted by Vreman et al.[20] This comparison provides a means of examining some of the trends and overall characteristics as predicted by LES. It is shown that

the VFDF performs well in predicting some of the phenomena pertaining to the SGS transport. The magnitude of the SGS Reynolds stresses as predicted by VFDF is significantly larger than those predicted by the other SGS models and much closer to the filtered DNS results. The temporal evolution of the production rate of the SGS kinetic energy is predicted well by VFDF as compared with those via the other closures. The VFDF is also capable of accounting the SGS backscatter without any numerical instability problems, although the level predicted is substantially less than that observed in DNS.

The results of a priori assessment against DNS data indicates that the values of the model coefficients as employed in VFDF (C_0 and C_ε) are of the range suggested in the equivalent models previously used in RAS. The results of a posteriori assessments via comparison with DNS data does not give any compelling reasons to use values other than those suggested in RAS, $C_0 = 2.1,\ C_\varepsilon = 1$. However, small values of C_ε are not acceptable as they would yield too much of SGS energy relative to that within the resolved scales.

Most of the overall flow features, including the mean velocity field and the resolved and total Reynolds stresses as predicted by VFDF are similar to those obtained via the dynamic Smagorinsky model. This is interesting in view of the fact that the model coefficients in VFDF are kept fixed. It may be possible to improve the predictive capabilities of the VFDF by two ways: (1) development of a dynamic procedure to determine the model coefficients, and/or (2) implementation of higher order closures

for the generalized Langevin model parameter G_{ij} (see Ref.[34]).

Work is in progress towards developments of a joint velocity-scalar FDF for LES of reacting flows. Compared to standard LES, this approach has the advantage of treating reaction in a closed form; and, compared to scalar FDF[6,8] has the advantage of treating convective transport (of momentum and species) in closed form. These modeling advantages have an associated computational penalty. For the cases considered here, VFDF is more expensive computationally than the dynamic Smagorinsky model by a factor of 15. It is expected that VFDF will not be more expensive than scalar FDF, at least for reacting flows with many species.

Acknowledgments

We are indebted to Drs. T.D. Dreeben, M. Germano, S. Heinz, R.D. Moser, M.M. Rogers, P. Sagaut and B. Vreman for their comments and very useful suggestions on the first draft of this manuscript. This work is sponsored by the U.S. Air Force Office of Scientific Research under Grant F49620-00-1-0035 to SUNY-Buffalo and Grant F49620-00-1-0171 to Cornell University. Dr. Julian M. Tishkoff is the Program Manager for both these grants. Additional support for the work at SUNY-Buffalo is provided by the NASA Langley Research Center under Grant NAG-1-2238 with Dr. J. Philip Drummond as the Technical Monitor. Computational resources are provided by the NCSA at the University of Illinois at Urbana and by the CCR at

SUNY-Buffalo.

References

[1] Pope, S. B., Computations of Turbulent Combustion: Progress and Challenges, Proc. Combust. Inst., 23:591–612 (1990).

[2] Madnia, C. K. and Givi, P., Direct Numerical Simulation and Large Eddy Simulation of Reacting Homogeneous Turbulence, in Galperin, B. and Orszag, S. A., editors, Large Eddy Simulations of Complex Engineering and Geophysical Flows, pp. 315–346, Cambridge University Press, Cambridge, UK, 1993.

[3] Gao, F. and O'Brien, E. E., A Large-Eddy Simulation Scheme for Turbulent Reacting Flows, Phys. Fluids A, 5:1282–1284 (1993).

[4] Frankel, S. H., Adumitroaie, V., Madnia, C. K., and Givi, P., Large Eddy Simulations of Turbulent Reacting Flows by Assumed PDF Methods, Engineering Applications of Large Eddy Simulations, 162:81–101 (1993).

[5] Cook, A. W. and Riley, J. J., A Subgrid Model for Equilibrium Chemistry in Turbulent Flows, Phys. Fluids, 6:2868–2870 (1994).

[6] Colucci, P. J., Jaberi, F. A., Givi, P., and Pope, S. B., Filtered Density Function for Large Eddy Simulation of Turbulent Reacting Flows, Phys. Fluids, 10(2):499–515 (1998).

[7] Réveillon, J. and Vervisch, L., Subgrid Scale Turbulent Micromixing: Dynamic Approach, AIAA J., 36(3):336–341 (1998).

[8] Jaberi, F. A., Colucci, P. J., James, S., Givi, P., and Pope, S. B., Filtered Mass Density Function for Large Eddy Simulation of Turbulent Reacting Flows, J. Fluid Mech., 401:85–121 (1999).

[9] Garrick, S. C., Jaberi, F. A., and Givi, P., Large Eddy Simulation of Scalar Transport in a Turbulent Jet Flow, in Knight, D. and Sakell, L., editors, Recent Advances in DNS and LES, Fluid Mechanics and its Applications, Vol. 54, pp. 155–166, Kluwer Academic Publishers, The Netherlands, 1999.

[10] James, S. and Jaberi, F. A., Large Scale Simulations of Two-Dimensional Non-premixed Methane Jet Flames, Combust. Flame, 123:465–487 (2000).

[11] Pope, S. B., Turbulent Flows, Cambridge University Press, Cambridge, UK, 2000.

[12] Zhou, X. Y. and Pereira, J. C. F., Large Eddy Simulation (2D) of a Reacting Plan Mixing Layer Using Filtered Density Function, Flow, Turbulence and Combustion, 64:279–300 (2000).

[13] Luo, K. H., DNS and LES of Turbulence-Combustion Interactions, In Geurts,[22] chapter 14, pp. 263–293.

[14] Poinsot, T. and Veynante, D., Theoretical and Numerical Combustion, R. T. Edwards, Inc., Philadelphia, PA, 2001.

[15] Tong, C., Measurements of Conserved Scalar Filtered Density Function in a Turbulent Jet, Phys. Fluids, 13(10):2923–2937 (2001).

[16] Smagorinsky, J., General Circulation Experiments with the Primitive Equations. I. The Basic Experiment, Monthly Weather Review, 91(3):99–164 (1963).

[17] Germano, M., Piomelli, U., Moin, P., and Cabot, W. H., A Dynamic Subgrid-Scale Eddy Viscosity Model, Phys. Fluids A, 3:1760–1765 (1991).

[18] Germano, M., Turbulence: The Filtering Approach, J. Fluid Mech., 238:325–336 (1992).

[19] Lilly, D. K., A Proposed Modification of the Germano Sub-Grid Closure Method, Phys. Fluids, A 4(3):633–635 (1992).

[20] Vreman, B., Geurts, B., and Kuerten, H., Large-Eddy Simulation of the Turbulent Mixing Layer, J. Fluid Mech., 339:357–390 (1997).

[21] Aldama, A. A., Filtering Techniques for Turbulent Flow Simulations, Lecture Notes in Engineering, Vol. 49, Springer-Verlag, New York, NY, 1990.

[22] Geurts, B. J., editor, Modern Simulation Strategies for Turbulent Flow, R. T. Edwards, Inc., Philadelphia, PA, 2001.

[23] Sagaut, P., Large Eddy Simulation for Incompressible Flows, Springer, New York, 2001.

[24] Vreman, B., Geurts, B., and Kuerten, H., Realizability Conditions for the Turbulent Stress Tensor in Large-Eddy Simulation, J. Fluid Mech., 278:351–362 (1994).

[25] O'Brien, E. E., The Probability Density Function (PDF) Approach to Reacting Turbulent Flows, in Libby, P. A. and Williams, F. A., editors, Turbulent Reacting Flows, chapter 5, pp. 185–218, Springer-Verlag, Heidelberg, 1980.

[26] Pope, S. B., PDF Methods for Turbulent Reacting Flows, Prog. Energy Combust. Sci., 11:119–192 (1985).

[27] Haworth, D. C. and Pope, S. B., A Generalized Langevin Model for Turbulent Flows, Phys. Fluids, 29(2):387–405 (1986).

[28] Haworth, D. C. and Pope, S. B., A PDF Modeling Study of Self-Similar Turbulent Free Shear Flows, Phys. Fluids, 30(4):1026–1044 (1987).

[29] Dreeben, T. D. and Pope, S. B., Probability Density Function and Reynolds-Stress Modeling of Near-Wall Turbulent Flows, Phys. Fluids, 9(1):154–163 (1997).

[30] Dreeben, T. D. and Pope, S. B., Wall-Function Treatment in PDF Methods for Turbulent Flows, Phys. Fluids, 9(9):2692–2703 (1997).

[31] Dreeben, T. D. and Pope, S. B., Probability Density Function/Monte Carlo Simulation of Near-Wall Turbulent Flows, J. Fluid Mech., 357:141–166 (1998).

[32] Pope, S. B., Lagrangian PDF Methods for Turbulent Flows, Ann. Rev. Fluid Mech., 26:23–63 (1994).

[33] Rotta, J., Statistiche Theorie Nichththomogener Turbulenz, J. Zeitsch fur Physik, 129:547 (1951), Translation in English available in NASA TM-14560 (1982).

[34] Pope, S. B., On the Relationship between Stochastic Lagrangian Models of Turbulence and Second-Moment Closures, Phys. Fluids, 6(2):973–985 (1994).

[35] Deardorff, J. W., The Use of Subgrid Transport Equations in a Three-Dimensional Model of Atmospheric Turbulence, J. Fluids Eng., 95:429–438 (1973).

[36] Risken, H., The Fokker-Planck Equation, Methods of Solution and Applications, Springer, New York, NY, 1989.

[37] Gardiner, C. W., Handbook of Stochastic Methods, Springer-Verlag, New York, NY, 1990.

[38] Karlin, S. and Taylor, H. M., A Second Course in Stochastic Processes, Academic Press, New York, NY, 1981.

[39] Pope, S. B., Mean Field Equations in PDF Particle Methods for Turbulent Reactive Flows, Technical Report FDA 97-06, Sibley School of Mechanical and Aerospace Engineering, Cornell University, Ithaca, NY, 1997.

[40] Muradoglu, M., Jenny, P., Pope, S. B., and Caughey, D. A., A Consistent Hybrid-Volume/Particle Method for the PDF Equations of Turbulent Reactive Flows, J. Comp. Phys., 154(2):342–371 (1999).

[41] Muradoglu, M., Pope, S. B., and Caughey, D. A., The Hybrid Method for the PDF Equations of Turbulent Reactive Flows: Consistency Conditions and Correction Algorithms, J. Comp. Phys., 172:841–878 (2001).

[42] Kloeden, P. E. and Platen, E., Numerical Solution of Stochastic Differential Equations, Applications of Mathematical Stochastic Modelling and Applied Probability, Vol. 23, Springer-Verlag, New York, NY, 1995.

[43] Billingsly, P., Probability and Measure, Wiley, New York, NY, 1979.

[44] Gillespie, D. T., Markov Processes, An Introduction for Physical Scientists, Academic Press, New York, NY, 1992.

[45] Itô, K., Differential Equations, Memoirs of the American Mathematical Society, Vol. 4, American Math Society, Providence, RI, 1951.

[46] Gikhman, I. I. and Skorokhod, A. V., Stochastic Differential Equations, Academic Press, New York, NY, 1972.

[47] Carpenter, M. H., A High-Order Compact Numerical Algorithm for Supersonic Flows, in Mortron, K. W., editor, Proc. 12th International Conference on Numerical Methods in Fluid Dynamics, Lecture Notes in Physics, Vol. 371, pp. 254–258, Springer-Verlag, 1990.

[48] MacCormack, R. W., The Effect of Viscosity in Hypervelocity Impact Catering, AIAA paper AIAA-69-354, 1969.

[49] Poinsot, T. J. and Lele, S. K., Boundary Conditions for Direct Simulations of Compressible Viscous Flows, J. Comp. Phys., 101:104–129 (1992).

[50] Rudy, D. H. and Strikwerda, J. C., Boundary Conditions for Subsonic Compressible Navier-Stokes Calculations, J. Comp. Phys., 36:327–338 (1980).

[51] Riley, J. J. and Metcalfe, R. W., Direct Numerical Simulations of a Perturbed, Turbulent Mixing Layer, AIAA paper AIAA-80-0274, 1980.

[52] Sandham, N. D. and Reynolds, W. C., Three-Dimensional Simulations of Large Eddies in the Compressible Mixing Layer, J. Fluid Mech., 224:133–158 (1991).

[53] Moser, R. D. and Rogers, M. M., The Three-Dimensional Evolution of a Plane Mixing Layer: Pairing and Transition to Turbulence, J. Fluid Mech., 247:275–320 (1993).

[54] Metcalfe, R. W., Orszag, S. A., Brachet, M. E., Menon, S., and Riley, J. J., Secondary Instabilities of a Temporally Growing Mixing Layer, J. Fluid Mech., 184:207–243 (1987).

[55] Lin, S. J. and Corcos, G. M., The Mixing Layer: Deterministic Models of a Turbulent Flow. Part 3. The Effect of Plane Strain on the Dynamics of Streamwise Vortices, J. Fluid Mech., 141:139–178 (1984).

[56] Moser, R. D. and Rogers, M. M., The Three-Dimensional Evolution of a Plane Mixing Layer: the Kelvin-Helmholtz Rollup, J. Fluid Mech., 243:183–226 (1992).

[57] Moser, R. D. and Rogers, M. M., Spanwise Scale Selection in Plane Mixing Layers, J. Fluid Mech., 247:321–337 (1993).

[58] Ferziger, J. H., Higher Level Simulations of Turbulent Flows, Stanford University Report TF-16, Department of Mechanical Engineering, Stanford University, Stanford, CA, 1981.

[59] Erlebacher, G., Hussaini, M. Y., Speziale, C. G., and Zang, T. A., Toward the Large Eddy Simulation of Compressible Turbulent Flows, J. Fluid Mech., 238:155–185 (1992).

[60] Rogallo, R. S. and Moin, P., Numerical Simulation of Turbulent Flow, Ann. Rev. Fluid Mech., 16:99–137 (1984).

[61] Deardorff, J. W., On the Magnitude of the Subgrid Scale Eddy Coefficient, J. Comp. Phys., 7:120–133 (1971).

[62] Piomelli, U., Large-Eddy Simulation: Achievements and Challenges, Progress in Aerospace Sciences, 35:335–362 (1999).

[63] Meneveau, C. and Katz, J., Scale-Invariance and Turbulence Models for Large-Eddy Simulations, Ann. Rev. Fluid Mech., 32:1–32 (2000).

[64] Piomelli, U., Cabot, W. H., Moin, P., and Lee, S., Subgrid-Scale Backscatter in Turbulent and Transitional Flows, Phys. Fluids A, 3(7):1766–1771 (1991).

[65] Mason, P. J. and Thomson, D. J., Stochastic Backscatter in Large Eddy Simulation of Boundary Layers, J. Fluid Mech., 242:51–78 (1992).

[66] Carati, D., Ghosal, S., and Moin, P., On the Representation of Backscatter in Dynamic Localizatiobn Models, Phys. Fluids, 7(3):606–616 (1995).

[67] Germano, M., A Statistical Formulation of the Dynamic Model, Phys. Fluids, 8:565–571 (1996).

[68] Deardorff, J. W., A Numerical Study of Three-Dimensional Turbulent Channel Flow at Large Reynolds Number, J. Fluid Mech., 41:453–480 (1970).

[69] Bilger, R. W., Future Progress in Turbulent Combustion Research, Prog. Energy Combust. Sci., 26(4-6):367–380 (2000).

[70] Peters, N., Turbulent Combustion, Cambridge University Press, Cambridge, UK, 2000.

[71] Bell, J. H. and Metha, R. D., Development of a Two-Stream Mixing Layer from Tripped and Untripped Boundary Layer, AIAA J., 28(12):2034–2042 (1990).

[72] Rogers, M. M. and Moser, R. D., Direct Simulation of a Self-Similar Turbulent Mixing Layer, Phys. Fluids, 6(2):903–923 (1994).

[73] Leonard, A. D. and Dai, F., Applications of a Coupled Monte Carlo PDF/Finite Volume, CFD Method for Turbulent Combustion, AIAA Paper AIAA-94-2904, 1994.

	Finite difference variables	Particle solver variables	Particle statistics used by the finite difference solver	Finite difference variables used by particle solver	Redundant quantities
VFDF 1	$\langle u_i \rangle_L$ $\langle p \rangle_L$	X_i U_i	$\tau_L(u_i, u_j)$	$\langle u_i \rangle_L$, $\frac{\partial \langle p \rangle_L}{\partial x_i}$ $\frac{\partial \langle u_i \rangle_L}{\partial x_k}$, $\frac{\partial^2 \langle u_i \rangle_L}{\partial x_k \partial x_k}$	$\langle u_i \rangle_L$
VFDF 2	$\langle u_i \rangle_L$ $\langle p \rangle_L$	X_i U_i	$\tau_L(u_i, u_j)$	$\langle u_i \rangle_L$, $\frac{\partial \langle p \rangle_L}{\partial x_i}$ $\frac{\partial^2 \langle u_i \rangle_L}{\partial x_k \partial x_k}$	$\langle u_i \rangle_L$
LES-FD	$\langle u_i \rangle_L$, $\langle p \rangle_L$ $\tau_L(u_i, u_j)$	X_i U_i	$\tau_L(u_i, u_j, u_k)$	$\langle u_i \rangle_L$, $\frac{\partial \langle p \rangle_L}{\partial x_i}$ $\frac{\partial^2 \langle u_i \rangle_L}{\partial x_k \partial x_k}$	$\langle u_i \rangle_L$ $\tau_L(u_i, u_j)$

Table 1: Recapitulation of the VFDF solution procedures.

	Resolution	N_E	Normalized CPU time
DNS	$193 \times 193 \times 193$	-	178
VFDF1	$33 \times 33 \times 33$	40	33.6
VFDF2	$33 \times 33 \times 33$	40	30
Dynamic Smagorinsky	$33 \times 33 \times 33$	-	2.19
Smagorinsky	$33 \times 33 \times 33$	-	1.05
No model	$33 \times 33 \times 33$	-	1

Table 2: Computer requirements for the 3D temporal mixing layer. 1 unit corresponds to 1657.2 seconds of CPU time on the SGI Origin 2000.

FIGURE CAPTIONS

Figure 1. Plot of the vorticity field contours, (a) VFDF2, (b) LES-FD. $\Delta_E = \Delta$, $N_E = 40$.

Figure 2. Scatter plots of the filtered velocity field as obtained via VFDF2 vs. LES-FD. (a), $\langle u \rangle_L$; (b), $\langle v \rangle_L$. $\Delta_E = \Delta$, $N_E = 40$.

Figure 3. Reynolds averaged values of the filtered streamwise velocity. (a) Cross-stream variations at $x = 7$, (b) streamwise variation at $y = 0$ (center-line). $N_E = 40$.

Figure 4. Cross-stream variations of the Reynolds averaged values of some of the components of the SGS stress tensor at $x = 7$ with $N_E = 40$. The LES-FD results are obtained with $\Delta_E = 0.5\Delta$, $N_E = 40$.

Figure 5. Percentage of the relative difference between the L_2 norms of the stresses as a function of $\frac{\Delta_E}{\Delta}$. (a) $x = 2.8$, (b) $x = 7$, (c) $x = 11.2$.

Figure 6. Cross-stream variations of the Reynolds averaged values of the filtered streamwise velocity at $x = 7$. The LES-FD results are obtained with $\Delta_E = 0.5\Delta$, $N_E = 40$.

Figure 7. Cross-stream variations of the Reynolds averaged values of some of the components of the SGS stress tensor at $x = 7$. The LES-FD results are obtained with $\Delta_E = 0.5\Delta$, $N_E = 40$.

Figure 8. Particle number density in VFDF2 simulation at $t = 60$. The iso-surface corresponds to $N_E = 40$ set as initial conditions. $C_0 = 2.1, C_\varepsilon = 1$.

Figure 9. Time variation of the model coefficients as obtained from a priori analysis of the DNS data.

Figure 10. Contour plots of the spanwise component of the vorticity at $z = 0.75L/L_r$, $t = 80$. (a) filtered DNS, (b) no model, (c), Smagorinsky model, (d) dynamic Smagorinsky model, (e) VFDF2, $C_0 = 2.1$, $C_\varepsilon = 1$, (f) VFDF1, $C_0 = 2.1$, $C_\varepsilon = 1$.

Figure 11. Contour plots of the streamwise component of the vorticity vector at $x = 0.25L/L_r$, $t = 80$. (a) filtered DNS, (b) no model, (c) Smagorinsky model, (d) dynamic Smagorinsky model, (e) VFDF2, $C_0 = 2.1$, $C_\varepsilon = 1$, (f) VFDF1, $C_0 = 2.1$, $C_\varepsilon = 1$.

Figure 12. Cross-stream variations of the Reynolds averaged values of the streamwise velocity at $t = 70$.

Figure 13. Temporal variations of the momentum thickness.

Figure 14. Temporal variations of (a) total resolved kinetic energy, (b) SGS kinetic energy production rate, (c) total backscatter, (d) total resolved dissipation.

Figure 15. Cross stream variations of some of the components of $\overline{a_{ij}}$ at $t = 60$.

Figure 16. Cross-stream variations of some of the components of $\overline{a_{ij}}$ at $t = 80$.

Figure 17. Cross-stream variations of some of the components of $\overline{R_{ij}}$ at $t = 60$.

Figure 18. Cross-stream variations of some of the components of $\overline{R_{ij}}$ at $t = 80$.

Figure 19. Cross stream variations of $\overline{r_{12}}$, (a) $t = 60$, (b) $t = 80$.

Figure 20. Cross stream variation of the Reynolds averaged values of the streamwise velocity at $t = 250$. Solid line denotes model predictions via the dynamic Smagorinsky model. Symbols denote experimental data of Bell and Mehta.[71]

Figure 21. Cross stream variations of the Reynolds averaged values of the streamwise velocity at $t = 250$. Solid lines denote model predictions via the dynamic Smagorinsky model. Symbols denote experimental data of Bell and Mehta.[71]

FIGURES

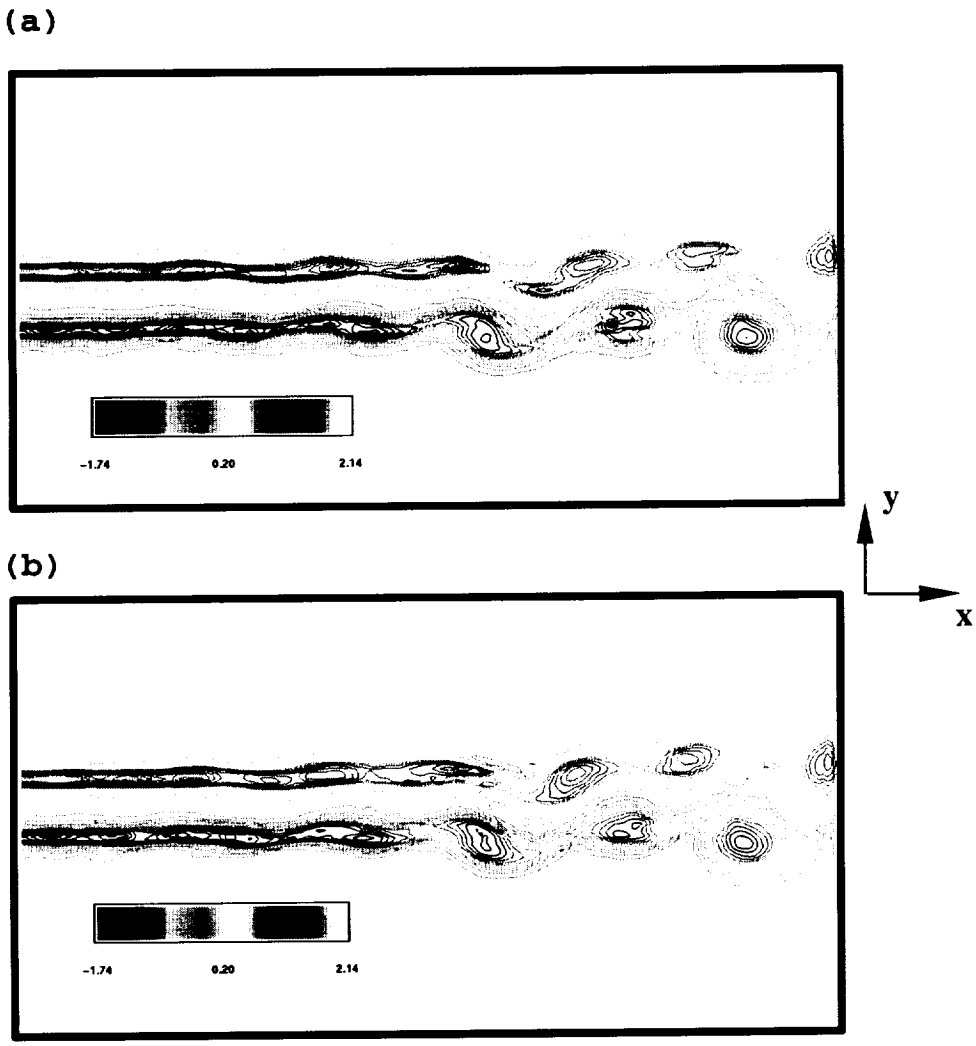

Figure 1: Plot of the vorticity field contours, (a) VFDF2, (b) LES-FD. $\Delta_E = \Delta$, $N_E = 40$. (Gicquel et al., Physics of Fluids.)

(a)

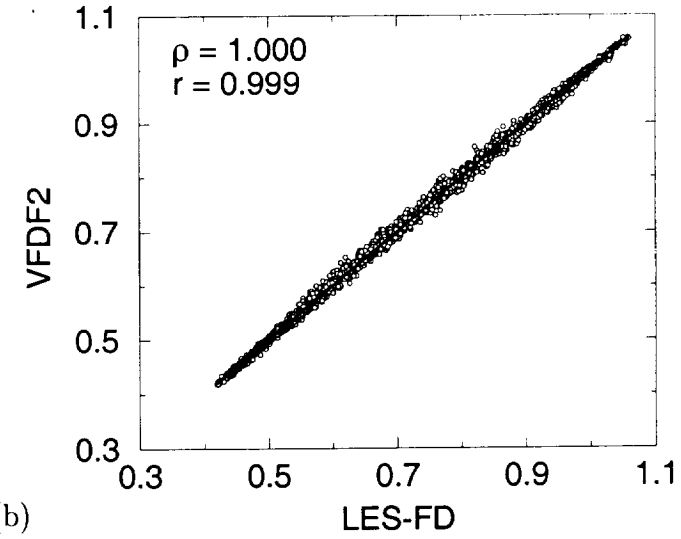

(b)

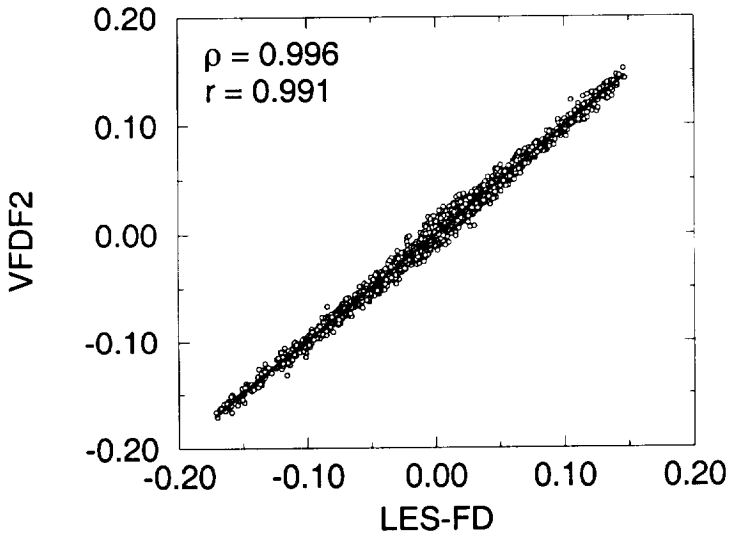

Figure 2: Scatter plots of the filtered velocity field as obtained via VFDF2 vs. LES-FD. (a), $\langle u \rangle_L$; (b), $\langle v \rangle_L$. $\Delta_E = \Delta$, $N_E = 40$. (Gicquel et al., Physics of Fluids.)

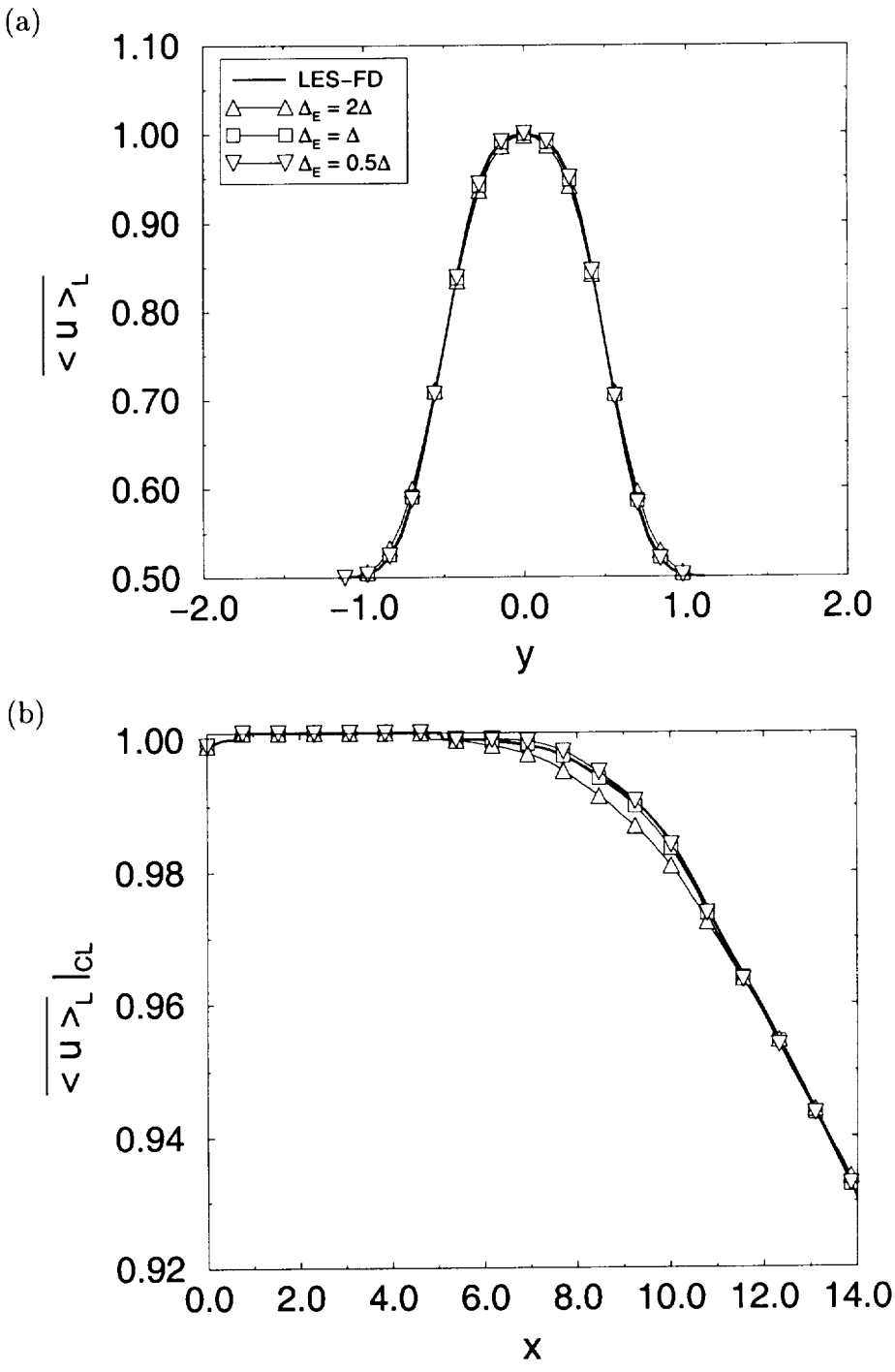

Figure 3: Reynolds averaged values of the filtered streamwise velocity. (a) Cross-stream variations at $x = 7$, (b) streamwise variation at $y = 0$ (center-line). $N_E = 40$. (Gicquel et al., Physics of Fluids.)

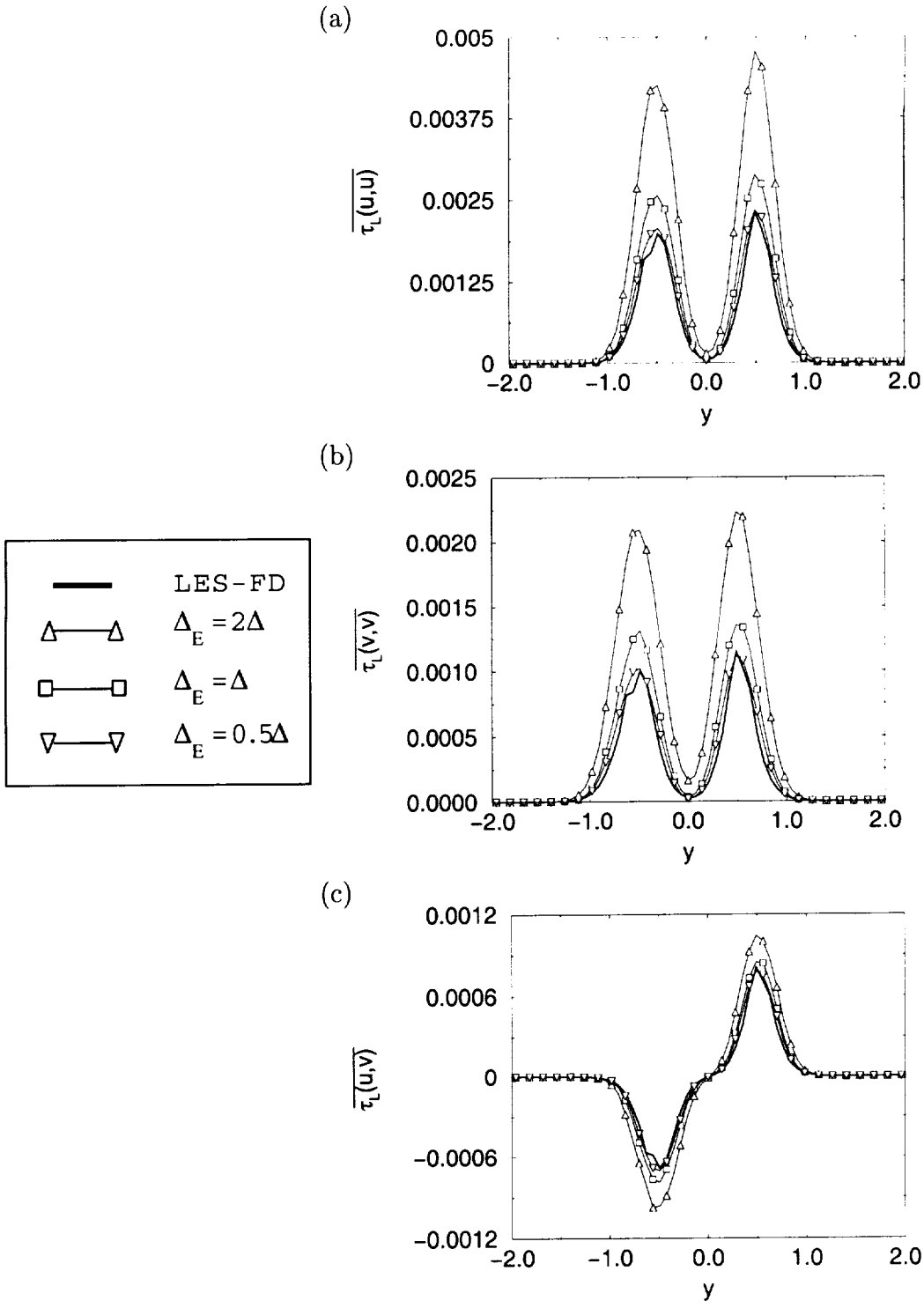

Figure 4: Cross-stream variations of the Reynolds averaged values of some of the components of the SGS stress tensor at $x = 7$ with $N_E = 40$. The LES-FD results are obtained with $\Delta_E = 0.5\Delta$, $N_E = 40$. (Gicquel et al., Physics of Fluids.)

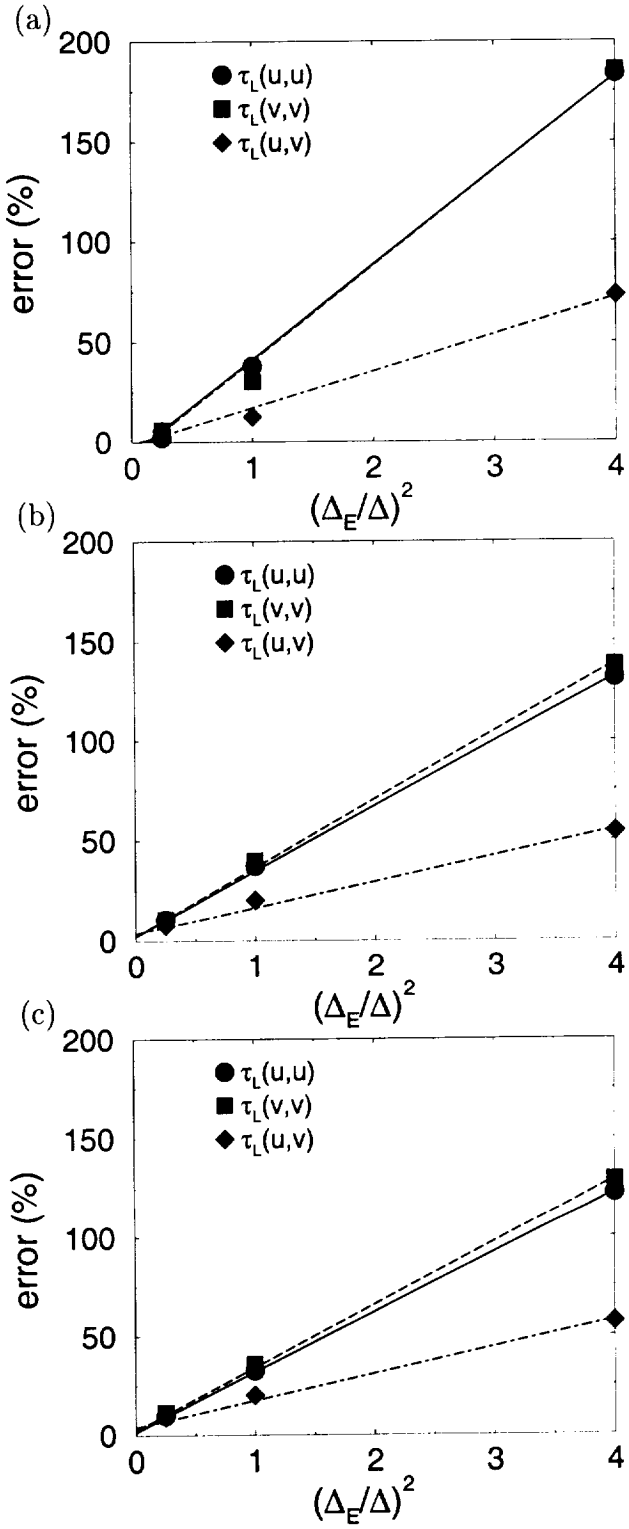

Figure 5: Percentage of the relative difference between the L_2 norms of the stresses a function of $\frac{\Delta_E}{\Delta}$. (a) $x = 2.8$, (b) $x = 7$, (c) $x = 11.2$. (Gicquel et al., Physics of Fluids.)

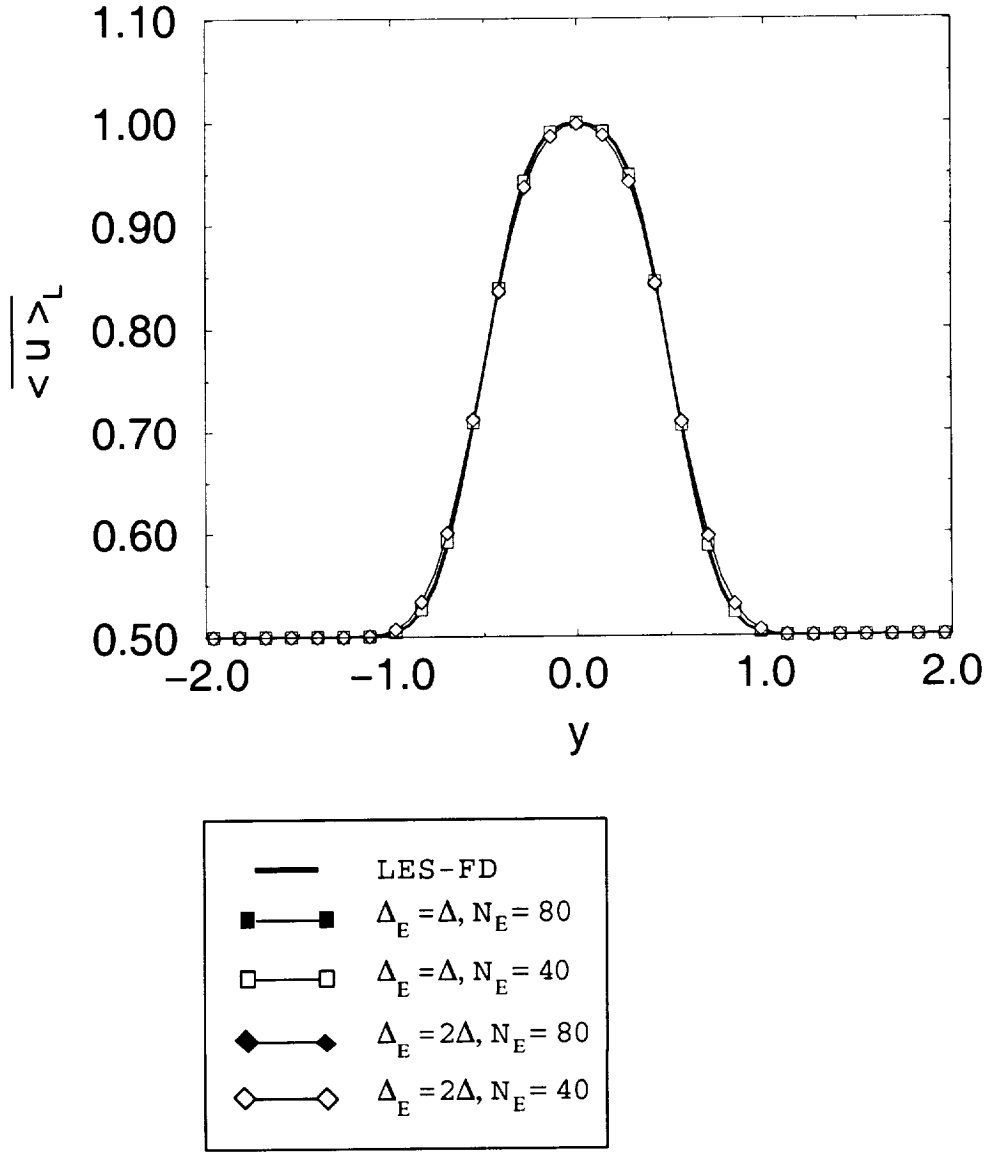

Figure 6: Cross-stream variations of the Reynolds averaged values of the filtered streamwise velocity at $x = 7$. The LES-FD results are obtained with $\Delta_E = 0.5\Delta$, $N_E = 40$.

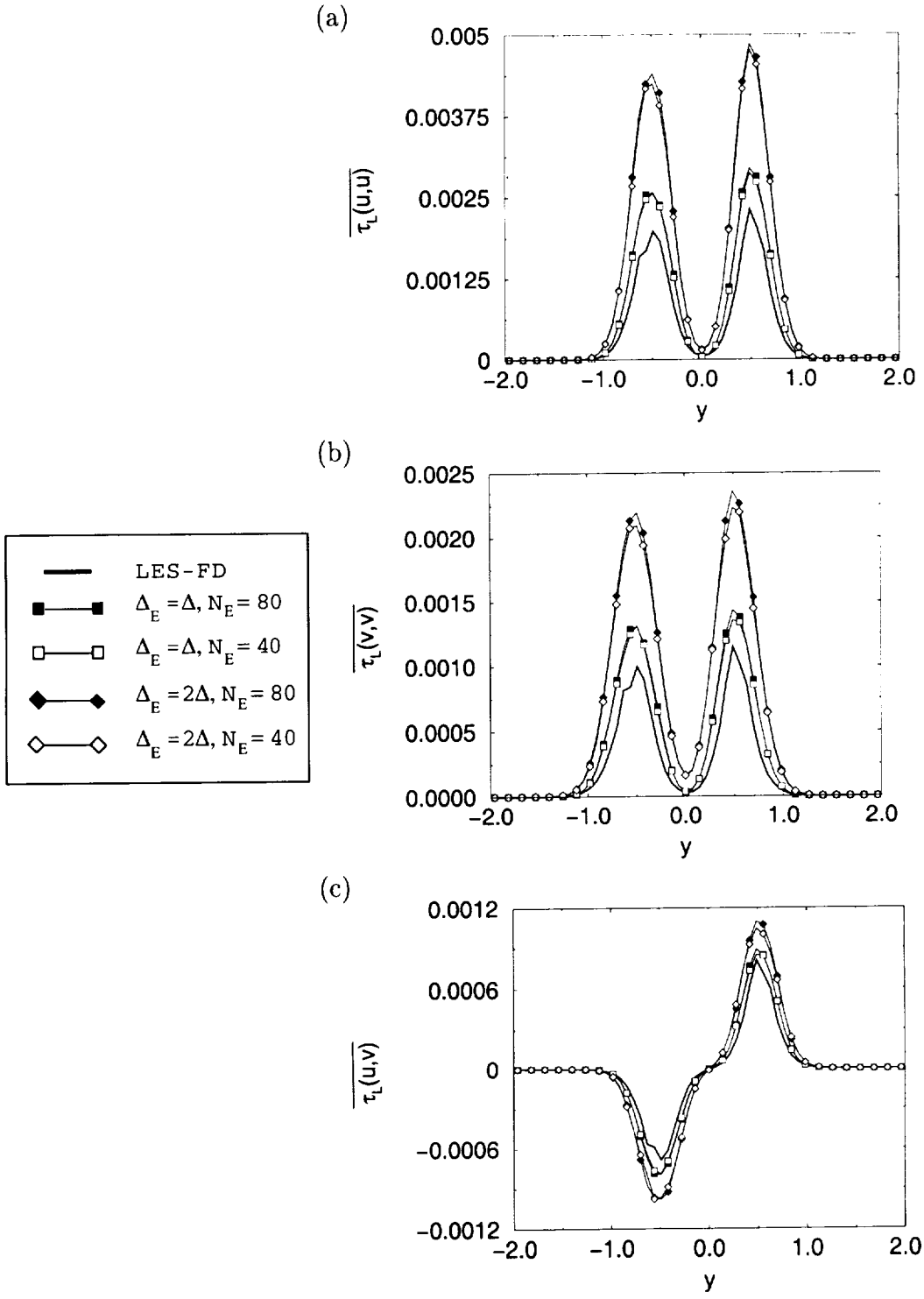

Figure 7: Cross-stream variations of the Reynolds averaged values of some of the components of the SGS stress tensor at $x = 7$. The LES-FD results are obtained with $\Delta_E = 0.5\Delta$, $N_E = 40$. (Gicquel et al., Physics of Fluids.)

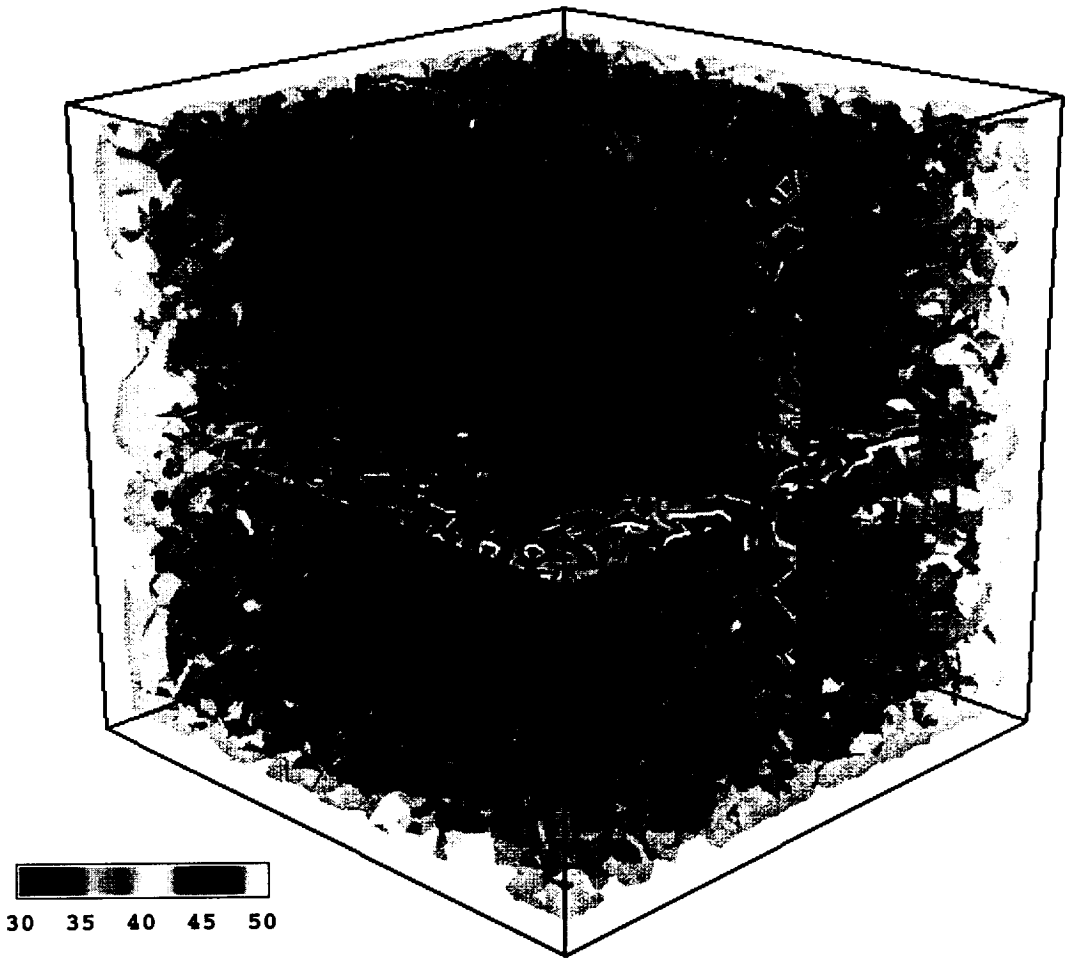

Figure 8: Particle number density in VFDF2 simulation at $t = 60$. The iso-surface corresponds to $N_E = 40$ set as initial conditions. $C_0 = 2.1, C_\varepsilon = 1$. (Gicquel et al., Physics of Fluids.)

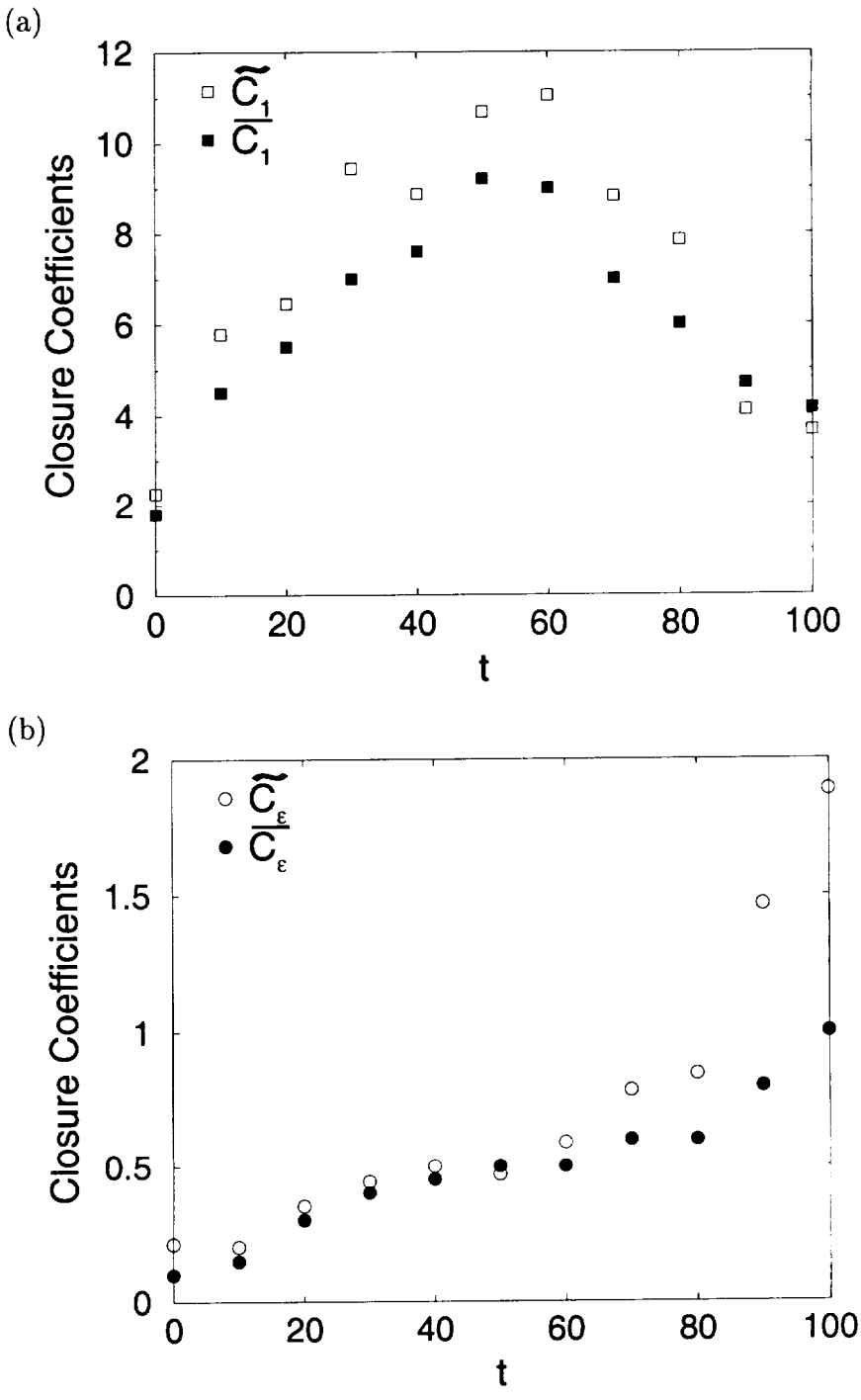

Figure 9: Time variation of the model coefficients as obtained from a priori analysis of the DNS data. (Gicquel et al., Physics of Fluids.)

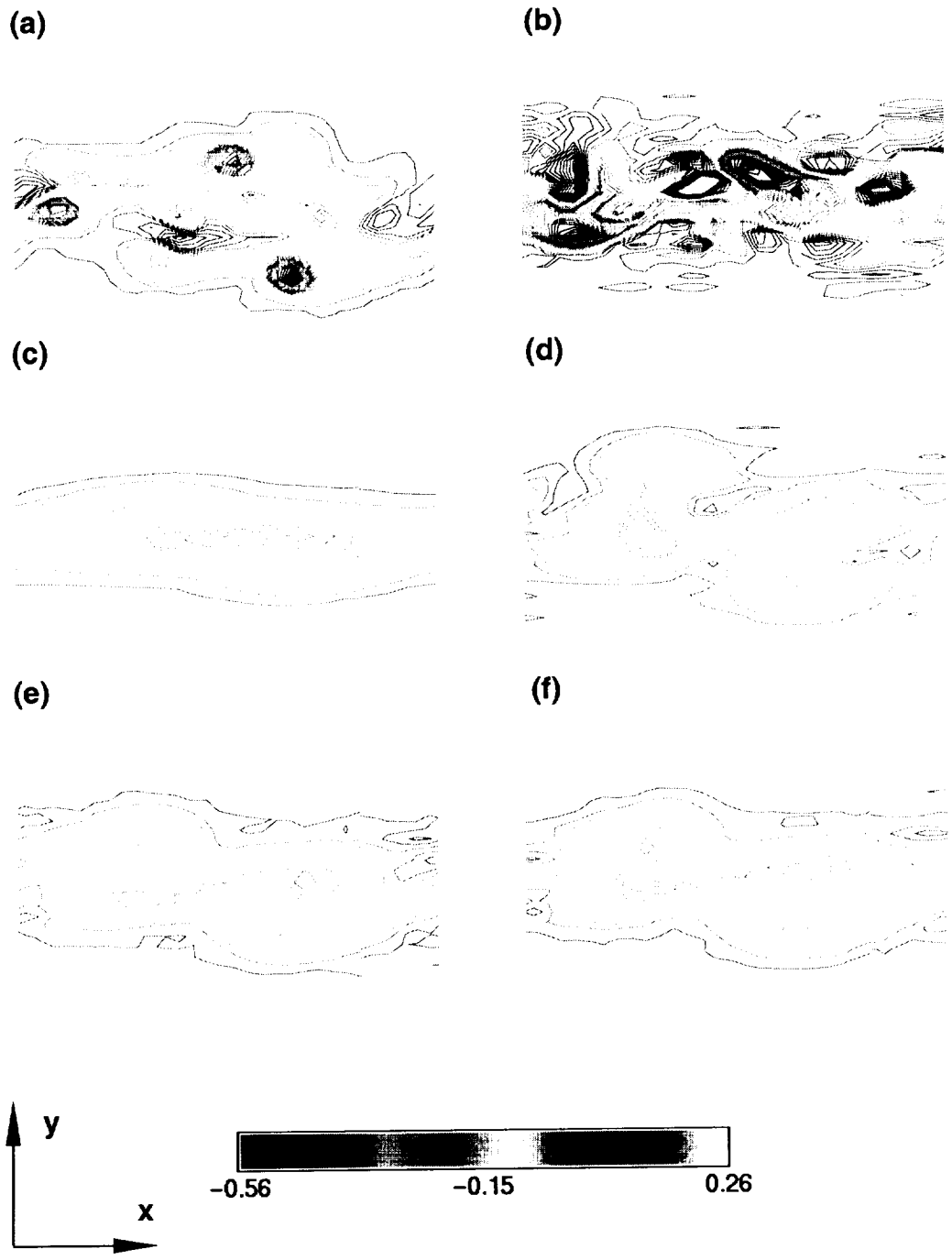

Figure 10: Contour plots of the spanwise component of the vorticity at $z = 0.75L/L_\tau$, $t = 80$. (a) filtered DNS, (b) no model, (c), Smagorinsky model, (d) dynamic Smagorinsky model, (e) VFDF2, $C_0 = 2.1$, $C_\varepsilon = 1$, (f) VFDF1, $C_0 = 2.1$, $C_\varepsilon = 1$. (Gicquel et al., Physics of Fluids.)

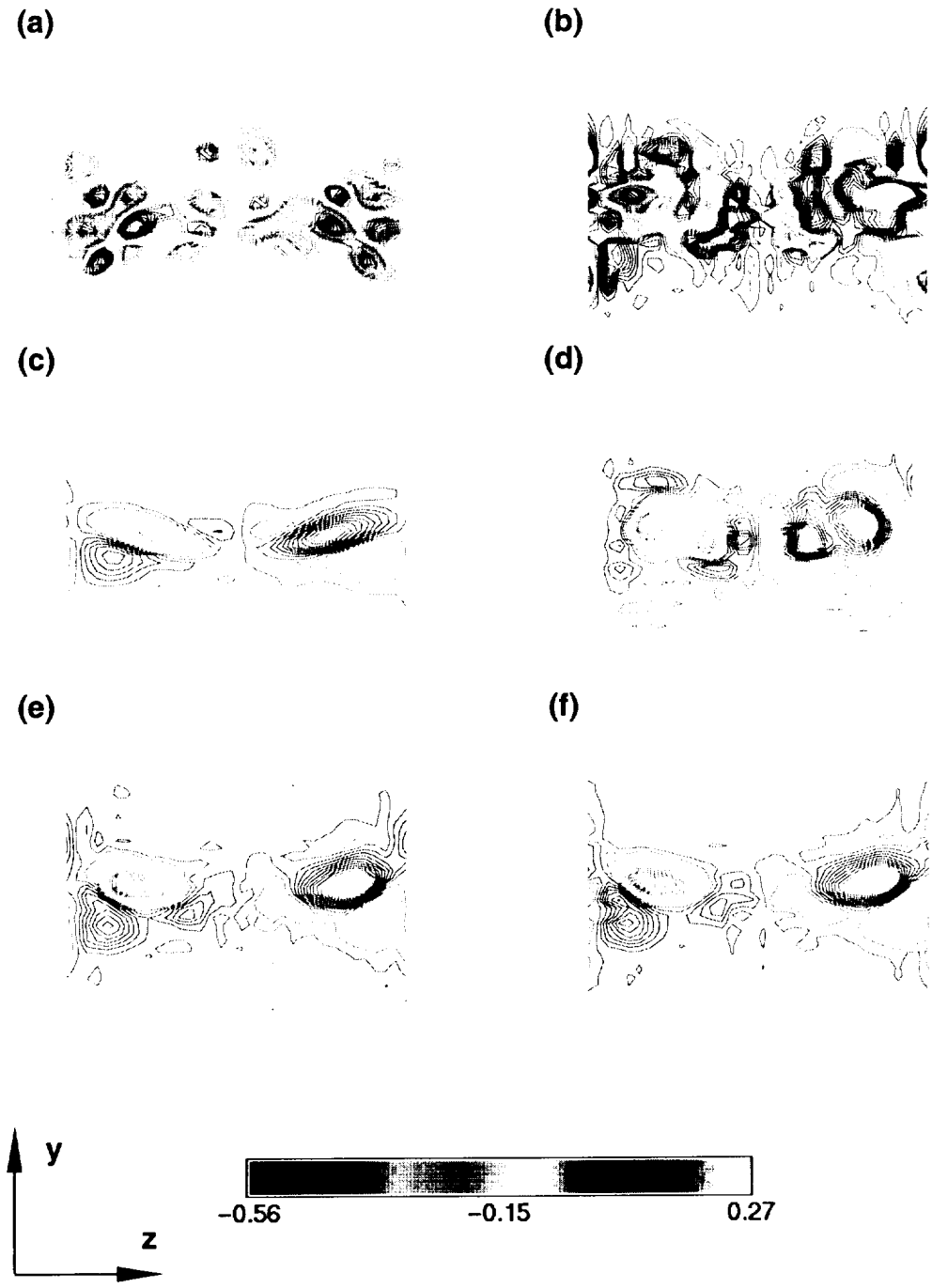

Figure 11: Contour plots of the streamwise component of the vorticity vector at $x = 0.25L/L_r$, $t = 80$. (a) filtered DNS, (b) no model, (c) Smagorinsky model, (d) dynamic Smagorinsky model, (e) VFDF2, $C_0 = 2.1$, $C_\epsilon = 1$, (f) VFDF1, $C_0 = 2.1$, $C_\epsilon = 1$. (Gicquel et al., Physics of Fluids.)

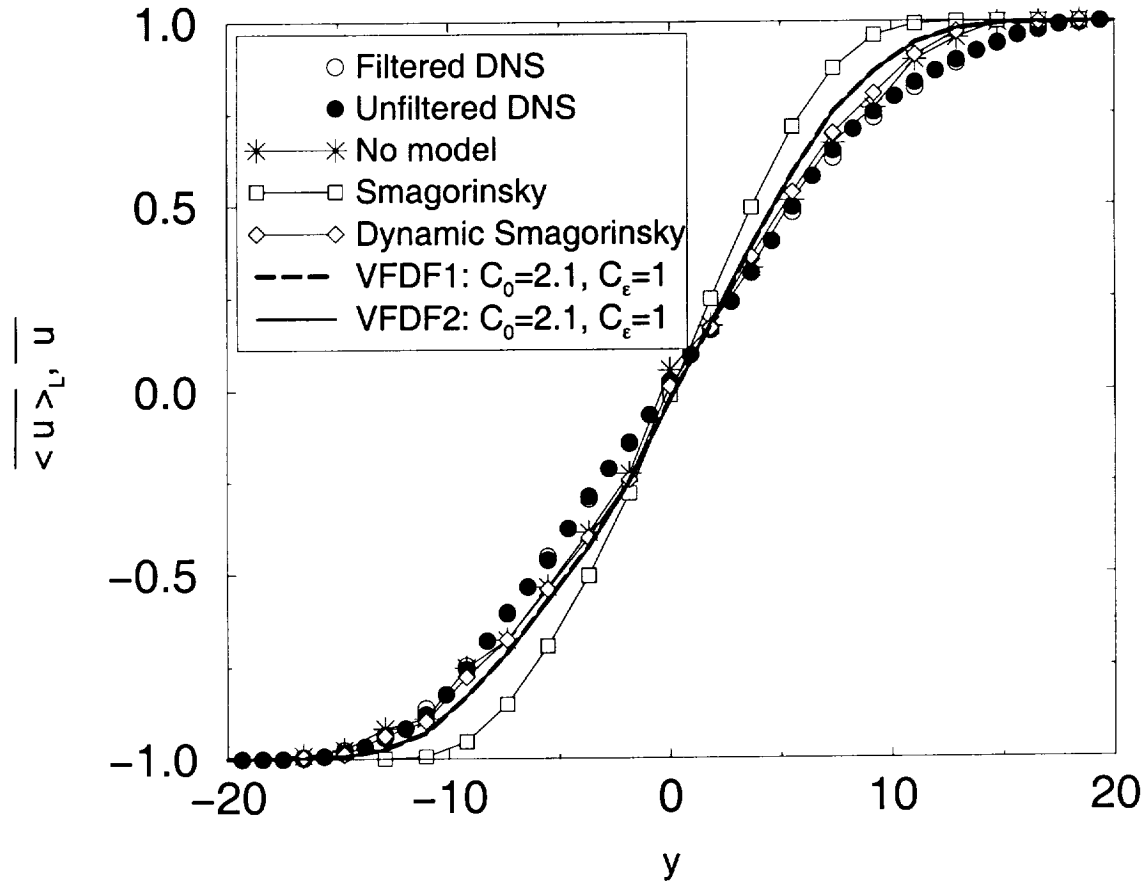

Figure 12: Cross-stream variations of the Reynolds averaged values of the streamwise velocity at $t = 70$. (Gicquel et al., Physics of Fluids.)

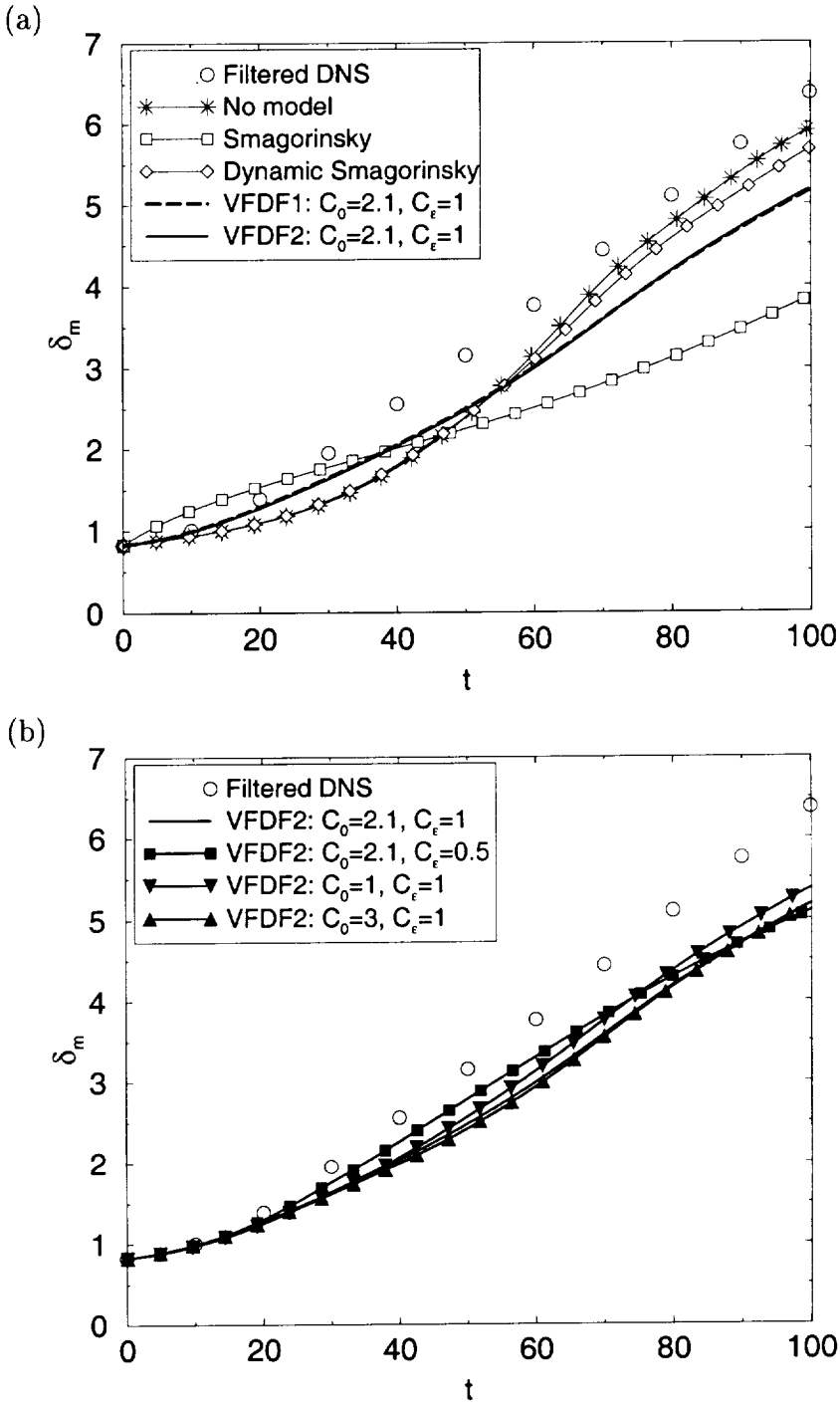

Figure 13: Temporal variations of the momentum thickness. (Gicquel et al., Physics of Fluids.)

(a)

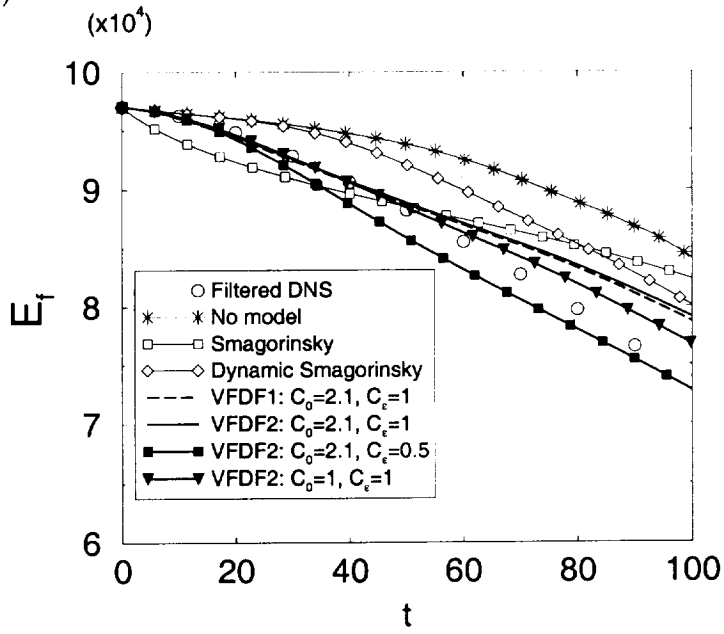
(x10^4)
10
9
8
7
6
E_T
0
20
40
60
80
100
t
Filtered DNS
No model
Smagorinsky
Dynamic Smagorinsky
VFDF1: C_0=2.1, C_ε=1
VFDF2: C_0=2.1, C_ε=1
VFDF2: C_0=2.1, C_ε=0.5
VFDF2: C_0=1, C_ε=1

(b)

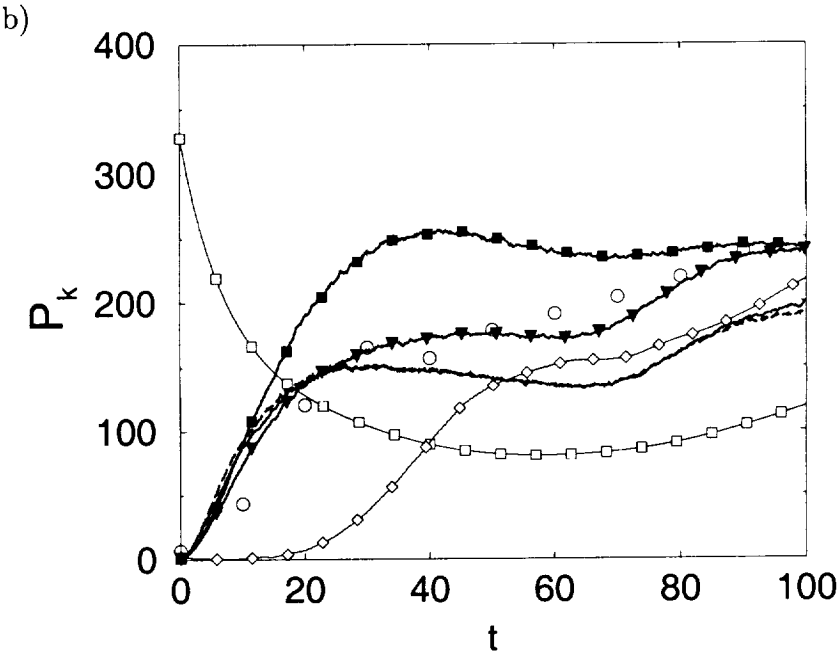
400
300
200
100
0
P_k
0
20
40
60
80
100
t

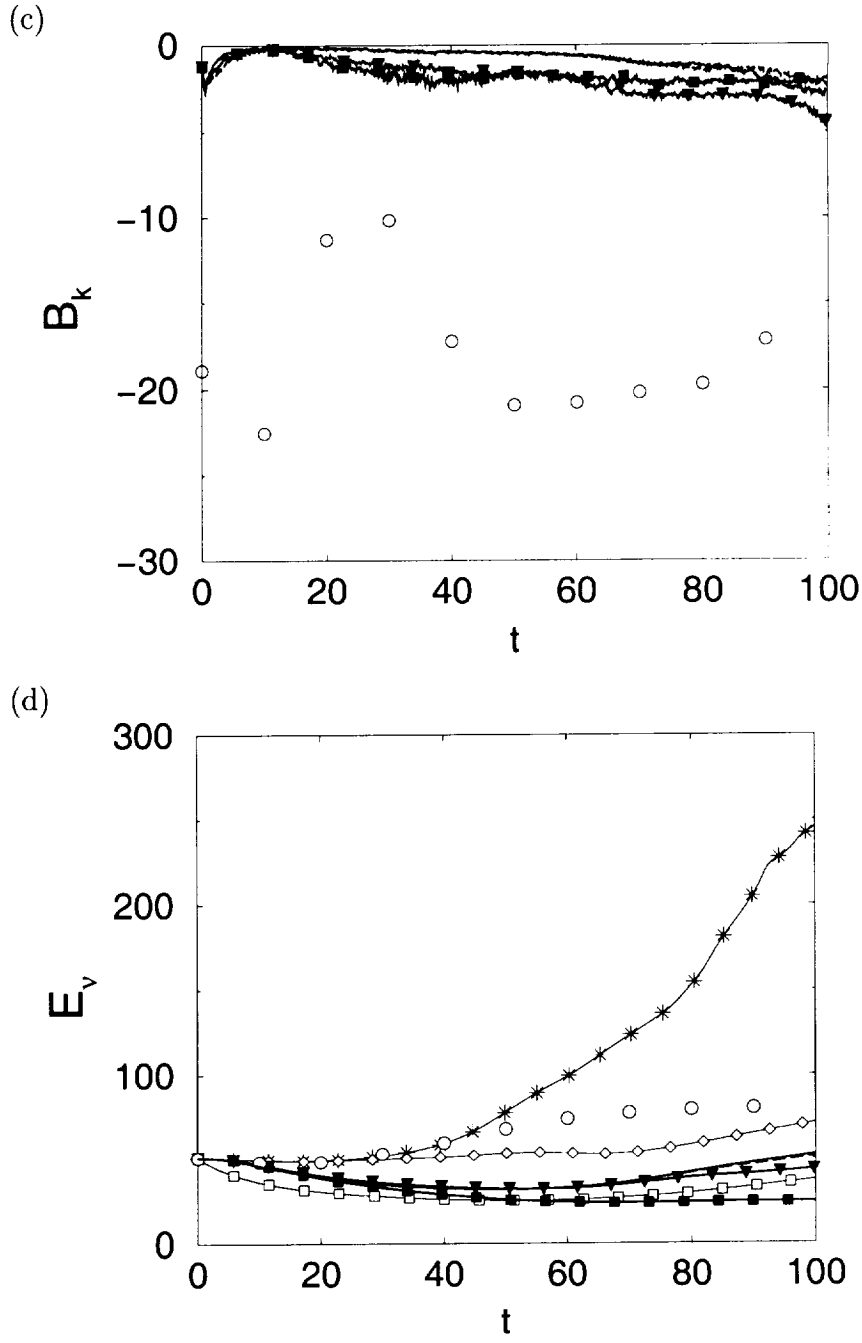

Figure 14: Temporal variations of (a) total resolved kinetic energy, (b) production rate of the SGS kinetic energy, (c) total backscatter, (d) total resolved dissipation. (Gicquel et al., Physics of Fluids.)

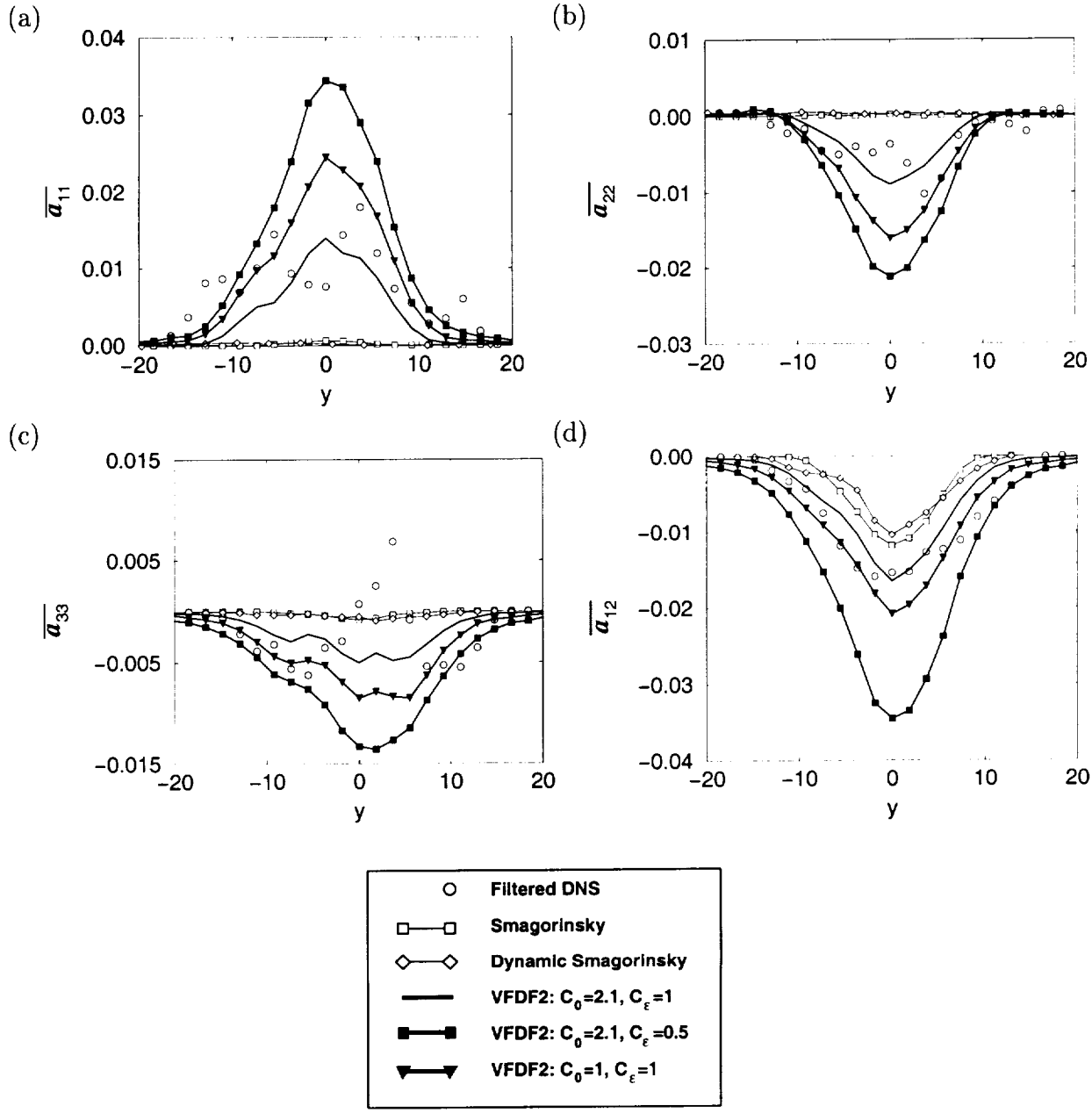

Figure 15: Cross stream variations of some of the components of $\overline{a_{ij}}$ at $t = 60$. (Gicquel et al., Physics of Fluids.)

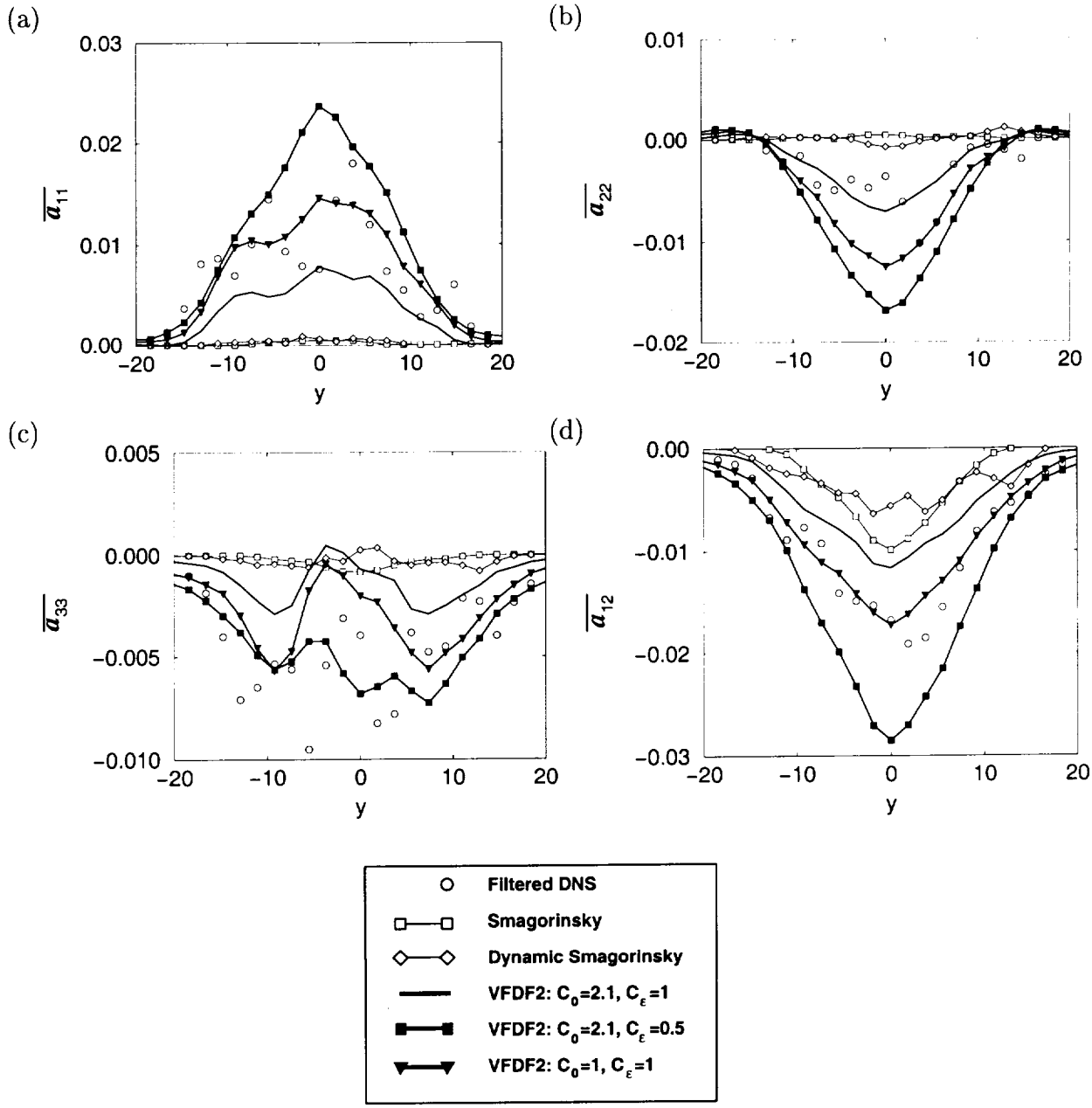

Figure 16: Cross-stream variations of some of the components of $\overline{a_{ij}}$ at $t = 80$. (Gicquel et al., Physics of Fluids.)

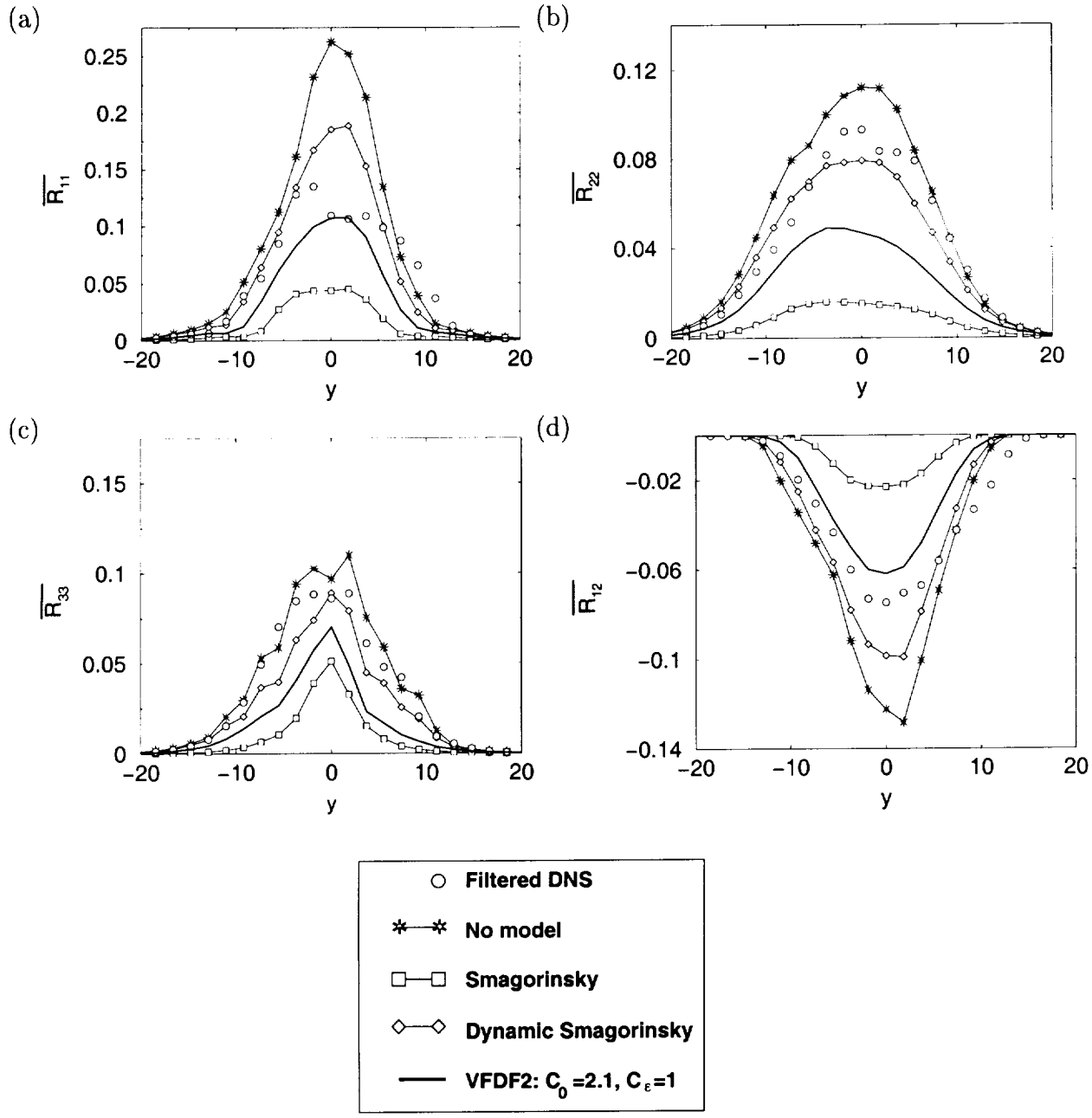

Figure 17: Cross-stream variations of some of the components of $\overline{R_{ij}}$ at $t = 60$. (Gicquel et al., Physics of Fluids.)

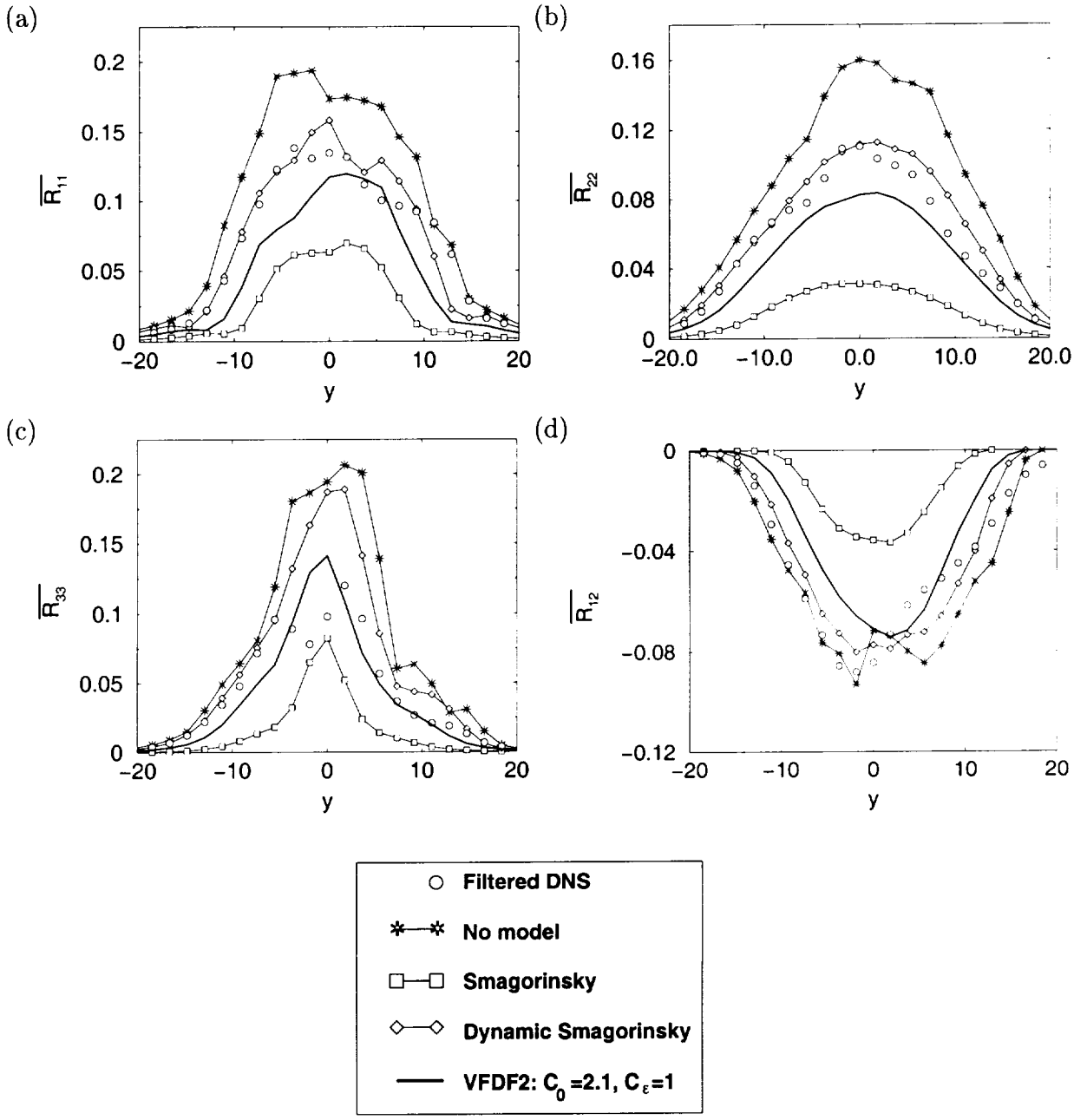

Figure 18: Cross-stream variations of some of the components of $\overline{R_{ij}}$ at $t = 80$. (Gicquel et al., Physics of Fluids.)

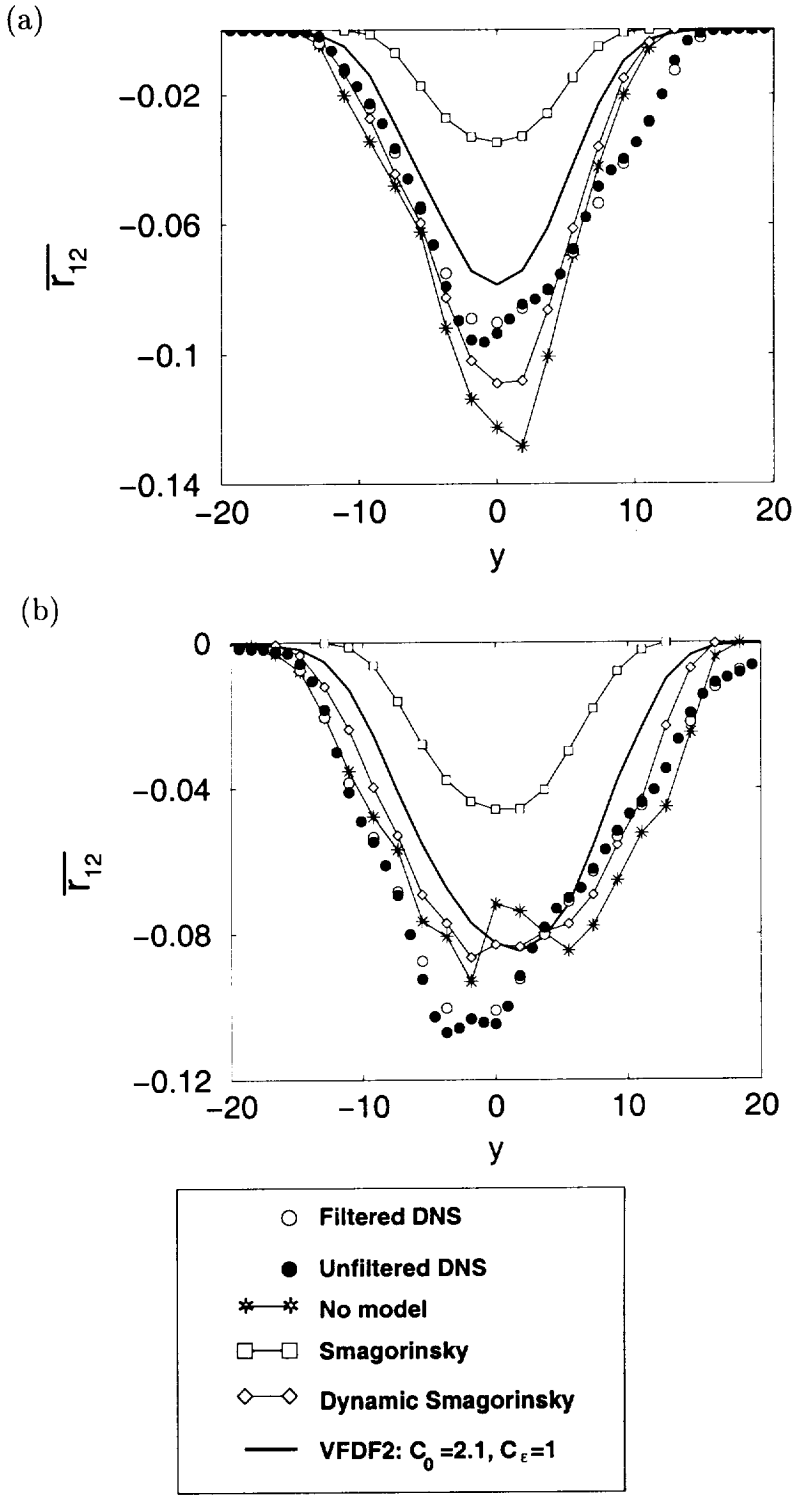

Figure 19: Cross-stream variations of $\overline{r_{12}}$. (a) $t = 60$, (b) $t = 80$. (Gicquel et al., Physics of Fluids.)

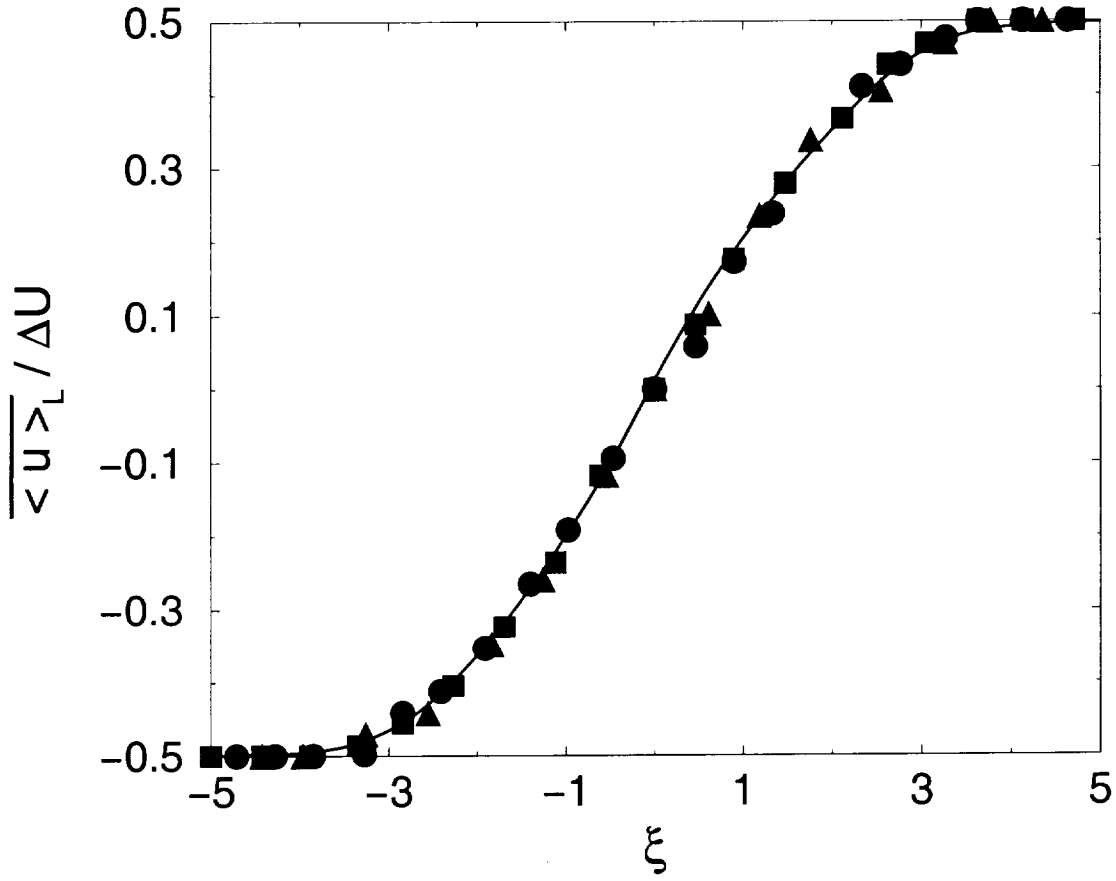

Figure 20: Cross stream variation of the Reynolds averaged values of the streamwise velocity at $t = 250$. Solid line denotes model predictions via the dynamic Smagorinsky model. Symbols denote experimental data of Bell and Mehta.[71] (Gicquel et al., Physics of Fluids.)

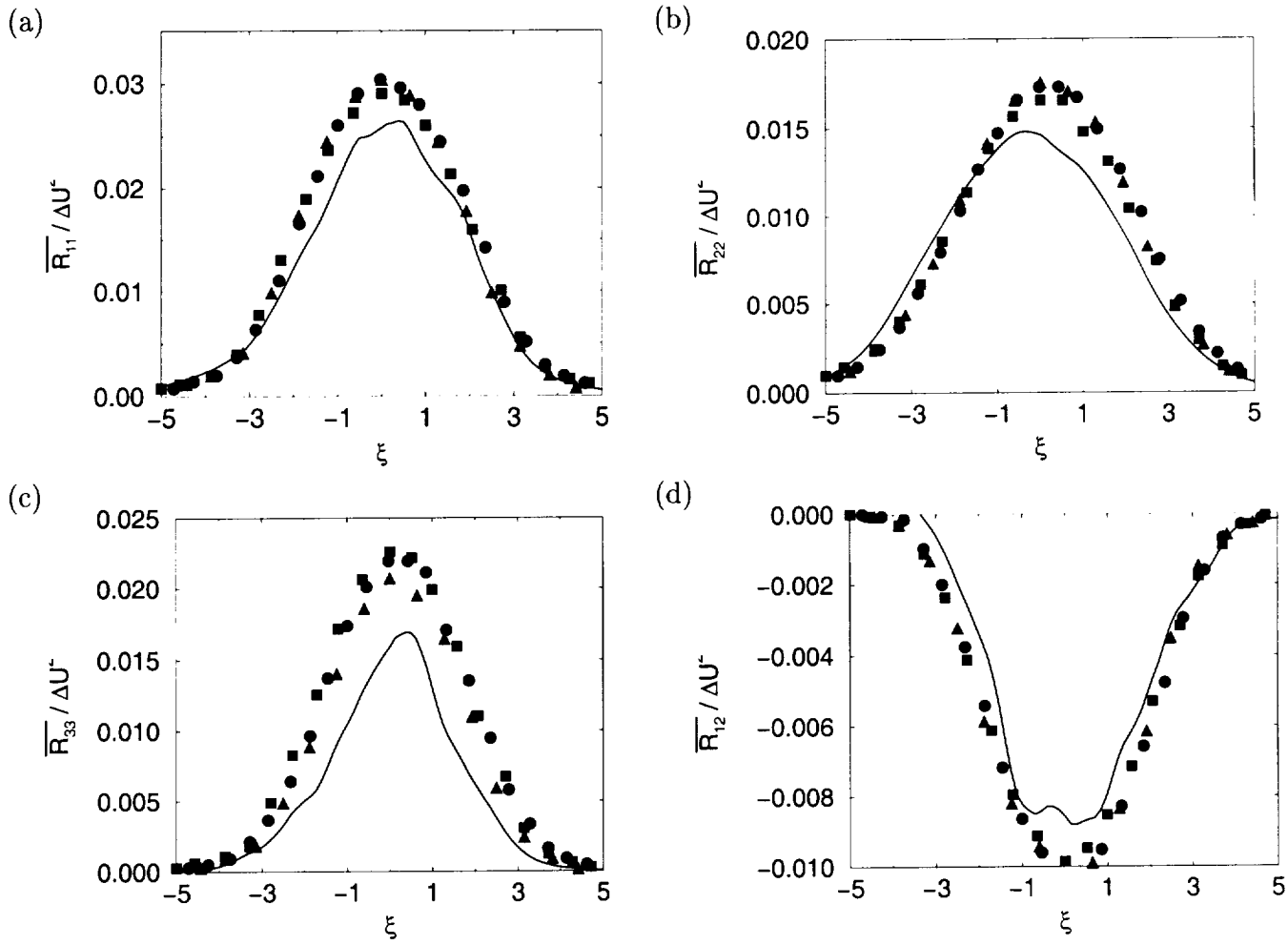

Figure 21: Cross stream variation of the resolved Reynolds stresses at $t = 250$. Solid lines denote model predictions via the dynamic Smagorinsky model. Symbols denote experimental data of Bell and Mehta.[71] (Gicquel et al., Physics of Fluids.)

Appendix II

This Appendix is submitted for publication.

Velocity-Scalar Filtered Density Function for Large Eddy Simulation of Turbulent Flows

M.R.H. Sheikhi, T.G. Drozda, and P. Givi*

Department of Mechanical and Aerospace Engineering

University at Buffalo, SUNY

Buffalo, NY 14260-4400

S.B. Pope

Sibley School of Mechanical and Aerospace Engineering

Cornell University

Ithaca, NY 14853-1301

(Dated: August 5, 2002)

Abstract

A methodology termed the "velocity-scalar filtered density function" (VSFDF) is developed and implemented for large eddy simulation (LES) of turbulent flows. In this methodology, the effects of the unresolved subgrid scales (SGS) are taken into account by considering the joint probability density function (PDF) of the velocity-scalar field. An exact transport equation is derived for the VSFDF in which the effects of the SGS convection and chemical reaction are closed. The unclosed terms in this equation are modeled. A system of stochastic differential equations (SDEs) which yields statistically equivalent results to the modeled VSFDF transport equation is constructed. These SDEs are solved numerically by a Lagrangian Monte Carlo procedure in which the Itô-Gikhman character of the SDEs is preserved. The consistency of the proposed SDEs and the convergence of the Monte Carlo solution are assessed by comparison with results obtained by a finite difference LES procedure in which the corresponding transport equations for the first two SGS moments are solved. The VSFDF results are compared with those obtained via other SGS closures, and all the results are assessed via comparison with data obtained by direct numerical simulation (DNS) of a temporally developing mixing layer involving transport of a passive scalar. It is shown that the values of both the SGS and the resolved components of all second order moments including the scalar fluxes are predicted well by VSFDF. The sensitivity of the model's (empirical) constants are assessed and it is shown that the magnitudes of these constants are in the same range as that typically employed in PDF methods.

Corresponding Author: Peyman Givi, Tel: (716) 645-2593 (x. 2320). Fax: 716-645-3875. E-mail: givi eng.buffalo.edu.

Keywords: large eddy simulation, filtered density function, probability density function, turbulent combustion, Monte Carlo simulation.

*Electronic address: **givi@eng.buffalo.edu**

I. INTRODUCTION

The probability density function (PDF) approach has proven useful for large eddy simulation (LES) of turbulent reacting flows [1]. The formal means of conducting such LES is by consideration of the "filtered density function" (FDF) [2] which is essentially the filtered fine-grained PDF of the transport quantities. In all previous contributions, the "marginal" FDF of the scalars [3–15], or the marginal FDF of the velocity vector [16] are considered; see Givi [17] for a recent review.

The objective of the present work is to extend the FDF methodology to account for the "joint" subgrid scale (SGS) velocity-scalar field. This is facilitated by consideration of the joint "velocity-scalar filtered density function" (VSFDF). With the definition of the VSFDF, the mathematical framework for its implementation in LES is established. A transport equation is developed for the VSFDF in which the effects of SGS convection and SGS chemical reaction (in a reacting flow) are closed. The unclosed terms in this equation are modeled in a fashion similar to those in the Reynolds-averaged simulation (RAS) procedures. A Lagrangian Monte Carlo procedure is developed and implemented for numerical simulation of the modeled VSFDF transport equation. The consistency of this procedure is assessed by comparing the first two moments of the VSFDF with those obtained by the Eulerian finite difference solutions of the same moments' transport equations. The results of the VSFDF simulations are compared with those predicted by the Smagorinsky [18] closure. All the results are assessed via comparisons with direct numerical simulation (DNS) data of a three-dimensional (3D) temporally developing mixing layer involving transport of a passive scalar variable.

II. FORMULATION

For the general formulation, we consider an incompressible (unit density), isothermal, turbulent reacting flow involving N_s species. The primary transport variables describing such a flow are the three components of the velocity vector $u_i(\mathbf{x},t)$ $(i=1,2,3)$, the pressure $p(\mathbf{x},t)$, and the species' mass fractions $\phi_\alpha(\mathbf{x},t)$ $(\alpha=1,2,\ldots,N_s)$. The equations which

govern the transport of these variables in space (x_i) and time (t) are

$$\frac{\partial u_k}{\partial x_k} = 0 \tag{1a}$$

$$\frac{\partial u_i}{\partial t} + \frac{\partial u_k u_i}{\partial x_k} = -\frac{\partial p}{\partial x_i} + \frac{\partial \sigma_{ik}}{\partial x_k} \tag{1b}$$

$$\frac{\partial \phi_\alpha}{\partial t} + \frac{\partial u_k \phi_\alpha}{\partial x_k} = -\frac{\partial J_k^\alpha}{\partial x_k} + S_\alpha \tag{1c}$$

where $S_\alpha \equiv \hat{S}_\alpha(\boldsymbol{\phi}(\mathbf{x}, t))$ denotes the chemical reaction term for species α, and $\boldsymbol{\phi} \equiv [\phi_1, \phi_2, \ldots, \phi_{N_s}]$ denotes the scalar variable array. For an incompressible, Newtonian fluid, with Fick's law of diffusion, the viscous stress tensor σ_{ik} and the scalar flux J_k^α are represented by

$$\sigma_{ik} = \nu \left(\frac{\partial u_i}{\partial x_k} + \frac{\partial u_k}{\partial x_i} \right) \tag{2a}$$

$$J_k^\alpha = -\Gamma \frac{\partial \phi_\alpha}{\partial x_k} \tag{2b}$$

where ν is the fluid kinematic viscosity and $\Gamma = \frac{\nu}{Sc}$ is the diffusion coefficient of all species with Sc denoting the molecular Schmidt number. We assume a constant value for $\nu = \Gamma$; that is $Sc = 1$. In reactive flows, molecular processes are much more complicated than portrayed by Eq. (2). Since the molecular diffusion is typically less important than that of SGS, this simple model is adopted with justifications and caveats given by in Refs. [19–21].

Large-eddy simulation involves the spatial filtering operation [22–25]

$$\langle f(x,t) \rangle = \int_{-\infty}^{+\infty} f(x',t) \mathcal{G}(x',x) dx' \tag{3}$$

where $\mathcal{G}(x',x)$ denotes a filter function, and $\langle f(x,t) \rangle$ is the filtered value of the transport variable $f(x,t)$. We will consider a filter function that is spatially and temporally invariant and localized, thus: $\mathcal{G}(x',x) \equiv G(x'-x)$ with the properties $G(x) \geq 0$, $\int_{-\infty}^{+\infty} G(x)dx 1$, and moments $\int_{-\infty}^{+\infty} x^m G(x)dx$ exist for $m > 0$. Applying the filtering operation to Eqs. (1) yields

$$\frac{\partial \langle u_k \rangle}{\partial x_k} = 0 \tag{4a}$$

$$\frac{\partial \langle u_i \rangle}{\partial t} + \frac{\partial \langle u_k \rangle \langle u_i \rangle}{\partial x_k} = -\frac{\partial \langle p \rangle}{\partial x_i} + \nu \frac{\partial^2 \langle u_i \rangle}{\partial x_k \partial x_k} - \frac{\partial \tau(u_k, u_i)}{\partial x_k} \tag{4b}$$

$$\frac{\partial \langle \phi_\alpha \rangle}{\partial t} + \frac{\partial \langle u_k \rangle \langle \phi_\alpha \rangle}{\partial x_k} = \nu \frac{\partial^2 \langle \phi_\alpha \rangle}{\partial x_k \partial x_k} - \frac{\partial \tau(u_k, \phi_\alpha)}{\partial x_k} + \langle S_\alpha \rangle \tag{4c}$$

where the second-order SGS correlations

$$\tau(a,b) \;=\; \langle ab\rangle - \langle a\rangle\,\langle b\rangle \tag{5}$$

are governed by

$$\frac{\partial\tau(u_i,u_j)}{\partial t} + \frac{\partial\,\langle u_k\rangle\,\tau(u_i,u_j)}{\partial x_k} = \Gamma\frac{\partial^2\tau(u_i,u_j)}{\partial x_k\partial x_k} - \tau(u_k,u_i)\frac{\partial\,\langle u_j\rangle}{\partial x_k} - \tau(u_k,u_j)\frac{\partial\,\langle u_i\rangle}{\partial x_k} - \left[2\Gamma\tau\left(\frac{\partial u_i}{\partial x_k},\frac{\partial u_j}{\partial x_k}\right) + \tau\left(u_i,\frac{\partial p}{\partial x_j}\right) + \tau\left(u_j,\frac{\partial p}{\partial x_i}\right)\right] - \frac{\partial\tau(u_k,u_i,u_j)}{\partial x_k} \tag{6a}$$

$$\frac{\partial\tau(u_i,\phi_\alpha)}{\partial t} + \frac{\partial\,\langle u_k\rangle\,\tau(u_i,\phi_\alpha)}{\partial x_k} = \Gamma\frac{\partial^2\tau(u_i,\phi_\alpha)}{\partial x_k\partial x_k} - \tau(u_k,u_i)\frac{\partial\,\langle\phi_\alpha\rangle}{\partial x_k} - \tau(u_k,\phi_\alpha)\frac{\partial\,\langle u_i\rangle}{\partial x_k} - \left[2\Gamma\tau\left(\frac{\partial u_i}{\partial x_k},\frac{\partial\phi_\alpha}{\partial x_k}\right) + \tau\left(\phi_\alpha,\frac{\partial p}{\partial x_i}\right)\right] + \tau(u_i,S_\alpha) - \frac{\partial\tau(u_k,u_i,\phi_\alpha)}{\partial x_k} \tag{6b}$$

$$\frac{\partial\tau(\phi_\alpha,\phi_\beta)}{\partial t} + \frac{\partial\,\langle u_k\rangle\,\tau(\phi_\alpha,\phi_\beta)}{\partial x_k} = \Gamma\frac{\partial^2\tau(\phi_\alpha,\phi_\beta)}{\partial x_k\partial x_k} - \tau(u_k,\phi_\alpha)\frac{\partial\,\langle\phi_\beta\rangle}{\partial x_k} - \tau(u_k,\phi_\beta)\frac{\partial\,\langle\phi_\alpha\rangle}{\partial x_k} - \left[2\Gamma\tau\left(\frac{\partial\phi_\alpha}{\partial x_k},\frac{\partial\phi_\beta}{\partial x_k}\right)\right] + \tau(\phi_\alpha,S_\beta) + \tau(\phi_\beta,S_\alpha) - \frac{\partial\tau(u_k,\phi_\alpha,\phi_\beta)}{\partial x_k} \tag{6c}$$

In this equation, the third order correlations

$$\begin{aligned}\tau(a,b,c) \;=\; &\langle abc\rangle - \langle a\rangle\,\tau(b,c)\\ &- \langle b\rangle\,\tau(a,c) - \langle c\rangle\,\tau(a,b) - \langle a\rangle\,\langle b\rangle\,\langle c\rangle\end{aligned} \tag{7}$$

are unclosed along with the other terms within square brackets.

III. VELOCITY-SCALAR FILTERED DENSITY FUNCTION (VSFDF)

A. Definitions

The "velocity-scalar filtered density function" (VSFDF), denoted by P, is formally defined as

$$P\left(\boldsymbol{v},\boldsymbol{\psi};\mathbf{x},t\right) = \int_{-\infty}^{+\infty}\varrho\left(\boldsymbol{v},\boldsymbol{\psi};\boldsymbol{u}(\mathbf{x}',t),\boldsymbol{\phi}(\mathbf{x}',t)\right)G(\mathbf{x}'-\mathbf{x})d\mathbf{x}' \tag{8}$$

$$\varrho\left(\boldsymbol{v},\boldsymbol{\psi};\boldsymbol{u}(\mathbf{x},t),\boldsymbol{\phi}(\mathbf{x},t)\right) = \prod_{i=1}^{3}\delta\left(v_i-u_i(\mathbf{x},t)\right)\times\prod_{\alpha=1}^{N_s}\delta\left(\psi_\alpha-\phi_\alpha(\mathbf{x},t)\right) \tag{9}$$

where δ denotes the delta function, and $\boldsymbol{v}, \boldsymbol{\psi}$ are the velocity vector and the scalar array in the sample space. The term ϱ is the "fine-grained" density [20, 26], hence Eq. (8) defines VSFDF as the spatially filtered value of the fine-grained density. With the condition of a positive filter kernel [27], P has all of the properties of the PDF [20]. For further developments it is useful to define the "conditional filtered value" of the variable $Q(\mathbf{x}, t)$ as

$$\begin{aligned}\left\langle Q(\mathbf{x},t) \,\middle|\, \boldsymbol{u}(\mathbf{x},t)=\boldsymbol{v}, \boldsymbol{\phi}(\mathbf{x},t)=\boldsymbol{\psi} \right\rangle &\equiv \left\langle Q \,\middle|\, \boldsymbol{v}, \boldsymbol{\psi} \right\rangle \\ &= \frac{\int_{-\infty}^{+\infty} Q(\mathbf{x}',t)\, \varrho(\boldsymbol{v}, \boldsymbol{\psi}; \boldsymbol{u}(\mathbf{x}',t), \boldsymbol{\phi}(\mathbf{x}',t))\, G(\mathbf{x}'-\mathbf{x})\, d\mathbf{x}'}{P(\boldsymbol{v}, \boldsymbol{\psi}; \mathbf{x}, t)}\end{aligned} \tag{10}$$

Equation (10) implies the followings:

(i) for $Q(\mathbf{x}, t) = c$, $$\left\langle Q(\mathbf{x},t) \,\middle|\, \boldsymbol{v}, \boldsymbol{\psi} \right\rangle = c \tag{11a}$$

(ii) for $Q(\mathbf{x}, t) \equiv \hat{Q}(\boldsymbol{u}(\mathbf{x},t), \boldsymbol{\phi}(\mathbf{x},t))$ $$\left\langle Q(\mathbf{x},t) \,\middle|\, \boldsymbol{v}, \boldsymbol{\psi} \right\rangle = \hat{Q}(\boldsymbol{v}, \boldsymbol{\psi}) \tag{11b}$$

(iii) Integral properties: $$\langle Q(\mathbf{x},t) \rangle = \int_{-\infty}^{+\infty} \left\langle Q(\mathbf{x},t) \,\middle|\, \boldsymbol{v}, \boldsymbol{\psi} \right\rangle P(\boldsymbol{v}, \boldsymbol{\psi}; \mathbf{x}, t) d\boldsymbol{v} d\boldsymbol{\psi} \tag{11c}$$

From Eqs. (11) it follows that the filtered value of any function of the velocity and/or scalar variables is obtained by its integration over the velocity and scalar sample spaces

$$\langle Q(\mathbf{x},t) \rangle = \int_{-\infty}^{+\infty} \hat{Q}(\boldsymbol{v}, \boldsymbol{\psi}) P(\boldsymbol{v}, \boldsymbol{\psi}; \mathbf{x}, t) d\boldsymbol{v} d\boldsymbol{\psi} \tag{12}$$

B. VSFDF Transport Equations

To develop the VSFDF transport equation, we consider the time derivative of the fine-grained density function (Eq. (9))

$$\frac{\partial \varrho}{\partial t} = -\left(\frac{\partial u_k}{\partial t} \frac{\partial \varrho}{\partial v_k} + \frac{\partial \phi_\alpha}{\partial t} \frac{\partial \varrho}{\partial \psi_\alpha} \right) \tag{13}$$

Substituting Eqs. (1b-1c), and Eqs. (2a-2b) into Eq. (13) we obtain

$$\frac{\partial \varrho}{\partial t} + \frac{\partial u_k \varrho}{\partial x_k} = \left(\frac{\partial p}{\partial x_i} - \nu \frac{\partial^2 u_i}{\partial x_k \partial x_k} \right) \frac{\partial \varrho}{\partial v_i} - \left(\nu \frac{\partial^2 \phi_\alpha}{\partial x_k \partial x_k} + S_\alpha(\boldsymbol{\phi}) \right) \frac{\partial \varrho}{\partial \psi_\alpha} \tag{14}$$

Integration of this according to Eq. (8), while employing Eq. (10) results in

$$\begin{aligned}\frac{\partial P}{\partial t}+\frac{\partial v_k P}{\partial x_k} &= \frac{\partial \langle p\rangle}{\partial x_k}\frac{\partial P}{\partial v_k}-\frac{\partial}{\partial \psi_\alpha}\left[S_\alpha(\psi)P\right] \\ &+ \frac{\partial}{\partial v_k}\left[\left(\left\langle \frac{\partial p}{\partial x_k}\,\middle|\,\boldsymbol{v},\boldsymbol{\psi}\right\rangle-\frac{\partial \langle p\rangle}{\partial x_k}\right)P\right] \\ &- \frac{\partial}{\partial v_i}\left(\left\langle \nu\frac{\partial^2 u_i}{\partial x_k \partial x_k}\,\middle|\,\boldsymbol{v},\boldsymbol{\psi}\right\rangle P\right) \\ &- \frac{\partial}{\partial \psi_\alpha}\left(\left\langle \nu\frac{\partial^2 \phi_\alpha}{\partial x_k \partial x_k}\,\middle|\,\boldsymbol{v},\boldsymbol{\psi}\right\rangle P\right) \end{aligned} \tag{15}$$

This is an exact transport equation for the VSFDF. It is observed that the effects of convection (second term on LHS) and chemical reaction (the last term on RHS) appear in closed forms. The unclosed terms denote convective effects in the velocity-scalar sample space. Alternatively, the VSFDF equation can be expressed as

$$\begin{aligned}\frac{\partial P}{\partial t}+\frac{\partial v_k P}{\partial x_k} &= \nu\frac{\partial^2 P}{\partial x_k \partial x_k}+\frac{\partial \langle p\rangle}{\partial x_k}\frac{\partial P}{\partial v_k}-\frac{\partial}{\partial \psi_\alpha}\left[S_\alpha(\psi)P\right] \\ &+ \frac{\partial}{\partial v_k}\left[\left(\left\langle \frac{\partial p}{\partial x_k}\,\middle|\,\boldsymbol{v},\boldsymbol{\psi}\right\rangle-\frac{\partial \langle p\rangle}{\partial x_k}\right)P\right] \\ &- \frac{\partial^2}{\partial v_i \partial v_j}\left[\left\langle \nu\frac{\partial u_i}{\partial x_k}\frac{\partial u_j}{\partial x_k}\,\middle|\,\boldsymbol{v},\boldsymbol{\psi}\right\rangle P\right] \\ &- 2\frac{\partial^2}{\partial v_i \partial \psi_\alpha}\left[\left\langle \nu\frac{\partial u_i}{\partial x_k}\frac{\partial \psi_\alpha}{\partial x_k}\,\middle|\,\boldsymbol{v},\boldsymbol{\psi}\right\rangle P\right] \\ &- \frac{\partial^2}{\partial \psi_\alpha \partial \psi_\beta}\left[\left\langle \nu\frac{\partial \psi_\alpha}{\partial x_k}\frac{\partial \psi_\beta}{\partial x_k}\,\middle|\,\boldsymbol{v},\boldsymbol{\psi}\right\rangle P\right] \end{aligned} \tag{16}$$

This is also an exact equation, but the unclosed terms are exhibited by the conditional filtered values of the dissipation fields as shown by the last three terms on the RHS.

C. Modeled VSFDF Transport Equation

For closure for the VSFDF transport equation, we consider the general diffusion process [28], given by the system of stochastic differential equations (SDEs):

$$\begin{aligned} dX_i^+(t) &= D_i^X(\mathbf{X}^+,\mathbf{U}^+,\phi^+;t)dt + B_{ij}^X(\mathbf{X}^+,\mathbf{U}^+,\phi^+;t)dW_j^X(t) \\ &+ F_{ij}^{XU}(\mathbf{X}^+,\mathbf{U}^+,\phi^+;t)dW_j^U(t) + F_{ij}^{X\phi}(\mathbf{X}^+,\mathbf{U}^+,\phi^+;t)dW_j^\phi(t) \qquad (17a) \\ dU_i^+(t) &= D_i^U(\mathbf{X}^+,\mathbf{U}^+,\phi^+;t)dt + B_{ij}^U(\mathbf{X}^+,\mathbf{U}^+,\phi^+;t)dW_j^U(t) \\ &+ F_{ij}^{UX}(\mathbf{X}^+,\mathbf{U}^+,\phi^+;t)dW_j^X(t) + F_{ij}^{U\phi}(\mathbf{X}^+,\mathbf{U}^+,\phi^+;t)dW_j^\phi(t) \qquad (17b) \\ d\phi_\alpha^+(t) &= D_\alpha^\phi(\mathbf{X}^+,\mathbf{U}^+,\phi^+;t)dt + B_{\alpha j}^\phi(\mathbf{X}^+,\mathbf{U}^+,\phi^+;t)dW_j^\phi(t) \\ &+ F_{\alpha j}^{\phi X}(\mathbf{X}^+,\mathbf{U}^+,\phi^+;t)dW_j^X(t) + F_{\alpha j}^{\phi U}(\mathbf{X}^+,\mathbf{U}^+,\phi^+;t)dW_j^U(t) \qquad (17c) \end{aligned}$$

where $X_i^+, U_i^+, \psi_\alpha^+$ are probabilistic representations of position, velocity vector, and scalar variables, respectively. The D terms denote drift in the composition space, The B terms denote diffusion, the F terms denote diffusion couplings, and the W terms denote the Wiener-Lévy processes [29, 30]. Following Haworth and Pope [31], Dreeben and Pope [32], Colucci *et al.* [7], and Gicquel *et al.* [16] we consider the generalized Langevin model (GLM) and the linear mean square estimation (LMSE) model [26]

$$\begin{aligned} dX_i^+ &= U_i^+dt + \sqrt{\nu_1}dW_i^X \qquad (18a) \\ dU_i^+ &= \left[-\frac{\partial\langle p\rangle}{\partial x_i} + \nu_2\frac{\partial^2\langle u_i\rangle}{\partial x_k\partial x_k} + G_{ij}\left(U_j^+ - \langle u_j\rangle\right)\right]dt \\ &+ \sqrt{\nu_3}\frac{\partial\langle u_i\rangle}{\partial x_k}dW_k^X + \sqrt{C_0\epsilon}dW_i^U \qquad (18b) \\ d\phi_\alpha^+ &= \left[\nu_{S_1}\frac{\partial^2\langle\phi_\alpha\rangle}{\partial x_k\partial x_k} - C_\phi\omega\left(\phi_\alpha^+ - \langle\phi_\alpha\rangle\right) + S_\alpha(\psi)\right]dt \\ &+ \sqrt{\nu_{S_2}}\frac{\partial\langle\phi_\alpha\rangle}{\partial x_k}dW_k^X \qquad (18c) \end{aligned}$$

where the variables $\nu_1, \nu_2, \ldots$ are all diffusion coefficients (to be specified), and

$$\begin{aligned} G_{ij} = -\omega\left(\frac{1}{2}+\frac{3}{4}C_0\right)\delta_{ij} \qquad \omega = \frac{\epsilon}{k} \\ \epsilon = C_\epsilon\frac{k^{3/2}}{\Delta_L} \qquad k = \frac{1}{2}\tau\left(u_k,u_k\right) \end{aligned} \qquad (19)$$

Here ω is the SGS mixing frequency, ϵ is the SGS dissipation rate, k is the turbulent kinetic energy, and Δ_L is the LES filter size. The parameters C_0, C_ϕ and C_ϵ are model constants

and need to be specified. The Fokker-Planck [33] equation for the diffusion process as given by Eq. (18) is:

$$\begin{aligned}
\frac{\partial f}{\partial t} + \frac{\partial}{\partial x_k}(v_k f) &= \left[\frac{\partial \langle p\rangle}{\partial x_i} - (\nu_2 - \sqrt{\nu_1\nu_3})\frac{\partial^2\langle u_i\rangle}{\partial x_k \partial x_k}\right]\frac{\partial f}{\partial v_i} - \frac{\partial}{\partial v_i}\left[G_{ij}\left(v_j - \langle u_j\rangle\right) f\right] \\
&- \left[\nu_{S_1} - \sqrt{\nu_1\nu_{S_2}}\right]\frac{\partial^2\langle\phi_\alpha\rangle}{\partial x_k\partial x_k}\frac{\partial f}{\partial\psi_\alpha} + \frac{\partial}{\partial\psi_\alpha}\left[C_\phi\omega\left(\psi_\alpha - \langle\phi_\alpha\rangle\right) f\right] - \frac{\partial}{\partial\psi_\alpha}\left[S_\alpha(\psi) f\right] \\
&+ \frac{\nu_1}{2}\frac{\partial^2 f}{\partial x_k\partial x_k} + \sqrt{\nu_1\nu_3}\frac{\partial\langle u_j\rangle}{\partial x_i}\frac{\partial^2 f}{\partial x_i\partial v_j} + \sqrt{\nu_1\nu_{S_2}}\frac{\partial\langle\phi_\alpha\rangle}{\partial x_i}\frac{\partial^2 f}{\partial x_i\partial\psi_\alpha} \\
&+ \frac{\nu_3}{2}\frac{\partial\langle u_i\rangle}{\partial x_k}\frac{\partial\langle u_j\rangle}{\partial x_k}\frac{\partial^2 f}{\partial v_i\partial v_j} + \frac{1}{2}C_0\epsilon\frac{\partial^2 f}{\partial v_k\partial v_k} + \sqrt{\nu_3\nu_{S_2}}\frac{\partial\langle u_i\rangle}{\partial x_k}\frac{\partial\langle\phi_\alpha\rangle}{\partial x_k}\frac{\partial^2 f}{\partial v_i\partial\psi_\alpha} \\
&+ \frac{\nu_{S_2}}{2}\frac{\partial\langle\phi_\alpha\rangle}{\partial x_k}\frac{\partial\langle\phi_\beta\rangle}{\partial x_k}\frac{\partial^2 f}{\partial\psi_\alpha\partial\psi_\beta}
\end{aligned} \tag{20}$$

The transport equations for the filtered variables are obtained by integration of Eq. (20) according to Eq. (12):

$$\frac{\partial\langle u_k\rangle}{\partial x_k} = 0 \tag{21a}$$

$$\frac{\partial\langle u_i\rangle}{\partial t} + \frac{\partial\langle u_k\rangle\langle u_i\rangle}{\partial x_k} = -\frac{\partial\langle p\rangle}{\partial x_i} + \left(\frac{\nu_1}{2} + \nu_2 - \sqrt{\nu_1\nu_3}\right)\frac{\partial^2\langle u_i\rangle}{\partial x_k\partial x_k} - \frac{\partial\tau(u_k,u_i)}{\partial x_k} \tag{21b}$$

$$\frac{\partial\langle\phi_\alpha\rangle}{\partial t} + \frac{\partial\langle u_k\rangle\langle\phi_\alpha\rangle}{\partial x_k} = \left(\nu_{S_1} - \sqrt{\nu_1\nu_{S_2}} + \frac{\nu_1}{2}\right)\frac{\partial^2\langle\phi_\alpha\rangle}{\partial x_k\partial x_k} + \langle S_\alpha(\phi)\rangle - \frac{\partial\tau(u_k,\phi_\alpha)}{\partial x_k} \tag{21c}$$

The transport equations for the second order SGS moments are

$$\begin{aligned}
\frac{\partial\tau(u_i,u_j)}{\partial t} + \frac{\partial\langle u_k\rangle\tau(u_i,u_j)}{\partial x_k} &= \frac{\nu_1}{2}\frac{\partial^2\tau(u_i,u_j)}{\partial x_k\partial x_k} - \tau(u_k,u_i)\frac{\partial\langle u_j\rangle}{\partial x_k} - \tau(u_k,u_j)\frac{\partial\langle u_i\rangle}{\partial x_k} + \\
&+ (\nu_1 - 2\sqrt{\nu_1\nu_3} + \nu_3)\frac{\partial\langle u_i\rangle}{\partial x_k}\frac{\partial\langle u_j\rangle}{\partial x_k} - \\
&+ [G_{ik}\tau(u_k,u_j) + G_{jk}\tau(u_k,u_i) + C_0\epsilon\delta_{ij}] - \frac{\partial\tau(u_k,u_i,u_j)}{\partial x_k}
\end{aligned} \tag{22a}$$

$$\begin{aligned}
\frac{\partial\tau(u_i,\phi_\alpha)}{\partial t} + \frac{\partial\langle u_k\rangle\tau(u_i,\phi_\alpha)}{\partial x_k} &= \frac{\nu_1}{2}\frac{\partial^2\tau(u_i,\phi_\alpha)}{\partial x_k\partial x_k} - \tau(u_k,u_i)\frac{\partial\langle\phi_\alpha\rangle}{\partial x_k} - \tau(u_k,\phi_\alpha)\frac{\partial\langle u_i\rangle}{\partial x_k} + \\
&+ \left(\nu_1 - \sqrt{\nu_1\nu_3} - \sqrt{\nu_1\nu_{S_2}} + \sqrt{\nu_3\nu_{S_2}}\right)\frac{\partial\langle u_i\rangle}{\partial x_k}\frac{\partial\langle\phi_\alpha\rangle}{\partial x_k} + \\
&+ [G_{ik}\tau(u_k,\phi_\alpha) - C_\phi\omega\tau(u_i,\phi_\alpha)] + \tau(u_i,S_\alpha) - \frac{\partial\tau(u_k,u_i,\phi_\alpha)}{\partial x_k}
\end{aligned} \tag{22b}$$

$$\frac{\partial \tau(\phi_\alpha,\phi_\beta)}{\partial t} + \frac{\partial \langle u_k\rangle \tau(\phi_\alpha,\phi_\beta)}{\partial x_k} = \frac{\nu_1}{2}\frac{\partial^2 \tau(\phi_\alpha,\phi_\beta)}{\partial x_k \partial x_k} - \tau(u_k,\phi_\alpha)\frac{\partial \langle \phi_\beta\rangle}{\partial x_k} - \tau(u_k,\phi_\beta)\frac{\partial \langle \phi_\alpha\rangle}{\partial x_k} +$$
$$+ \left(\nu_1 - 2\sqrt{\nu_1 \nu_{S_2}} + \nu_{S_2}\right)\frac{\partial \langle \phi_\alpha\rangle}{\partial x_k}\frac{\partial \langle \phi_\beta\rangle}{\partial x_k} -$$
$$- \left[2C_\phi \omega \tau(\phi_\alpha,\phi_\beta)\right] + \tau(\phi_\alpha,S_\beta) + \tau(\phi_\beta,S_\alpha) - \frac{\partial \tau(u_k,\phi_\alpha,\phi_\beta)}{\partial x_k} \tag{22c}$$

A term-by-term comparison of the exact moment transport equations (Eqs. (4),(6)), with the modeled equations (Eqs. (21),(22)), suggests $\nu_1 = \nu_2 = \nu_3 = \nu_{S_1} = \nu_{S_2} = 2\nu$. However, this violates the realizability of the scalar field. A set of coefficients yielding a realizable stochastic model requires: $\nu_1 = \nu_2 = \nu_3 = 2\nu$ and $\nu_{S_1} = \nu_{S_2} = 0$. That is,

$$dX_i^+ = U_i^+ dt + \sqrt{2\nu} dW_i^X \tag{23a}$$
$$dU_i^+ = \left[-\frac{\partial \langle p\rangle}{\partial x_i} + 2\nu\frac{\partial^2 \langle u_i\rangle}{\partial x_k \partial x_k} + G_{ij}\left(U_j^+ - \langle u_j\rangle\right)\right] dt$$
$$+ \sqrt{2\nu}\frac{\partial \langle u_i\rangle}{\partial x_k} dW_k^X + \sqrt{C_0\epsilon}\, dW_i^U \tag{23b}$$
$$d\phi_\alpha^+ = -C_\phi\omega\left(\phi_\alpha^+ - \langle \phi_\alpha\rangle\right) dt \tag{23c}$$

The Fokker-Planck equation for this system is

$$\frac{\partial f}{\partial t} + \frac{\partial}{\partial x_k}(v_k f) = \frac{\partial \langle p\rangle}{\partial x_i}\frac{\partial f}{\partial v_i} - \frac{\partial}{\partial v_i}\left[G_{ij}\left(v_j - \langle u_j\rangle\right) f\right] + \frac{\partial}{\partial \psi_\alpha}\left[C_\phi\omega\left(\psi_\alpha - \langle \phi_\alpha\rangle\right) f\right]$$
$$+ \nu\frac{\partial^2 f}{\partial x_k \partial x_k} + 2\nu\frac{\partial \langle u_j\rangle}{\partial x_i}\frac{\partial^2 f}{\partial x_i \partial v_j} + \nu\frac{\partial \langle u_i\rangle}{\partial x_k}\frac{\partial \langle u_j\rangle}{\partial x_k}\frac{\partial^2 f}{\partial v_i \partial v_j} + \frac{1}{2}C_0\epsilon\frac{\partial^2 f}{\partial v_k \partial v_k} \tag{24}$$

and the corresponding equations for the moments are:

$$\frac{\partial \langle u_k\rangle}{\partial x_k} = 0 \tag{25a}$$
$$\frac{\partial \langle u_i\rangle}{\partial t} + \frac{\partial \langle u_k\rangle \langle u_i\rangle}{\partial x_k} = -\frac{\partial \langle p\rangle}{\partial x_i} + \nu\frac{\partial^2 \langle u_i\rangle}{\partial x_k \partial x_k} - \frac{\partial \tau(u_k,u_i)}{\partial x_k} \tag{25b}$$
$$\frac{\partial \langle \phi_\alpha\rangle}{\partial t} + \frac{\partial \langle u_k\rangle \langle \phi_\alpha\rangle}{\partial x_k} = \nu\frac{\partial^2 \langle \phi_\alpha\rangle}{\partial x_k \partial x_k} - \frac{\partial \tau(u_k,\phi_\alpha)}{\partial x_k} \tag{25c}$$

$$\frac{\partial \tau(u_i,u_j)}{\partial t} + \frac{\partial \langle u_k\rangle \tau(u_i,u_j)}{\partial x_k} = \nu\frac{\partial^2 \tau(u_i,u_j)}{\partial x_k \partial x_k} - \tau(u_k,u_i)\frac{\partial \langle u_j\rangle}{\partial x_k} - \tau(u_k,u_j)\frac{\partial \langle u_i\rangle}{\partial x_k} +$$
$$+ \left[G_{ik}\tau(u_k,u_j) + G_{jk}\tau(u_k,u_i) + C_0\epsilon\delta_{ij}\right] - \frac{\partial \tau(u_k,u_i,u_j)}{\partial x_k} \tag{26a}$$

$$\frac{\partial \tau(u_i,\phi_\alpha)}{\partial t} + \frac{\partial \langle u_k\rangle \tau(u_i,\phi_\alpha)}{\partial x_k} = \nu\frac{\partial^2 \tau(u_i,\phi_\alpha)}{\partial x_k \partial x_k} - \tau(u_k,u_i)\frac{\partial \langle \phi_\alpha\rangle}{\partial x_k} - \tau(u_k,\phi_\alpha)\frac{\partial \langle u_i\rangle}{\partial x_k} +$$
$$+ \left[G_{ik}\tau(u_k,\phi_\alpha) - C_\phi\omega\tau(u_i,\phi_\alpha)\right] - \frac{\partial \tau(u_k,u_i,\phi_\alpha)}{\partial x_k} \tag{26b}$$

$$\frac{\partial \tau(\phi_\alpha,\phi_\beta)}{\partial t} + \frac{\partial \langle u_k\rangle \tau(\phi_\alpha,\phi_\beta)}{\partial x_k} = \nu\frac{\partial^2 \tau(\phi_\alpha,\phi_\beta)}{\partial x_k \partial x_k} - \tau(u_k,\phi_\alpha)\frac{\partial \langle \phi_\beta\rangle}{\partial x_k} - \tau(u_k,\phi_\beta)\frac{\partial \langle \phi_\alpha\rangle}{\partial x_k} +$$
$$+ \left[2\nu\frac{\partial \langle \phi_\alpha\rangle}{\partial x_k}\frac{\partial \langle \phi_\beta\rangle}{\partial x_k} - 2C_\phi\omega\tau(\phi_\alpha,\phi_\beta)\right] - \frac{\partial \tau(u_k,\phi_\alpha,\phi_\beta)}{\partial x_k} \quad (26c)$$

Therefore, the stochastic diffusion process described by the SDEs (23) implies the following closure for the VSFDF:

$$\frac{\partial}{\partial v_k}\left[\left(\left\langle \frac{\partial p}{\partial x_k}\,\middle|\, \boldsymbol{v},\boldsymbol{\psi}\right\rangle - \frac{\partial \langle p\rangle}{\partial x_k}\right)P\right] - \nu\frac{\partial^2}{\partial v_i \partial v_j}\left[\left\langle \frac{\partial u_i}{\partial x_k}\frac{\partial u_j}{\partial x_k}\,\middle|\, \boldsymbol{v},\boldsymbol{\psi}\right\rangle P\right]$$
$$-2\nu\frac{\partial^2}{\partial v_i \partial \psi_\alpha}\left[\left\langle \frac{\partial u_i}{\partial x_k}\frac{\partial \psi_\alpha}{\partial x_k}\,\middle|\, \boldsymbol{v},\boldsymbol{\psi}\right\rangle P\right] - \nu\frac{\partial^2}{\partial \psi_\alpha \partial \psi_\beta}\left[\left\langle \frac{\partial \psi_\alpha}{\partial x_k}\frac{\partial \psi_\beta}{\partial x_k}\,\middle|\, \boldsymbol{v},\boldsymbol{\psi}\right\rangle P\right]$$
$$\approx \nu\frac{\partial \langle u_i\rangle}{\partial x_k}\frac{\partial \langle u_j\rangle}{\partial x_k}\frac{\partial^2 f}{\partial v_i \partial v_j} + \frac{1}{2}C_0\epsilon\frac{\partial^2 f}{\partial v_k \partial v_k} + 2\nu\frac{\partial \langle u_i\rangle}{\partial x_k}\frac{\partial^2 f}{\partial x_k \partial v_i}$$
$$-\frac{\partial}{\partial v_i}\left[G_{ij}\left(v_j - \langle u_j\rangle\right) f\right] + \frac{\partial}{\partial \psi_\alpha}\left[C_\phi\omega\left(\psi_\alpha - \langle \phi_\alpha\rangle\right) f\right] \quad (27)$$

which yields the closures at the second order levels:

$$-\left[2\nu\,\tau\left(\frac{\partial u_i}{\partial x_k},\frac{\partial u_j}{\partial x_k}\right) + \tau\left(u_i,\frac{\partial p}{\partial x_j}\right) + \tau\left(u_j,\frac{\partial p}{\partial x_i}\right)\right] = G_{ik}\tau(u_k,u_j) + G_{jk}\tau(u_k,u_i) + C_0\epsilon\delta_{ij}$$
$$= -\omega\left(1+\frac{3}{2}C_0\right)\left[\tau(u_i,u_j) - \frac{2}{3}k\delta_{ij}\right] - \frac{2}{3}\epsilon\delta_{ij} \quad (28a)$$

$$-\left[2\nu\,\tau\left(\frac{\partial u_i}{\partial x_k},\frac{\partial \phi_\alpha}{\partial x_k}\right) + \tau\left(\phi_\alpha,\frac{\partial p}{\partial x_i}\right)\right] = G_{ik}\tau(u_k,\phi_\alpha) - C_\phi\omega\tau(u_i,\phi_\alpha)$$
$$= -\omega\left(\frac{1}{2}+\frac{3}{4}C_0 + C_\phi\right)\tau\left(u_i,\phi_\alpha\right) \quad (28b)$$

$$-2\nu\,\tau\left(\frac{\partial \phi_\alpha}{\partial x_k},\frac{\partial \phi_\beta}{\partial x_k}\right) = -2C_\phi\omega\tau(\phi_\alpha,\phi_\beta) + 2\nu\frac{\partial \langle \phi_\alpha\rangle}{\partial x_k}\frac{\partial \langle \phi_\beta\rangle}{\partial x_k} \quad (28c)$$

IV. NUMERICAL SOLUTION PROCEDURE

Numerical solution of the modeled VSFDF transport equation is obtained by a Lagrangian Monte Carlo (MC) procedure. The basis of this procedure is the same as that used in RAS [34–36] and in previous FDF simulations [7, 9, 16]. In this procedure, the FDF is represented by an ensemble of N_p statistically identical Monte Carlo particles. Each particle carries information pertaining to its position, $\mathbf{X}^{(n)}(t)$, velocity,$\boldsymbol{U}^{(n)}(t)$, and scalar value, $\boldsymbol{\phi}^{(n)}(t)$, $n = 1,\ldots,N_p$. This information is updated via temporal integration of the SDEs. The

simplest way of performing this integration is via Euler-Maruyamma approximation [37]. For example, for Eq. (17a),

$$X_i^n(t_{k+1}) = X_i^n(t_k) + \left(D_i^X(t_k)\right)^n \Delta t + \left(B_{ij}^X(t_k)\right)^n (\Delta t)^{1/2} \left(\zeta_j^X(t_k)\right)^n + \left(F_{ij}^{XU}(t_k)\right)^n (\Delta t)^{1/2} \left(\zeta_j^U(t_k)\right)^n + \left(F_{ij}^{X\phi}(t_k)\right)^n (\Delta t)^{1/2} \left(\zeta_j^\phi(t_k)\right)^n \quad (29)$$

where $D_i(t_k) = D_i(\mathbf{X}^{(n)}(t_k), \boldsymbol{U}^{(n)}(t_k), \boldsymbol{\phi}^{(n)}(t_k); t_k)$, ..., and $\zeta(t_k)$'s are independent standardized Gaussian random variables. This scheme preserves the Itô character of the SDEs [38].

The computational domain is discretized on equally spaced finite difference grid points. These points are used for three purposes: (1) identify the regions where the statistical information from the MC simulations are obtained, (2) perform a part of the simulations via finite difference discretization coupled with the MC solver, and (3) perform a set of complementary LES primarily by the finite difference methodology for assessing the consistency and convergence of the MC results. The LES procedure via the finite difference discretization is referred to as LES-FD and will be further discussed below.

Statistical information is obtained by considering an ensemble of N_E computational particles residing within an ensemble domain of characteristic length Δ_E centered around each of the finite-difference grid points. This is illustrated schematically in Fig. 1. For reliable statistics with minimal numerical dispersion, it is desired to minimize the size of ensemble domain and maximize the number of the MC particles. In this way, the ensemble statistics would tend to the desired filtered values:

$$\langle a \rangle_E \equiv \frac{1}{N_E} \sum_{n \in \Delta_E} a^{(n)} \xrightarrow[\substack{N_E \to \infty \\ \Delta_E \to 0}]{} \langle a \rangle$$

$$\tau_E(a,b) \equiv \frac{1}{N_E} \sum_{n \in \Delta_E} \left(a^{(n)} - \langle a \rangle_E\right) \left(b^{(n)} - \langle b \rangle_E\right) \xrightarrow[\substack{N_E \to \infty \\ \Delta_E \to 0}]{} \tau(a,b) \quad (30)$$

where $a^{(n)}$ denotes the information carried by n^{th} MC particle pertaining to transport variable a.

The LES-FD solver is based on the compact parameter finite difference scheme [39, 40]. This is a variant of the MacCormack scheme in which fourth-order compact differencing schemes are used to approximate the spatial derivatives, and second-order symmetric predictor-corrector sequence is employed for time discretization. All of the finite difference operations are conducted on fixed grid points. The transfer of information from the grid

points to the MC particles is accomplished via a second-order interpolation. The transfer of information from the particles to the grid points is accomplished via ensemble averaging as described above.

The LES-FD procedure determines the pressure field which is used in the MC solver. The LES-FD also determines the filtered velocity and scalar fields. That is, there is a "redundancy" in the determination of the first filtered moments as both the LES-FD and the MC procedures provides the solution of this field. This redundancy is actually very useful in monitoring the accuracy of the simulated results as shown in previous work [9, 16, 34–36]. To establish consistency and convergence of the MC solver, the modeled transport equations for the generalized second order SGS moments (Eq. (26) are also solved via LES-FD. In doing so, the unclosed third order correlations are taken from the MC solver. The comparison of all of the first and second refer moments as obtained by LES-FD with those obtained by the MC solver is useful to establish the accuracy of the MC solver. These simulations are referred to as VSFDF-C. Attributes of all of the simulation procedures are summarized in Table ??. In this table and hereinafter, VSFDF simulations refer to the coupled MC/LES-FD procedure in which the LES-FD is used for only the first order filtered variables. In VSFDF-C, the LES-FD procedure is used for both first and second order filtered values. Further discussions about the simulation methods are available in Refs. [7, 16, 34–36].

V. RESULTS

A. Flows Simulated

Simulations are conducted of a two-dimensional (2D) and a 3D temporally developing mixing layer involving transport of a passive scalar variable. The 2D simulations are performed to establish and demonstrate the consistency of the MC solver. The 3D simulations are used to assess the overall predictive capabilities of the VSFDF methodology. These predictions are compared with data obtained by direct numerical simulation (DNS) of the same layer.

The temporal mixing layer consists of two parallel streams traveling in opposite directions with the same speed [41–43]. In the representation below, x, y (and z) denote the streamwise, the cross-stream, (and the span-wise) directions (in 3D), respectively. The ve-

locity components along these directions are denoted by u, v, (and w) in the x, y, (and z) directions, respectively. Both the filtered streamwise velocity and the scalar fields are initialized with a hyperbolic tangent profiles with $\langle u \rangle = 0.5$, $\langle \phi \rangle = 1$ on the top stream and $\langle u \rangle = -0.5$, $\langle \phi \rangle = 0$ on the bottom stream. The length L is specified such that $L = 2^{N_P} \lambda_u$, where N_P is the desired number of successive vortex pairings and λ_u is the wavelength of the most unstable mode corresponding to the mean streamwise velocity profile imposed at the initial time. The flow variables are normalized with respect to the half initial vorticity thickness, $L_r = \frac{\delta_v(t=0)}{2}$, ($\delta_v = \frac{\Delta U}{|\partial \overline{\langle u \rangle}_L / \partial y|_{max}}$, where $\overline{\langle u \rangle}_L$ is the Reynolds averaged value of the filtered streamwise velocity and ΔU is the velocity difference across the layer). The reference velocity is $U_r = \Delta U/2$.

All 2D simulations are conducted for $0 \leq x \leq 30$, and $-20 \leq y \leq 20$. The dimensions are chosen to trigger the most unstable linear mode. The formation of large scale structures is facilitated by introducing small harmonic, phase-shifted, disturbances containing sub-harmonics of the most unstable mode into the stream-wise and cross-stream velocity profiles. For $N_p = 1$, this results in formation of two large vortices and one subsequent pairing of these vortices. The 3D simulations are conducted for a cubic box, $0 \leq x \leq 60$, $-30 \leq y \leq 30$, $(0 \leq z \leq 60)$. The 3D field is parameterized in a procedure somewhat similar to that by Vreman *et al.* [44]. The formation of the large scale structures are expedited through eigenfunction based initial perturbations [45, 46]. This includes two-dimensional [42, 44, 47] and three-dimensional [42, 48] perturbations with a random phase shift between the $3D$ modes. This results in the formation of two successive vortex pairings and strong three-dimensionality.

B. Numerical Specifications

Simulations are conducted on equally-spaced grid points with grid spacings $\Delta x = \Delta y = \Delta z(\text{for 3D}) = \Delta$. All 2D simulations are performed on 32×41 grid points. The 3D simulations are conducted on 193^3 and 33^3 points for DNS and LES, respectively. **The Reynolds number is** $Re = \frac{U_r L_r}{\nu} = 50$.

To filter the DNS data, a top-hat function of the form below is used

$$G(\mathbf{x}' - \mathbf{x}) = \prod_{i=1}^{3} \widetilde{G}(x_i' - x_i)$$
$$\widetilde{G}(x_i' - x_i) = \begin{cases} \frac{1}{\Delta_L} & |x_i' - x_i| \leq \frac{\Delta_L}{2}, \\ 0 & |x_i' - x_i| > \frac{\Delta_L}{2}, \end{cases} \tag{31}$$

No attempt is made to investigate the sensitivity of the results to the filter function [27] or the size of the filter [49].

The MC particles are initially distributed throughout the computational region. All simulations are performed with a uniform "weight" [20] of the particles. Due to flow periodicity in the streamwise (and span-wise in 3D) direction(s), if the particle leaves the domain at one of these boundaries new particles are introduced at the other boundary with the same compositional values. In the cross-stream directions, the free-slip boundary condition is satisfied by the mirror-reflection of the particles leaving through these boundaries. The density of the MC particles is determined by the average number of particles N_E within the ensemble domain of size $\Delta_E \times \Delta_E (\times \Delta_E)$. The effects of both of these parameters are assessed to ensure the consistency and the statistical accuracy of the VSFDF simulations.

All results are analyzed both "instantaneously" and "statistically." In the former, the instantaneous contours (snap-shots) and scatter plots of the variables of interest are analyzed. In the latter, the "Reynolds-averaged" statistics constructed from the instantaneous data are considered. These are constructed by spatial averaging over x (and z in 3D). All Reynolds averaged results are denoted by an overbar.

C. Consistency and Convergence Assessments

The objective of this section is to demonstrate the consistency of the VSFDF formulation and the convergence of its MC simulation procedure. For this purpose, the results via MC and LES-FD are compared against each other in VSFDF-C simulations. Since the accuracy of the FD procedure is well-established (at least for the first order filtered quantities), such a comparative assessment provides a good means of assessing the performance of the MC solution. No attempt is made to determine the appropriate values of the model constants; the values suggested in the literature are adopted [50] $C_0 = 2.1$, $C_\epsilon = 1$ and $C_\phi = 1$. The influence of these parameters are assessed in Section(V D.

The uniformity of the MC particle is checked by monitoring their distributions at all times, as the particle number density must be proportional to fluid density. The Reynolds averaged density field as obtained by both LES-FD and by MC are shown in Fig. 2. Close to unity values for the density at all times is the first measure of accuracy of simulations. Figures 3 and 4 show the instantaneous contour plots of the filtered scalar and vorticity fields at several times. These figures provide a visual demonstration of the consistency of the VSFDF. This consistency is observed for all first order moments (filter values) without any statistical variability. Also, all of the first moments show very little dependence on the Δ_E and N_E values. So, in the presentation below we only focus on second order moments. Specifically, the scalar-velocity correlations are shown since all other second order SGS moments behave similarly.

Figure 5-6 show the statistical variability of the results for several simulations with $N_E = 40$. It is observed that these moments exhibit spreads with variances decreasing as the size of the ensemble domain is reduced. Figures 7-10 show the sensitivity to N_E and Δ_E. All these results clearly display convergence suggested by Eq. (30). As the ensemble domain size decreases, the VSFDF results converge to those of LES-FD. Ideally, the LES-FD results should become independent of the MC results, as the latter become more reliable, *i.e.* when $N_E \to \infty$, and $\Delta_E \to 0$). It is observed that best match is achieved with $\Delta_E \leq \Delta/2$ and $N_E \geq 40$. This conclusion is consistent with previous assessment studies on the scalar FDF [7, 9], and the velocity FDF [16]. All the subsequent simulations are conducted with $\Delta_E = \Delta/2$ and $N_E = 40$.

D. Comparative Assessments of the VFDF

The objective of this section is to analyze some of the characteristics of the VSFDF via comparative assessments against DNS data. In addition, comparisons are also made with

LES via the "conventional" Smagorinsky [18, 51] model:

$$\begin{aligned} \tau_L(u_i,u_j) - \frac{2}{3}\, k\, \delta_{ij} &= -2\, \nu_t\, S_{ij}, \\ \tau_L(u_i,\phi) &= -\Gamma_t \frac{\partial \langle phi \rangle}{\partial x_i}, \\ S_{ij} &= \frac{1}{2}\left(\frac{\partial \langle u_i \rangle_L}{\partial x_j} + \frac{\partial \langle u_j \rangle_L}{\partial x_i}\right), \\ \nu_t &= C_\nu\, \Delta_L^2\, S, \quad \Gamma_t = \frac{\nu_t}{Sc_t}. \end{aligned} \tag{32}$$

$C_\nu = 0.04$, $Sc_t = 1$, $S = \sqrt{S_{ij}S_{ij}}$ and Δ_L is the characteristic length of the filter. This model considers the anisotropic part of the SGS stress tensor $a_{ij} = \tau_L(u_i,u_j) - 2/3\ k\ \delta_{ij}$. The isotropic components are absorbed in the pressure field.

The predicted results via VSFDF and the Smagorinsky model are compared with those obtained by DNS of the same flow. For this comparison, the DNS data are filtered and are transposed from the original high resolution 193^3 points to the coarse 33^3 points. In the comparisons, we also consider the "resolved" and the "total" components of the Reynolds averaged moments. The former are denoted by $\overline{R(a,b)}$ with $R(a,b) = \left(\langle a \rangle - \overline{\langle a \rangle}\right)\left(\langle b \rangle - \overline{\langle b \rangle}\right)$; and the latter is $\overline{r(a,b)}$ with $r(a,b) = (a-\overline{a})\,(b-\overline{b})$. n DNS, the "total" SGS components are directly available, while in LES they are approximated by $\overline{r(a,b)} \approx \overline{R(a,b)} + \overline{\tau(a,b)}$ [44]. Unless indicated otherwise, the values of the model constants are ($C_0 = 2.1$, $C_\varepsilon = 1$, $C_\phi = 1$; but the effects of these parameters on the predicted results are assessed.

Figure 11 show the instantaneous iso-surface of the $\langle \phi \rangle = 0.5$ field $t = 80$. By this time, the flow has gone through several pairings and exhibits strong 3D effects. This is evident by the formation of large scale span-wise rollers with presence of mushroom like structures in streamwise planes [45]. Similar to previous results of Gicquel *et al.* [16], the amount of SGS diffusion with the Smagorinsky model is significant, especially at initial times. Therefore, the predicted results are overly smooth. The Reynolds averaged values of the filtered scalar field at $t = 80$ are shown in Fig. 12 and the temporal variation of the "scalar thickness,"

$$\delta_s(t) = \left|y(\overline{\langle \phi \rangle} = 0.9)\right| + \left|y(\overline{\langle \phi \rangle} = 0.1)\right| \tag{33}$$

is shown in in Fig. 13. The filtered and unfiltered DNS data yield virtually indistinguishable results. The dissipative nature of the Smagorinsky model at initial times resulting in a slow growth of the layer is shown. All VSFDF predictions compare well with DNS data in predicting the spread of the layer.

Several components of the planar averaged values of the second order SGS moments are compared with DNS data in Figs. 14-15 for several values of the model constants. In general, the the VSFDF results are in better agreement with DNS data than those predicted by the Smagorinsky model. In this regard, therefore, the VSFDF is expected to be more effective than the Smagorinsky type closures for LES of reacting flows since the extent of SGS mixing is heavily influenced by these SGS moments [52, 53]. However, it is not possible to suggest "optimum" values for the model constants, except that at small C_ϵ and C_ϕ values, the SGS energy is very large.

Several components of the resolved second order moments are presented in Figs. 16-17. As expected, the performance of the Smagorinsky model is not very good as it does not predict the spread and the peak value accurately. The VSFDF yields reasonable predictions of the resolved field, except for small C_ϕ values. However, the total values of these moments are fairly independent of the model constants and yield very good agreement with DNS data as shown in Figs. 18-19. It is also interesting to note that while the SGS moments and/or the resolved moments may be over- and/or under-estimated depending on the values of the model coefficients, the total values of the moments are fairly independent of these coefficients, at least in the range of these values as considered. But low values of C_ϕ, C_ϵ are not recommended as they would result into too much SGS energy in comparison to the resolved energy.

VI. SUMMARY AND CONCLUDING REMARKS

The filtered density function (FDF) methodology has proven very effective for LES of turbulent reactive flows. In previous investigations, the FDF of either only the marginal FDF of the scalar, or that of the velocity were considered. The objective of present work is to develop the joint velocity-scalar FDF methodology. For this purpose, the exact transport equation governing the evolution of VSFDF is derived. It is shown that effects of the SGS convection and chemical reaction appear in a closed form. The unclosed terms are modeled in a fashion similar to those typically followed in PDF methods. The modeled VSFDF transport equation is solved numerically via a Lagrangian Monte Carlo scheme via consideration of a system of equivalent stochastic differential equations (SDEs). These SDEs are discretized via the Euler-Maruyamma approximation. The consistency of the VSFDF

method and the convergence of its Monte Carlo solutions are assessed in LES of a two-dimensional (2D) temporally developing mixing layer. This assessment is done by comparing the results obtained via Monte Carlo procedure with those of the finite-difference scheme (LES-FD) for the solution of the transport equations of the first two moments of VSFDF. With inclusion of the third moments from the VSFDF into the LES-FD, the consistency and convergence of the Monte Carlo solution is demonstrated by good agreements of the first two SGS moments with those obtained by LES-FD.

The VFDF predictions are compared with those with LES results with the Smagorinsky [18] SGS model. All of these results are also compared with direct numerical simulation (DNS) data of a three-dimensional, temporally developing mixing layer. This comparison provides a means of examining some of the trends and overall characteristics as predicted by LES. It is shown that the VFDF performs well in predicting some of the phenomena pertaining to the SGS transport. The magnitude of the second order SGS moments as predicted by VSFDF is significantly larger than those predicted by the Smagorinsky model and are much closer to the filtered DNS results. Most of the overall flow features, including the mean field, the resolved and total stresses as predicted by VSFDF are in good agreement with DNS data. It may be possible to improve the predictive capabilities of the VFDF by two ways: (1) development of a dynamic procedure to determine the model coefficients, and/or (2) implementation of higher order closures for the generalized Langevin model parameter G_{ij} (see Ref. [50]).

Work is in progress on further development and application of VSFDF for LES of variable density involving exothermic chemical reactions.

Captions

Table 1. Attributes of the computational methods.

Figure 1. Concept of ensemble averaging. Shown are three different ensemble domains: $1(\Delta_E = \Delta/2,\ N_E \approx 10)$, $2(\Delta_E = \Delta,\ N_E \approx 40)$, $3(\Delta_E = 2\Delta,\ N_E \approx 160)$. Black squares denote the finite-difference grid points, and the circles denote the MC particles.

Figure 2. Cross-stream variation of the Reynolds-averaged values of $\langle\rho\rangle$ at t=34.3: (a) $N_E = 40$, (b) $\Delta_E = \Delta/2$.

Figure 3. Temporal evolution of the scalar (with superimposed vorticity iso-lines) (left) and the vorticity (right) fields for LES-FD, with $\Delta_E = \Delta/2$ and $N_E = 40$ at several times.

Figure 4. Temporal evolution of the scalar (with superimposed vorticity iso-lines) (left) and the vorticity (right) fields for VSFDF with $\Delta_E = \Delta/2$ and $N_E = 40$ at several times.

Figure 5. Statistical variability of LES-FD and VSFDF simulations with $N_E = 40$ for Reynolds-averaged values of $\tau(u, \phi)$ at t=34.4.

Figure 6. Statistical variability of LES-FD and VSFDF simulations with $N_E = 40$ for Reynolds-averaged values of $\tau(v, \phi)$ at t=34.4.

Figure 7. Cross-stream variations of the Reynolds-averaged values of $\tau(u, \phi)$ (a) $\Delta_E = \Delta/2$, (b) $\Delta_E = \Delta$, (c) $\Delta_E = 2\Delta$.

Figure 8. Cross-stream variations of the Reynolds-averaged values of $\tau(v, \phi)$ (a) $\Delta_E = \Delta/2$, (b) $\Delta_E = \Delta$, (c) $\Delta_E = 2\Delta$.

Figure 9. Cross-stream variations of the Reynolds-averaged values of $\tau(u, \phi)$ (a) $N_E = 20$, (b) $N_E = 40$, (c) $N_E = 80$.

Figure 10. Cross-stream variations of the Reynolds-averaged values of $\tau(v, \phi)$ (a) $N_E = 20$, (b) $N_E = 40$, (c) $N_E = 80$.

Figure 11. Contours surface of the $\langle\phi\rangle$ field in the 3D mixing layer at $t = 80$.

Figure 12. Cross-stream variations of the Reynolds averaged values of the filtered scalar field at $t = 80$.

Figure 13. Temporal variations of the scalar thickness.

Figure 14. Cross stream variations of some of the components of τ at $t = 60$.

Figure 15. Cross stream variations of some of the components of τ at $t = 80$.

Figure 16. Cross-stream variations of some of the components of $\overline{R}$ at $t = 60$.

Figure 17. Cross-stream variations of some of the components of $\overline{R}$ at $t = 80$.

Figure 18. Cross stream variations of $\overline{r}$ at $t = 60$.

Figure 19. Cross stream variations of $\overline{r}$ at $t = 80$.

Acknowledgments

This work is sponsored by the U.S. Air Force Office of Scientific Research under Grant F49620-00-1-0035 to SUNY-Buffalo and Grant F49620-00-1-0171 to Cornell University. Dr. Julian M. Tishkoff is the Program Manager for both these grants. Additional support for the work at SUNY-Buffalo is provided by the NASA Langley Research Center under Grant NAG-1-2238 with Dr. J. Philip Drummond as the Technical Monitor. Computational resources are provided by the NCSA at the University of Illinois at Urbana and by the CCR at SUNY-Buffalo.

---

[1] Pope, S. B., *Turbulent Flows*, Cambridge University Press, Cambridge, UK, 2000.

[2] Pope, S. B., Computations of Turbulent Combustion: Progress and Challenges, *Proc. Combust. Inst.*, **23**:591–612 (1990).

[3] Madnia, C. K. and Givi, P., Direct Numerical Simulation and Large Eddy Simulation of Reacting Homogeneous Turbulence, in Galperin, B. and Orszag, S. A., editors, *Large Eddy Simulations of Complex Engineering and Geophysical Flows*, chapter 15, pp. 315–346, Cambridge University Press, Cambridge, England, 1993.

[4] Gao, F. and O'Brien, E. E., A Large-Eddy Simulation Scheme for Turbulent Reacting Flows, *Phys. Fluids A*, **5**(6):1282–1284 (1993).

[5] Frankel, S. H., Adumitroaie, V., Madnia, C. K., and Givi, P., Large Eddy Simulations of Turbulent Reacting Flows by Assumed PDF Methods, in Ragab, S. A. and Piomelli, U., editors, *Engineering Applications of Large Eddy Simulations*, pp. 81–101, ASME, FED-Vol. 162, New York, NY, 1993.

[6] Cook, A. W. and Riley, J. J., A Subgrid Model for Equilibrium Chemistry in Turbulent Flows, *Phys. Fluids*, **6**(8):2868–2870 (1994).

[7] Colucci, P. J., Jaberi, F. A., Givi, P., and Pope, S. B., Filtered Density Function for Large Eddy Simulation of Turbulent Reacting Flows, *Phys. Fluids*, **10**(2):499–515 (1998).

[8] Réveillon, J. and Vervisch, L., Subgrid-Scale Turbulent Micromixing: Dynamic Approach, *AIAA J.*, **36**(3):336–341 (1998).

[9] Jaberi, F. A., Colucci, P. J., James, S., Givi, P., and Pope, S. B., Filtered Mass Density Function for Large Eddy Simulation of Turbulent Reacting Flows, *J. Fluid Mech.*, **401**:85-121 (1999).

[10] Garrick, S. C., Jaberi, F. A., and Givi, P., Large Eddy Simulation of Scalar Transport in a Turbulent Jet Flow, in Knight, D. and Sakell, L., editors, *Recent Advances in DNS and LES*, *Fluid Mechanics and its Applications*, Vol. 54, pp. 155–166, Kluwer Academic Publishers, The Netherlands, 1999.

[11] James, S. and Jaberi, F. A., Large Scale Simulations of Two-Dimensional Nonpremixed Methane Jet Flames, *Combust. Flame*, **123**:465–487 (2000).

[12] Zhou, X. Y. and Pereira, J. C. F., Large Eddy Simulation (2D) of a Reacting Plan Mixing Layer Using Filtered Density Function, *Flow, Turbulence and Combustion*, **64**:279–300 (2000).

[13] Luo, K. H., DNS and LES of Turbulence-Combustion Interactions, In Geurts [24], chapter 14, pp. 263–293.

[14] Poinsot, T. and Veynante, D., *Theoretical and Numerical Combustion*, R. T. Edwards, Inc., Philadelphia, PA, 2001.

[15] Tong, C., Measurements of Conserved Scalar Filtered Density Function in a Turbulent Jet, *Phys. Fluids*, **13**(10):2923–2937 (2001).

[16] Gicquel, L. Y. M., Givi, P., Jaberi, F. A., and Pope, S. B., Velocity Filtered Density Function for Large Eddy Simulation of Turbulent Flows, *Phys. Fluids*, **14**(3):1196–1213 (2002).

[17] Givi, P., A Review of Modern Developments in Large Eddy Simulation of Turbulent Reacting Flows, in Liu, C., Sakell, L., and Herklotz, R., editors, *DNS/LES-Progress and Challenges*, pp. 81–92, Greyden Press, Columbus, OH, 2001.

[18] Smagorinsky, J., General Circulation Experiments With the Primitive Equations. I. The Basic Experiment, *Monthly Weather Review*, **91**(3):99–164 (1963).

[19] Libby, P. A. and Williams, F. A., editors, *Turbulent Reacting Flows*, *Topics in Applied Physics*, Vol. 44, Springer-Verlag, Heidelberg, 1980.

[20] Pope, S. B., PDF Methods for Turbulent Reactive Flows, *Prog. Energy Combust. Sci.*, **11**:119–192 (1985).

[21] Bilger, R. W., Molecular Transport Effects in Turbulent Diffusion Flames at Moderate

Reynolds Number, *AIAA J.*, **20**:962–970 (1982).

[22] Piomelli, U., Large-Eddy Simulation: Achievements and Challenges, *Progress in Aerospace Sciences*, **35**:335–362 (1999).

[23] Meneveau, C. and Katz, J., Scale-Invariance and Turbulence Models for Large-Eddy Simulations, *Ann. Rev. Fluid Mech.*, **32**:1–32 (2000).

[24] Geurts, B. J., editor, *Modern Simulation Strategies for Turbulent Flow*, R. T. Edwards, Inc., Philadelphia, PA, 2001.

[25] Sagaut, P., *Large Eddy Simulation for Incompressible Flows*, Springer, New York, 2001.

[26] O'Brien, E. E., The Probability Density Function (PDF) Approach to Reacting Turbulent Flows, In Libby and Williams [19], chapter 5, pp. 185–218.

[27] Vreman, B., Geurts, B., and Kuerten, H., Realizability Conditions for the Turbulent Stress Tensor in Large-Eddy Simulation, *J. Fluid Mech.*, **278**:351–362 (1994).

[28] Karlin, S. and Taylor, H. M., *A Second Course in Stochastic Processes*, Academic Press, New York, NY, 1981.

[29] Wax, N., *Selected Papers on Noise and Stochastic Processes*, Dover Publications, Inc., New York, NY, 1954.

[30] Gardiner, C. W., *Handbook of Stochastic Methods*, Springer-Verlag, New York, NY, 1990.

[31] Haworth, D. C. and Pope, S. B., A Generalized Langevin Model for Turbulent Flows, *Phys. Fluids*, **29**(2):387–405 (1986).

[32] Dreeben, T. D. and Pope, S. B., Probability Density Function and Reynolds-Stress Modeling of Near-Wall Turbulent Flows, *Phys. Fluids*, **9**(1):154–163 (1997).

[33] Risken, H., *The Fokker-Planck Equation, Methods of Solution and Applications*, Springer-Verlag, New York, NY, 1989.

[34] Pope, S. B., Mean Field Equations in PDF Particle Methods for Turbulent Reactive Flows, Technical Report FDA 97-06, Cornell University, Ithaca, NY, 1997.

[35] Muradoglu, M., Jenny, P., Pope, S. B., and Caughey, D. A., A Consistent Hybrid-Volume/Particle Method for the PDF Equations of Turbulent Reactive Flows, *J. Comp. Phys.*, **154**(2):342–371 (1999).

[36] Muradoglu, M., Pope, S. B., and Caughey, D. A., The Hybrid Method for the PDF Equations of Turbulent Reactive Flows: Consistency Conditions and Correction Algorithms, *J. Comp. Phys.*, **172**:841–878 (2001).

[37] Kloeden, P. E., Platen, E., and Schurz, H., *Numerical Solution of Stochastic Differential Equations through Computer Experiments*, Springer-Verlag, New York, NY, corrected second printing edition, 1997.

[38] Gikhman, I. I. and Skorokhod, A. V., *Stochastic Differential Equations*, Springer-Verlag, New York, NY, 1972.

[39] Carpenter, M. H., A High-Order Compact Numerical Algorithm for Supersonic Flows. in Morton, K. W., editor, *Twelfth International Conference on Numerical Methods in Fluid Dynamics, Lecture Notes in Physics*, Vol. 371, pp. 254–258, Springer-Verlag, New York, NY, 1990.

[40] Kennedy, C. A. and Carpenter, M. H., Several New Numerical Methods for Compressible Shear-Layer Simulations, *Appl. Num. Math.*, **14**:397–433 (1994).

[41] Riley, J. J. and Metcalfe, R. W., Direct Numerical Simulations of a Perturbed, Turbulent Mixing Layer, AIAA Paper 80-0274, 1980.

[42] Sandham, N. D. and Reynolds, W. C., Three-Dimensional Simulations of Large Eddies in the Compressible Mixing Layer, *J. Fluid Mech.*, **224**:133–158 (1991).

[43] Moser, R. D. and Rogers, M. M., The Three-Dimensional Evolution of a Plane Mixing Layer: Pairing and Transition to Turbulence, *J. Fluid Mech.*, **247**:275–320 (1993).

[44] Vreman, B., Geurts, B., and Kuerten, H., Large-Eddy Simulation of the Turbulent Mixing Layer, *J. Fluid Mech.*, **339**:357–390 (1997).

[45] Metcalfe, R. W., Orszag, S. A., Brachet, M. E., Menon, S., and Riley, J. J., Secondary Instabilities of a Temporally Growing Mixing Layer, *J. Fluid Mech.*, **184**:207–243 (1987).

[46] Lin, S. J. and Corcos, G. M., The Mixing Layer: Deterministic Models of a Turbulent Flow. Part 3. The Effect of Plane Strain on the Dynamics of Streamwise Vortices, *J. Fluid Mech.*, **141**:139–178 (1984).

[47] Moser, R. D. and Rogers, M. M., The Three-Dimensional Evolution of a Plane Mixing Layer: the Kelvin-Helmholtz Rollup, *J. Fluid Mech.*, **243**:183–226 (1992).

[48] Moser, R. D. and Rogers, M. M., Spanwise Scale Selection in Plane Mixing Layers, *J. Fluid Mech.*, **247**:321–337 (1993).

[49] Erlebacher, G., Hussaini, M. Y., Speziale, C. G., and Zang, T. A., Toward the Large Eddy Simulation of Compressible Turbulent Flows, *J. Fluid Mech.*, **238**:155–185 (1992).

[50] Pope, S. B., On the Relation Between Stochastic Lagrangian Models of Turbulence and

Second-Moment Closures, *Phys. Fluids*, **6**(2):973–985 (1994).

[51] Rogallo, R. S. and Moin, P., Numerical Simulation of Turbulent Flow, *Ann. Rev. Fluid Mech.*, **16**:99–137 (1984).

[52] Bilger, R. W., Future Progress in Turbulent Combustion Research, *Prog. Energy Combust. Sci.*, **26**(4-6):367–380 (2000).

[53] Peters, N., *Turbulent Combustion*, Cambridge University Press, Cambridge, UK, 2000.

	LES-FD variables	VSFDF variables	VSFDF quantities used by the LES-FD system	LES-FD quantities used by the VSFDF system	Redundant quantities
VSFDF	$\langle p \rangle$, $\langle u_i \rangle$	X_i^+	$\tau(u_i, u_j)$	$\langle u_i \rangle$, $\frac{\partial \langle p \rangle}{\partial x_i}$	$\langle u_i \rangle$
	$\langle \phi_\alpha \rangle$	U_i^+	$\tau(u_i, \phi_\alpha)$	$\frac{\partial \langle u_i \rangle}{\partial x_k}$, $\frac{\partial^2 \langle u_i \rangle}{\partial x_k \partial x_k}$	$\langle \phi_\alpha \rangle$
		ϕ_α^+	$\langle S_\alpha(\boldsymbol{\phi}) \rangle$	$\langle \phi_\alpha \rangle$	
VSFDF-C	$\langle p \rangle$, $\langle u_i \rangle$	X_i^+	$\tau(u_i, u_j)$	$\langle u_i \rangle$, $\frac{\partial \langle p \rangle}{\partial x_i}$	$\langle u_i \rangle$,$\langle \phi_\alpha \rangle$
	$\langle \phi_\alpha \rangle$	U_i^+	$\tau(u_i, \phi_\alpha)$	$\frac{\partial \langle u_i \rangle}{\partial x_k}$, $\frac{\partial^2 \langle u_i \rangle}{\partial x_k \partial x_k}$	$\tau(u_i, u_j)$
	$\tau(u_i, u_j)$	ϕ_α^+	$\tau(u_i, u_j, u_k)$	$\langle \phi_\alpha \rangle$, k	$\tau(u_i, \phi_\alpha)$
	$\tau(u_i, \phi_\alpha)$		$\tau(u_i, u_j, \phi_\alpha)$		$\tau(\phi_\alpha, \phi_\beta)$
	$\tau(\phi_\alpha, \phi_\beta)$		$\tau(u_i, \phi_\alpha, \phi_\beta)$		

Table 1

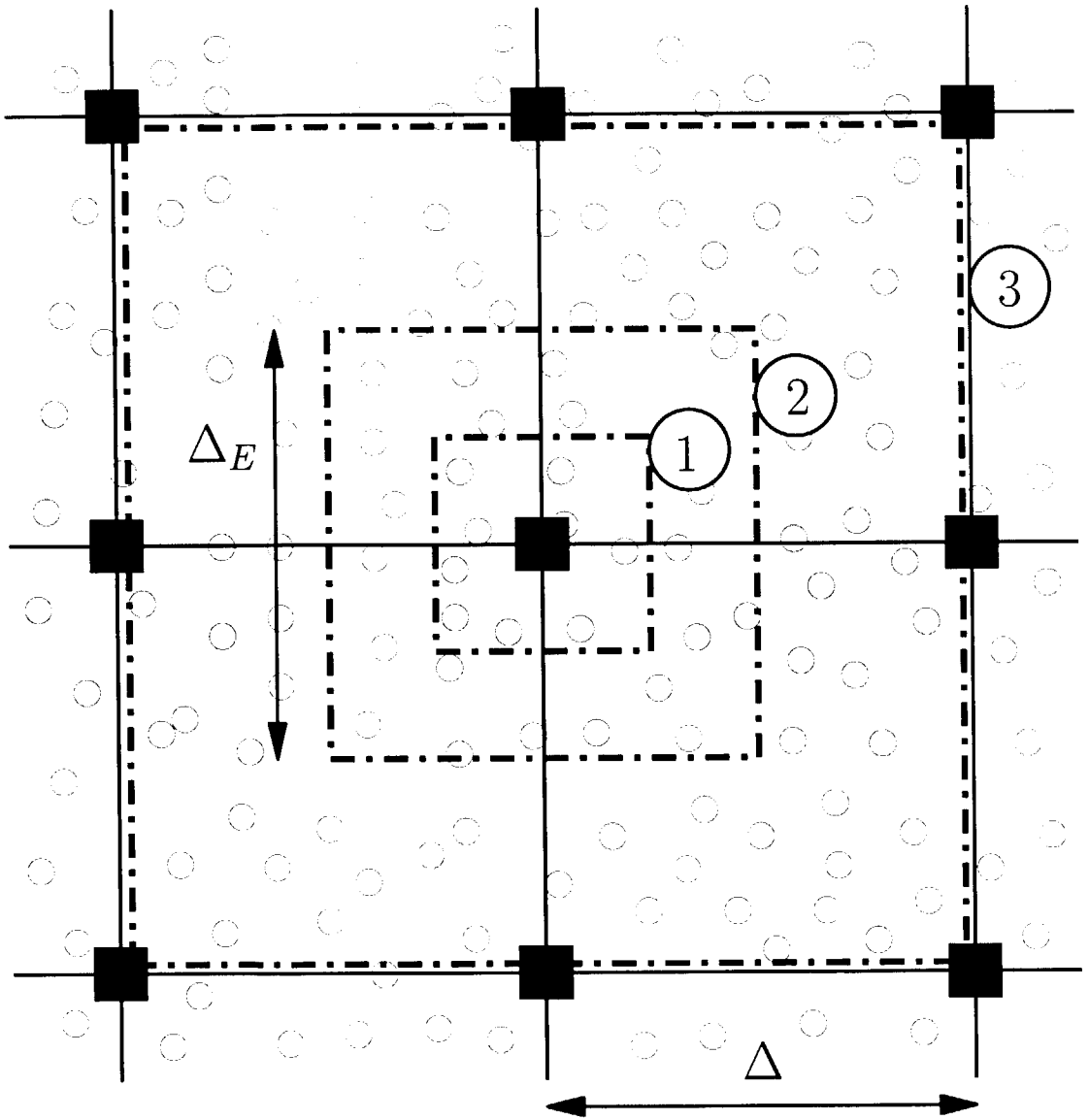

Figure 1

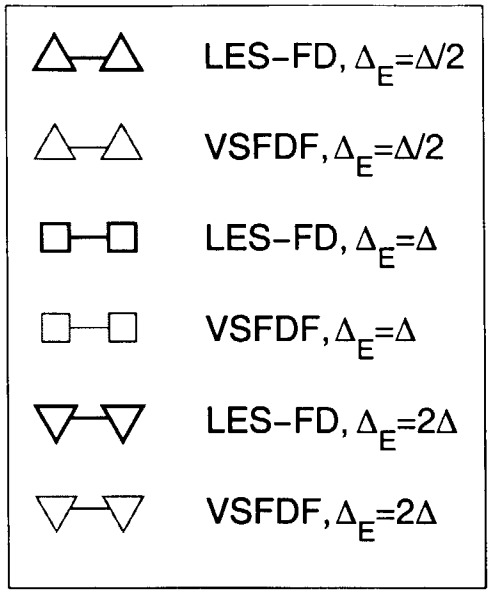
LES-FD, $\Delta_E=\Delta/2$
VSFDF, $\Delta_E=\Delta/2$
LES-FD, $\Delta_E=\Delta$
VSFDF, $\Delta_E=\Delta$
LES-FD, $\Delta_E=2\Delta$
VSFDF, $\Delta_E=2\Delta$

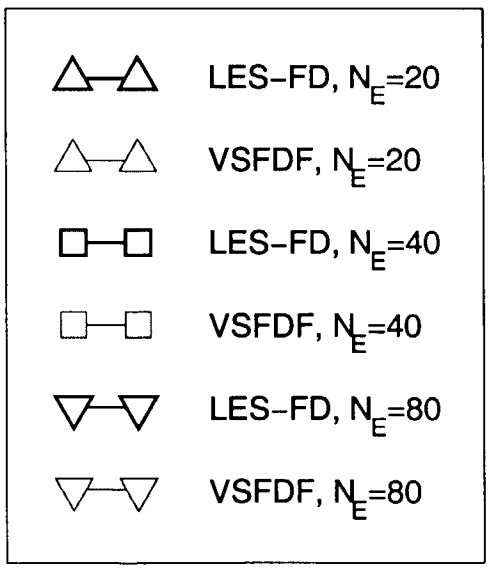
LES-FD, $N_E=20$
VSFDF, $N_E=20$
LES-FD, $N_E=40$
VSFDF, $N_E=40$
LES-FD, $N_E=80$
VSFDF, $N_E=80$

(a)

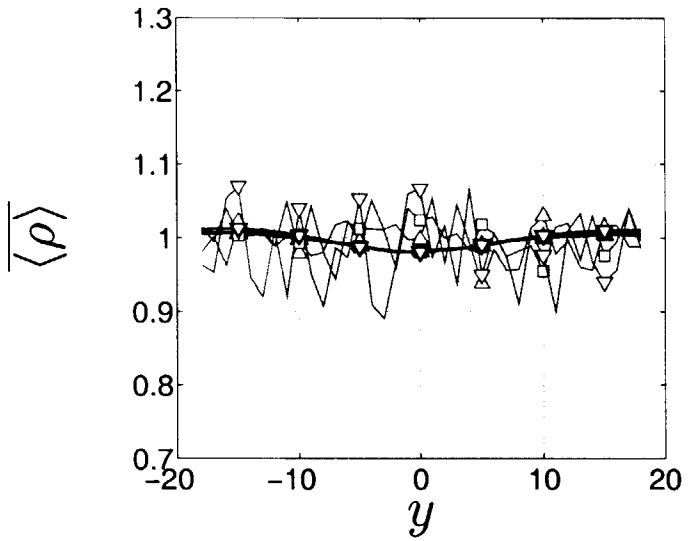
1.3
1.2
1.1
1
0.9
0.8
0.7
$\langle\rho\rangle$
−20
−10
0
10
20
y

(b)

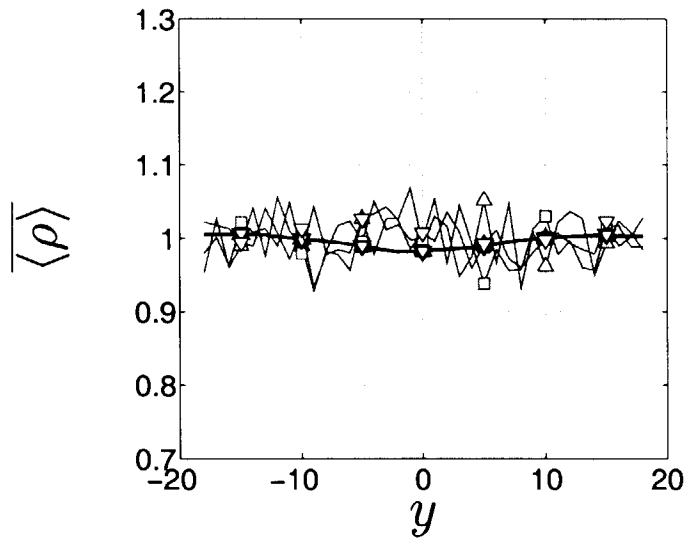
1.3
1.2
1.1
1
0.9
0.8
0.7
$\langle\rho\rangle$
−20
−10
0
10
20
y

Figure 2

(a) t=13.98 (b) t=23.94 (c) t=33.90

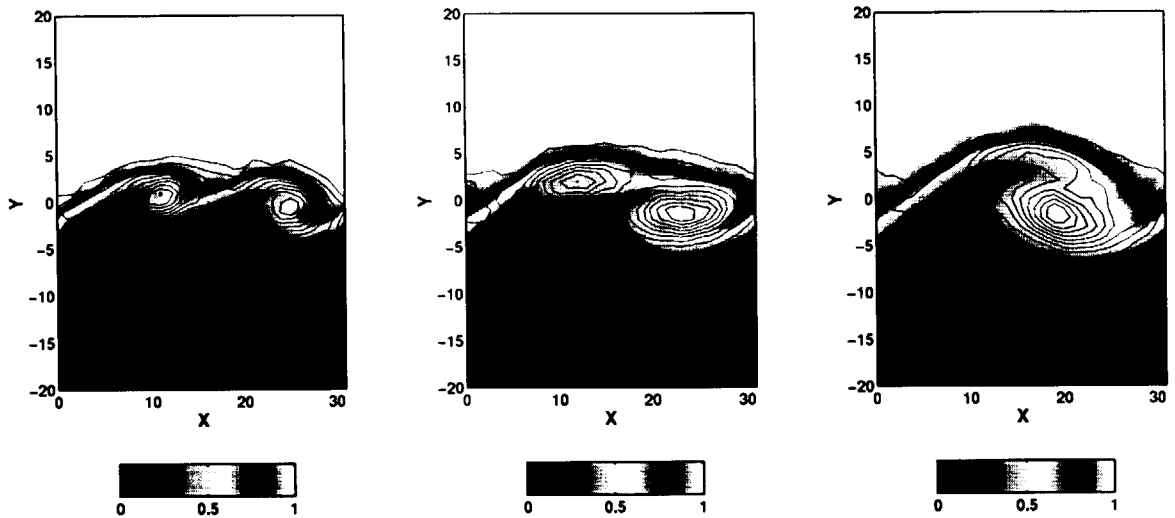

(d) t=13.98 (e) t=23.94 (f) t=33.90

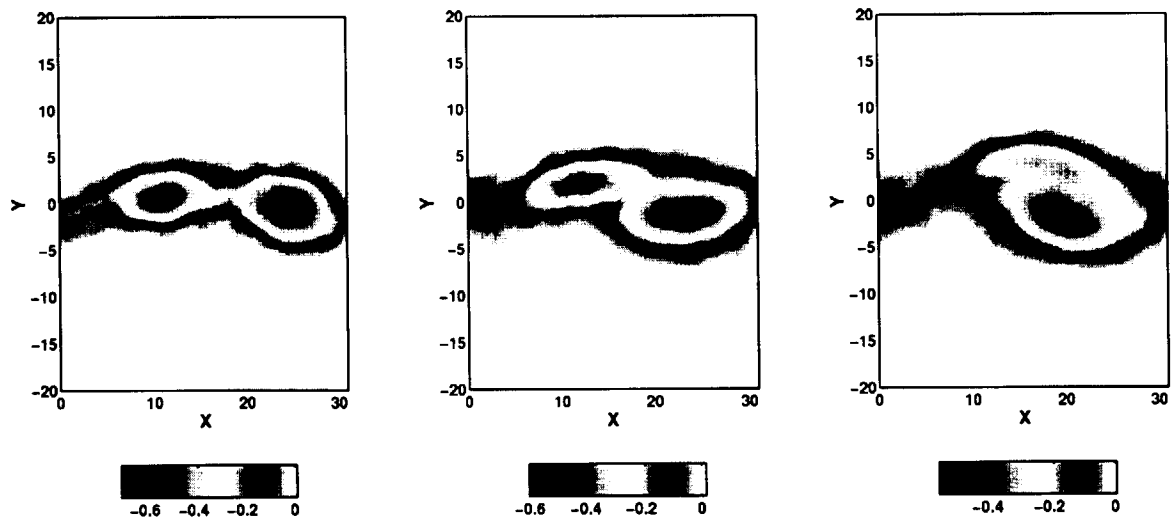

Figure 3

(a) t=13.98 (b) t=23.94 (c) t=33.90

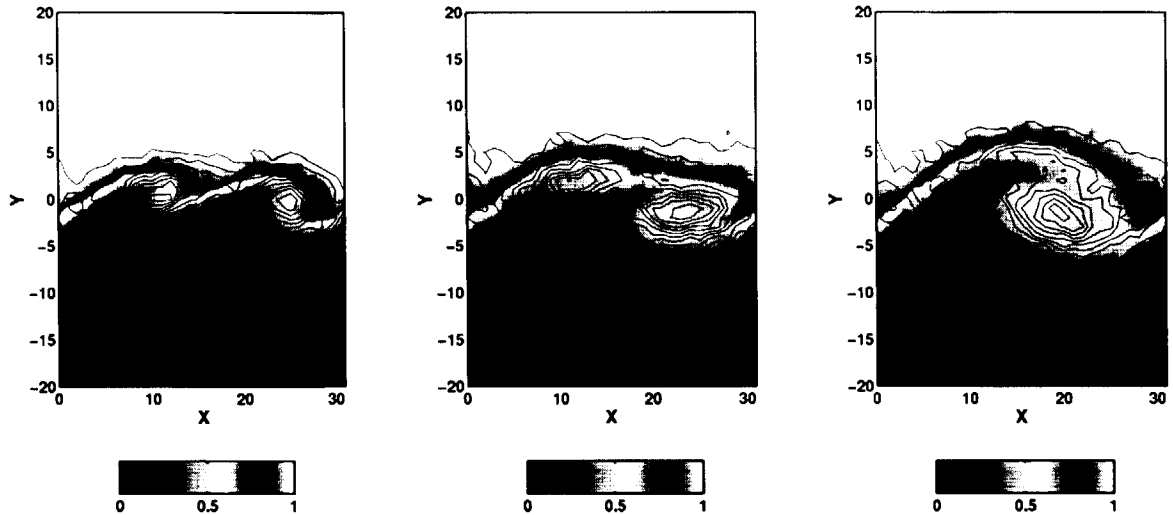

(d) t=13.98 (e) t=23.94 (f) t=33.90

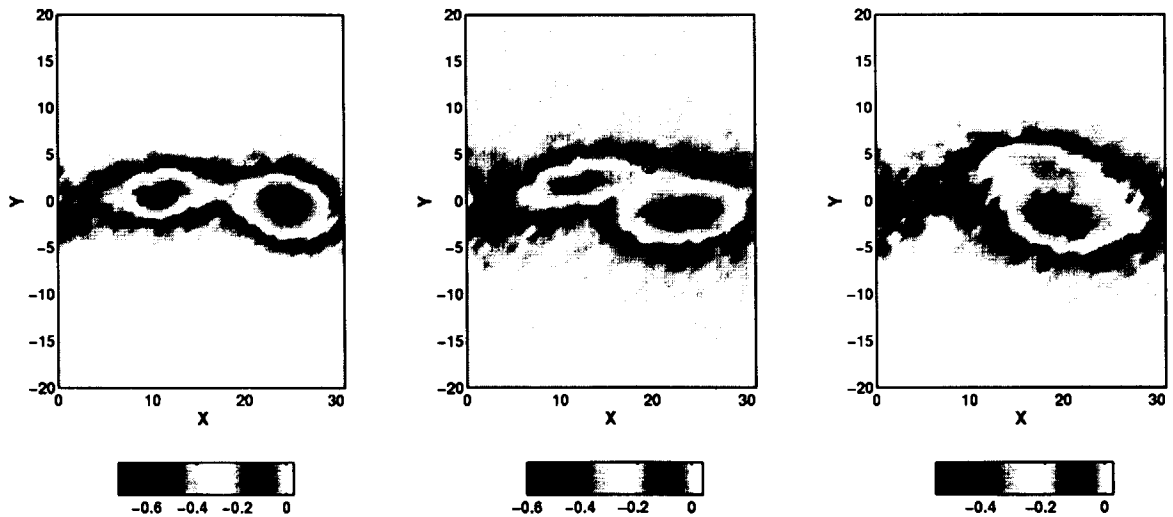

Figure 4

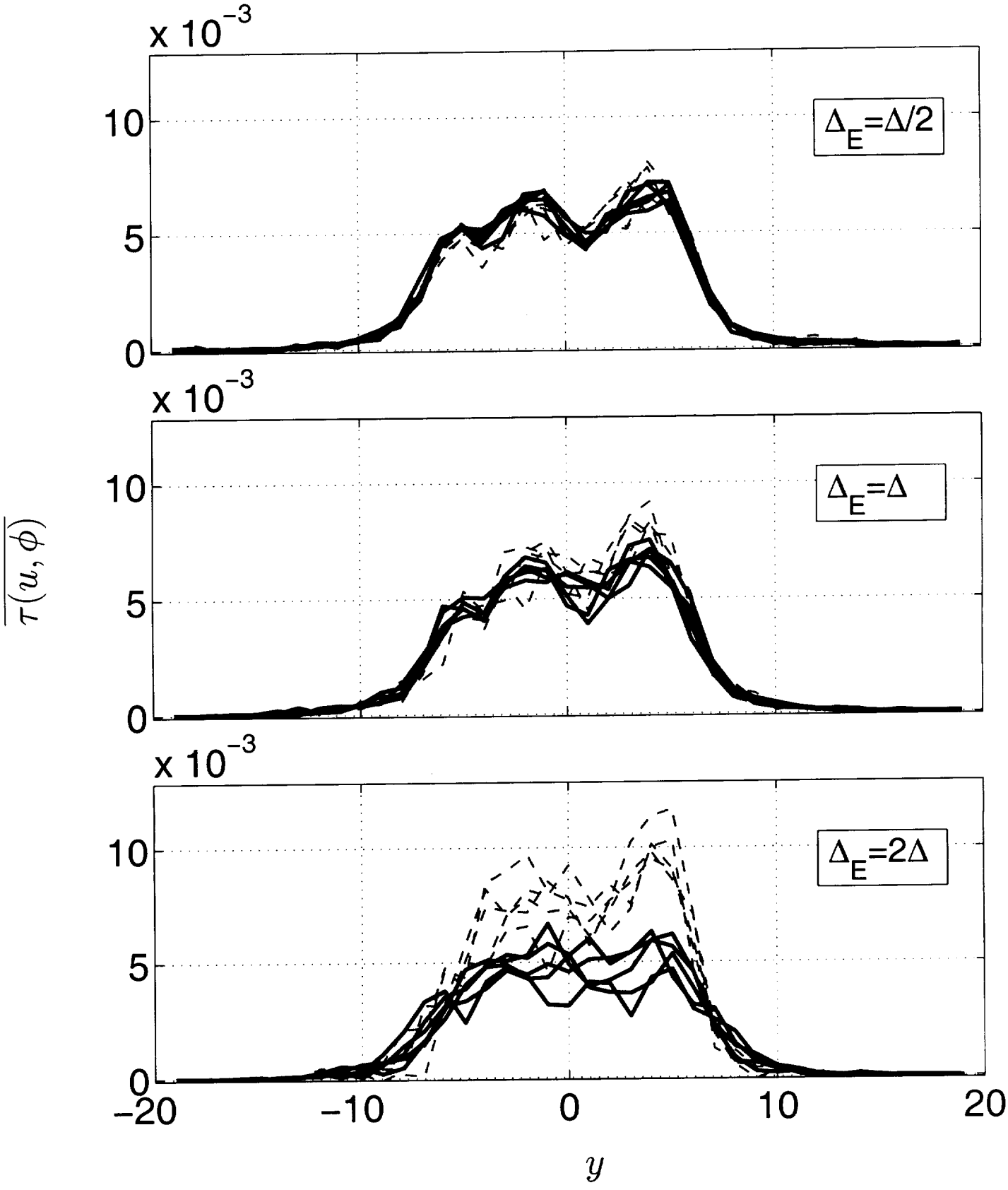

Figure 5

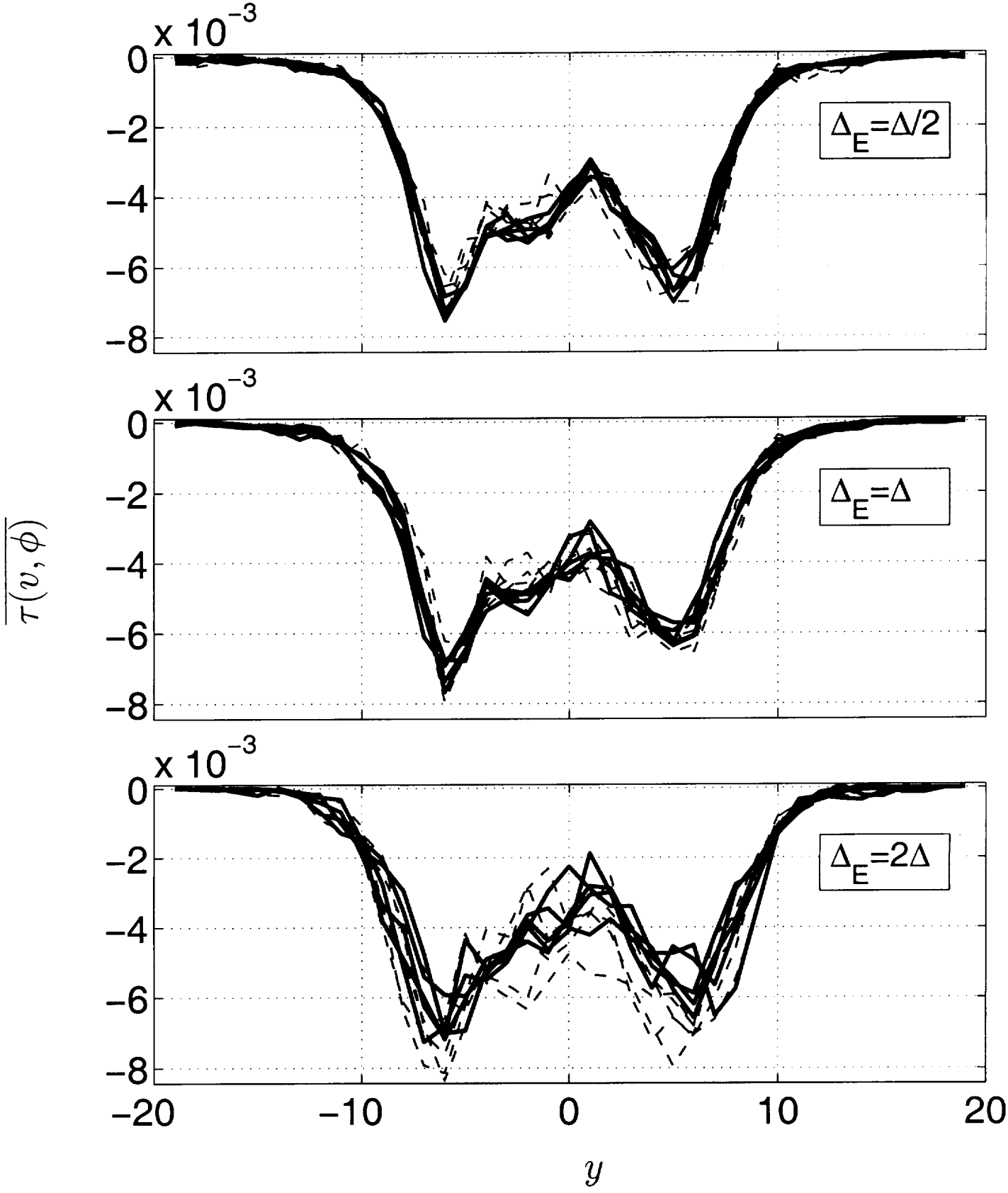

Figure 6

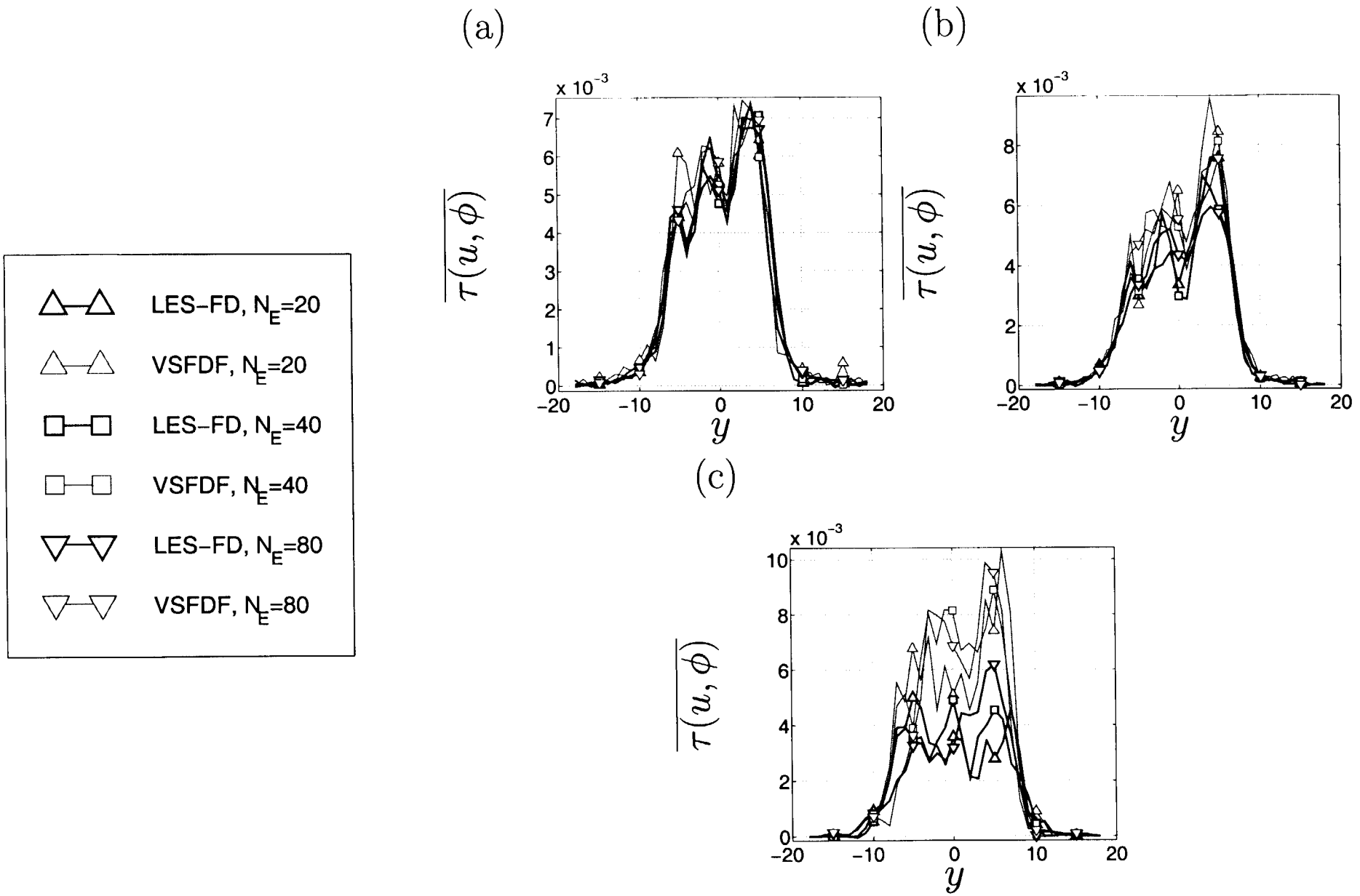
(a)
(b)
(c)
LES–FD, N_E=20
VSFDF, N_E=20
LES–FD, N_E=40
VSFDF, N_E=40
LES–FD, N_E=80
VSFDF, N_E=80
x 10^-3
$\overline{\tau(u,\phi)}$
y

Figure 7

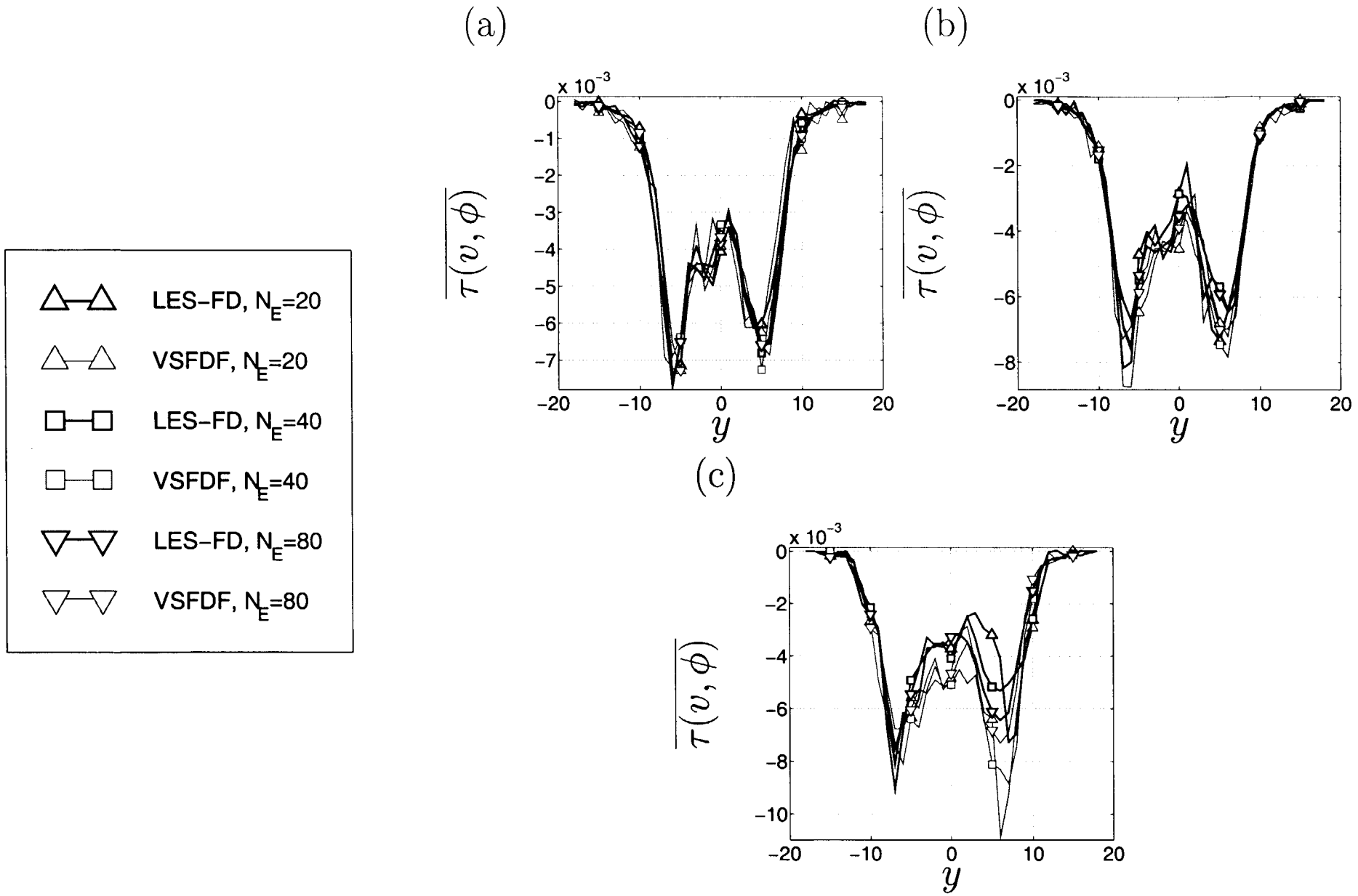
(a)
(b)
(c)
LES–FD, N_E=20
VSFDF, N_E=20
LES–FD, N_E=40
VSFDF, N_E=40
LES–FD, N_E=80
VSFDF, N_E=80
x 10^-3
$\overline{\tau(v,\phi)}$
y

Figure 8

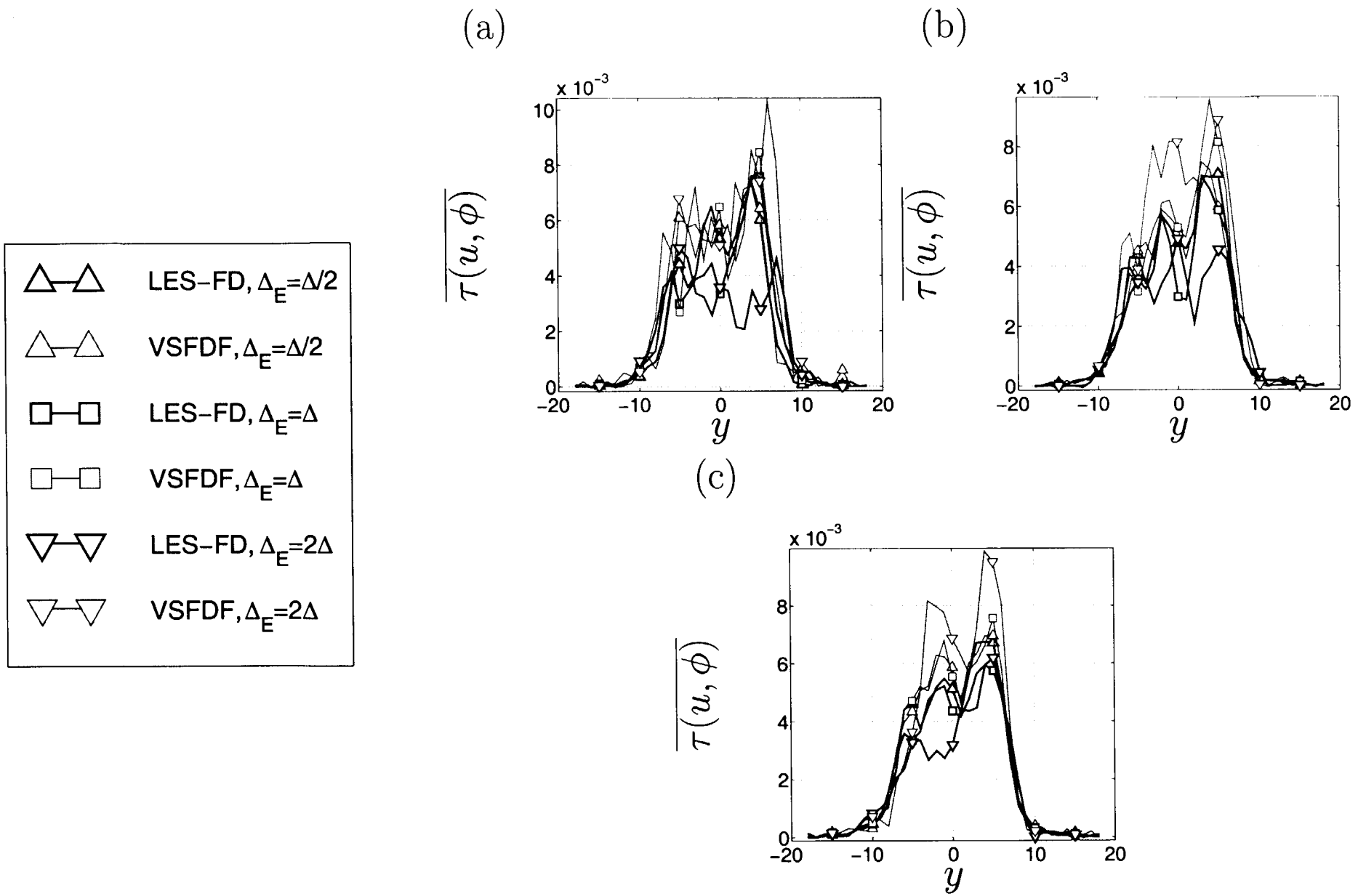
(a)
(b)
(c)
LES–FD, $\Delta_E=\Delta/2$
VSFDF, $\Delta_E=\Delta/2$
LES–FD, $\Delta_E=\Delta$
VSFDF, $\Delta_E=\Delta$
LES–FD, $\Delta_E=2\Delta$
VSFDF, $\Delta_E=2\Delta$
x 10^{-3}
$\overline{\tau(u,\phi)}$
y

Figure 9

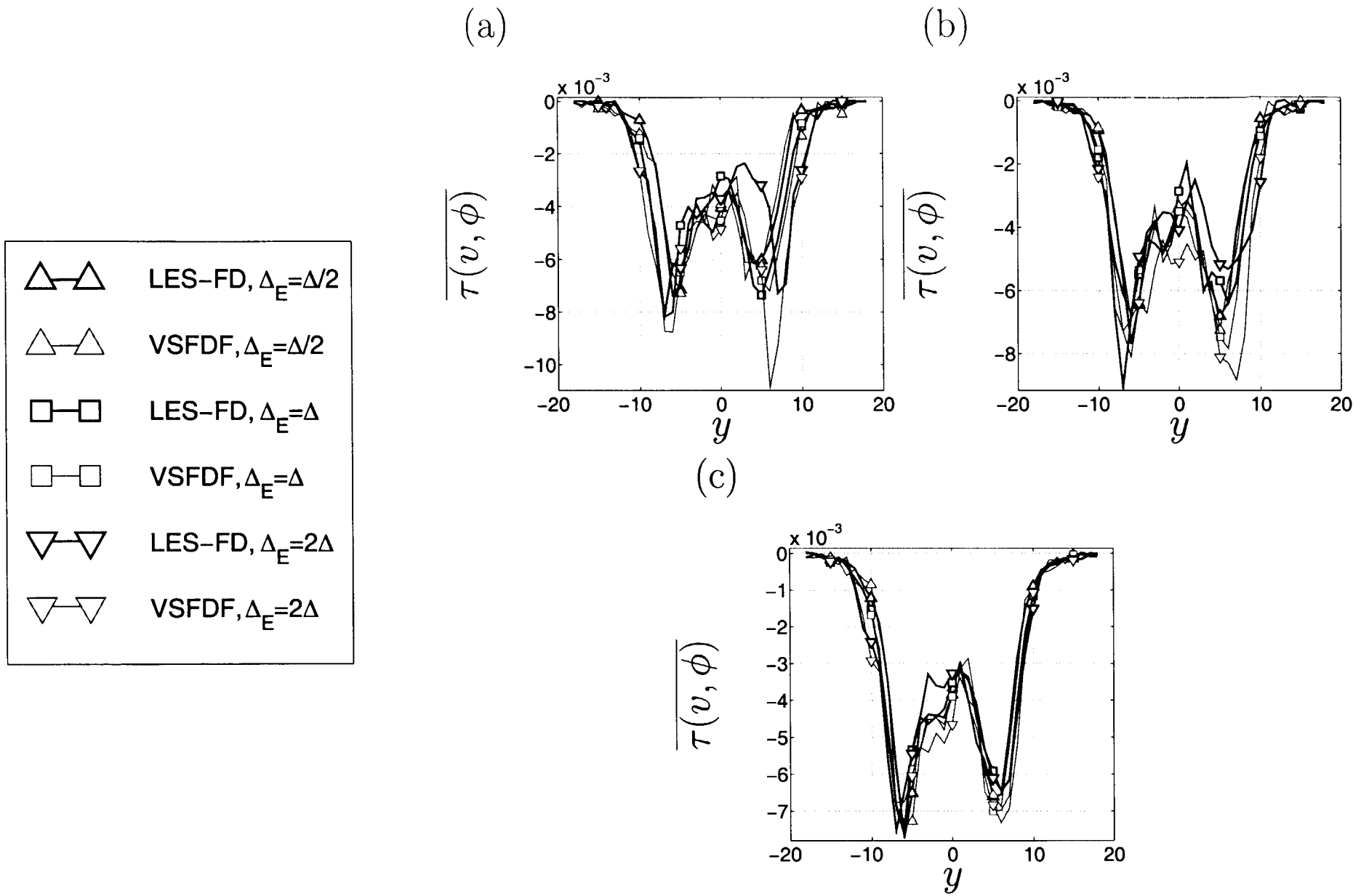
(a)
(b)
(c)
x 10^-3
$\overline{\tau(v,\phi)}$
y
LES–FD, Δ_E=Δ/2
VSFDF, Δ_E=Δ/2
LES–FD, Δ_E=Δ
VSFDF, Δ_E=Δ
LES–FD, Δ_E=2Δ
VSFDF, Δ_E=2Δ

Figure 10

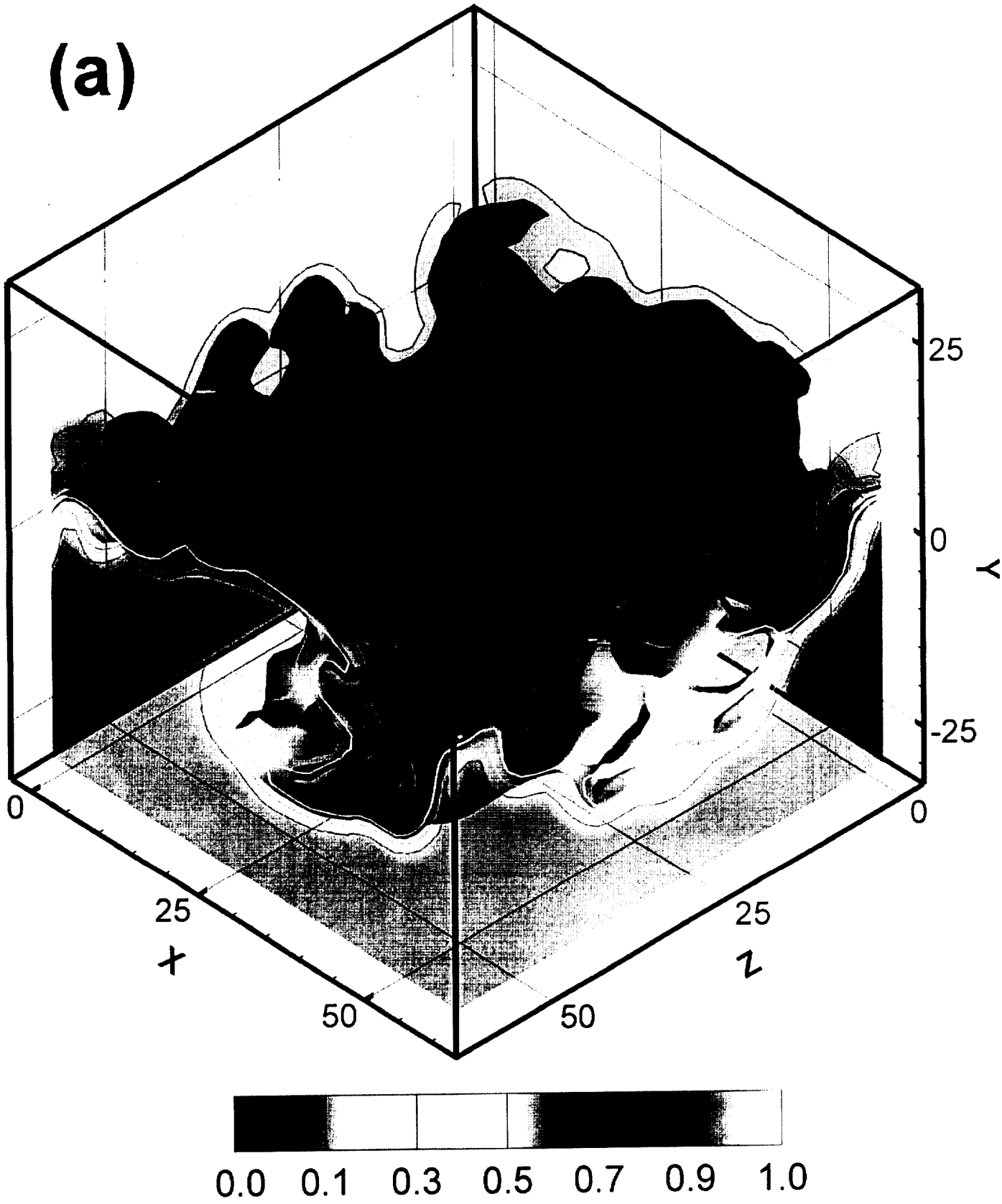

Figure 11

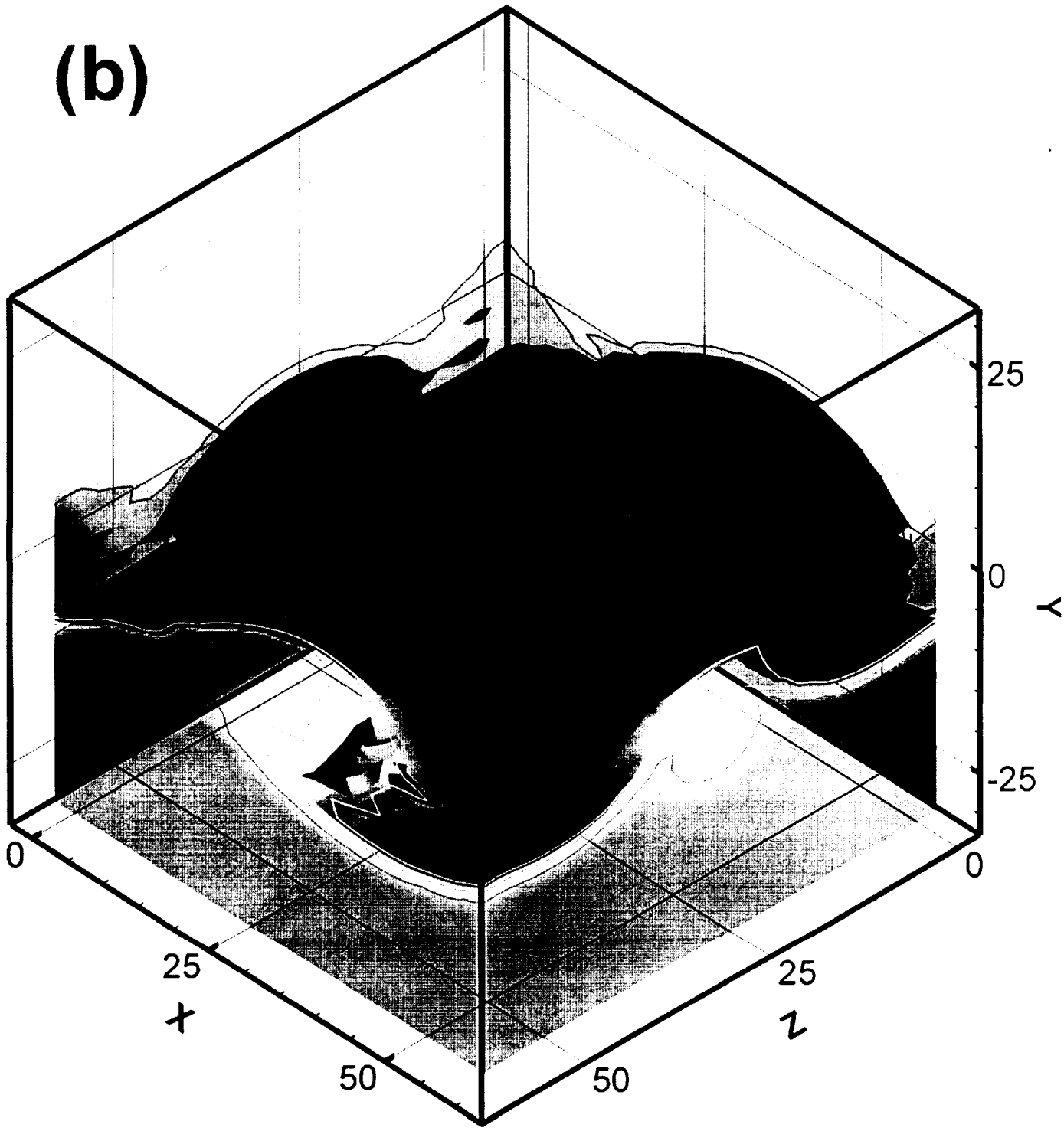
(b)
25
0
-25
y
0
25
50
x
0
25
50
z

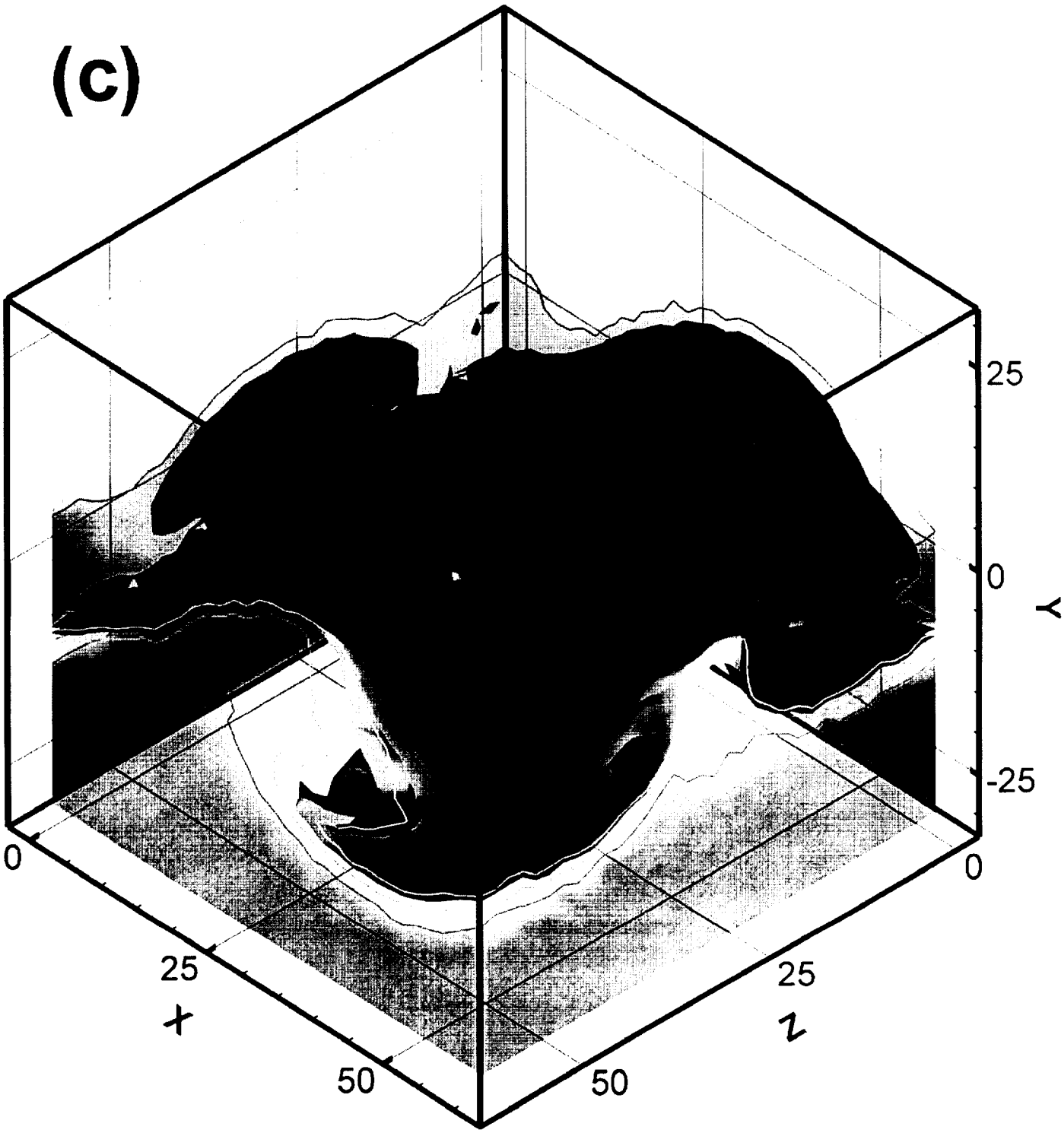
(c)
25
0
-25
Y
0
25
50
x
0
25
50
z

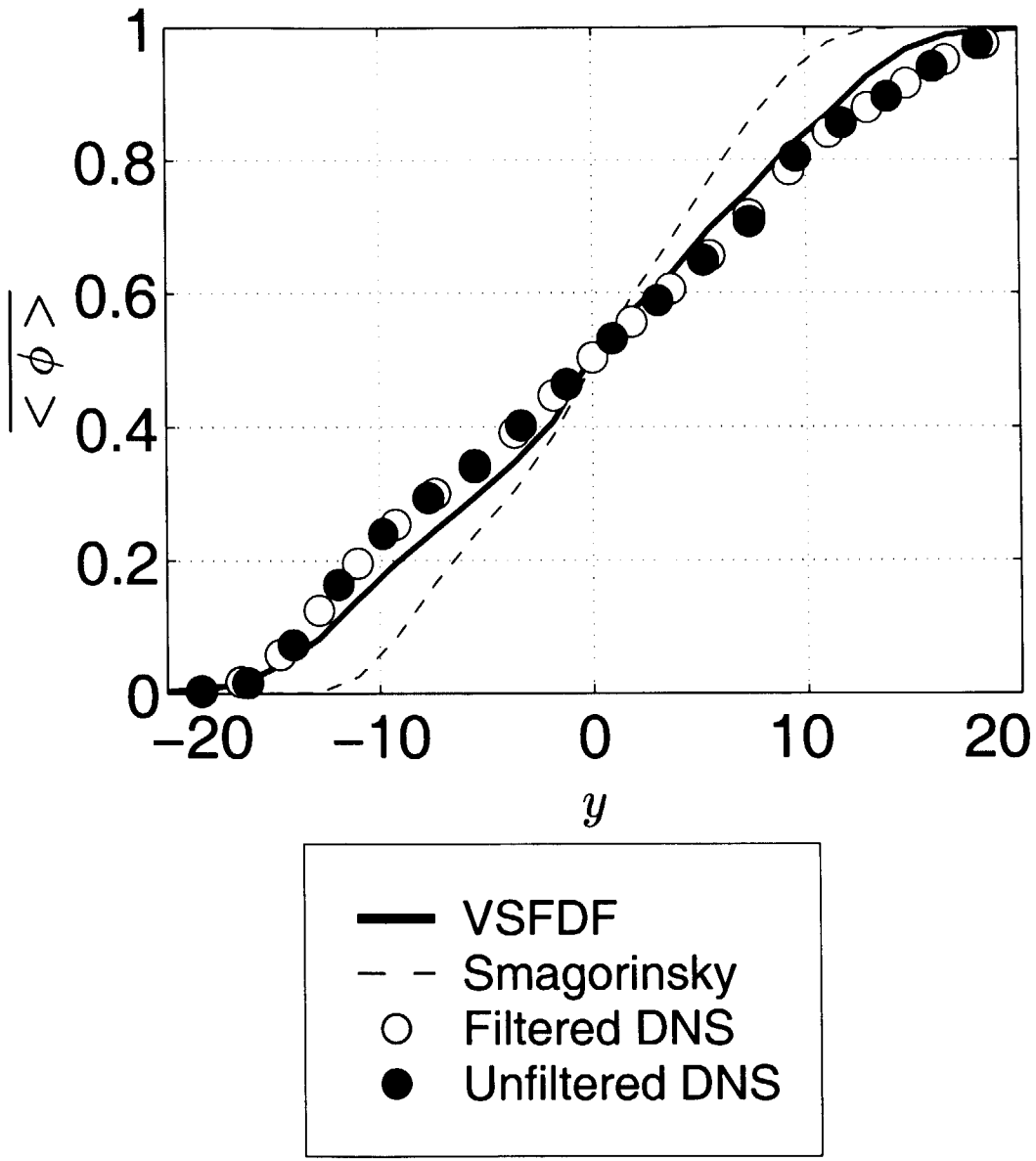
1
0.8
0.6
0.4
0.2
0
$\langle\phi\rangle$
−20
−10
0
10
20
y
VSFDF
Smagorinsky
Filtered DNS
Unfiltered DNS

Figure 12

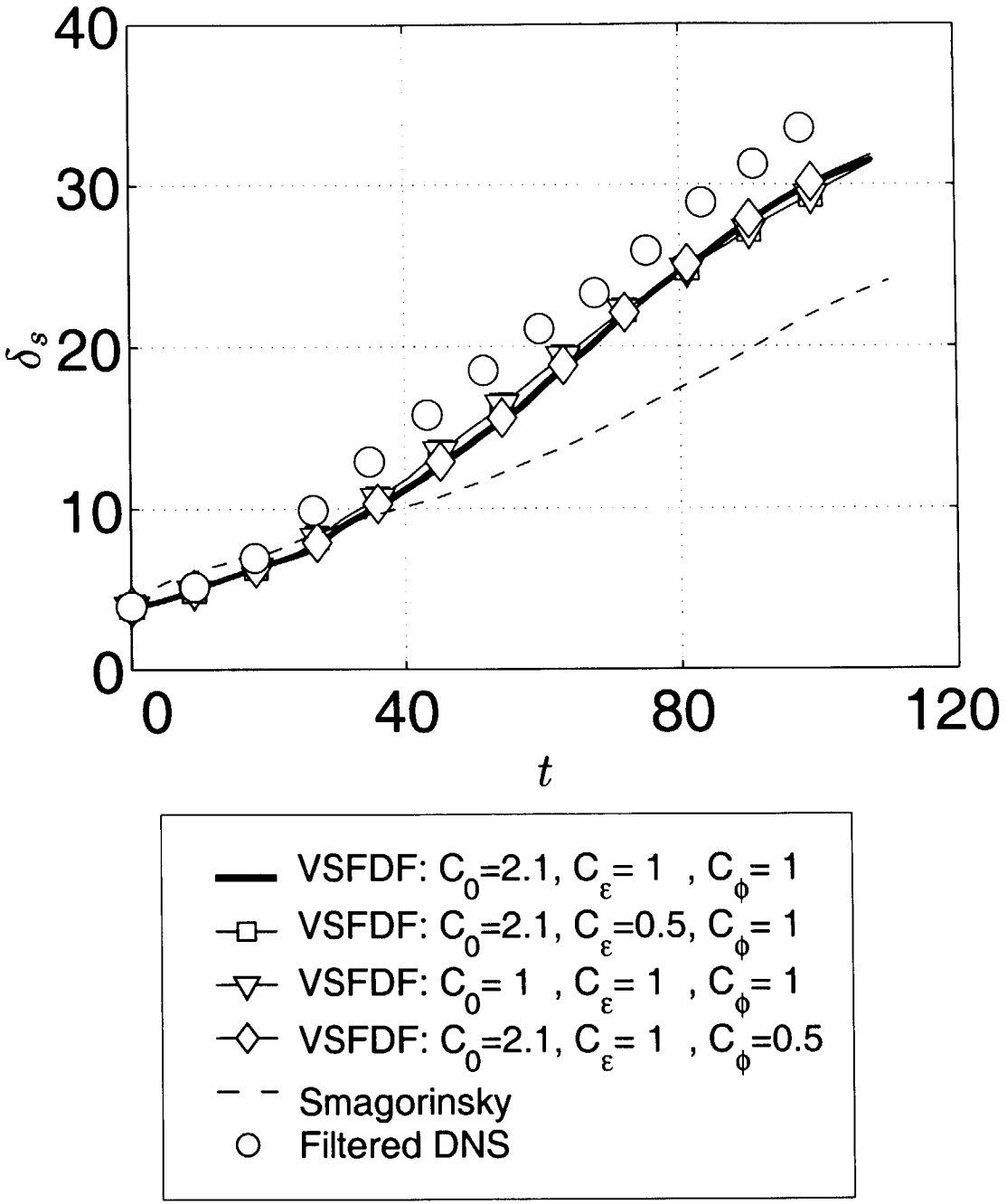
40
30
20
10
0
δ_s
0
40
80
120
t
VSFDF: C_0=2.1, C_ε= 1 , C_ϕ= 1
VSFDF: C_0=2.1, C_ε=0.5, C_ϕ= 1
VSFDF: C_0= 1 , C_ε= 1 , C_ϕ= 1
VSFDF: C_0=2.1, C_ε= 1 , C_ϕ=0.5
Smagorinsky
Filtered DNS

Figure 13

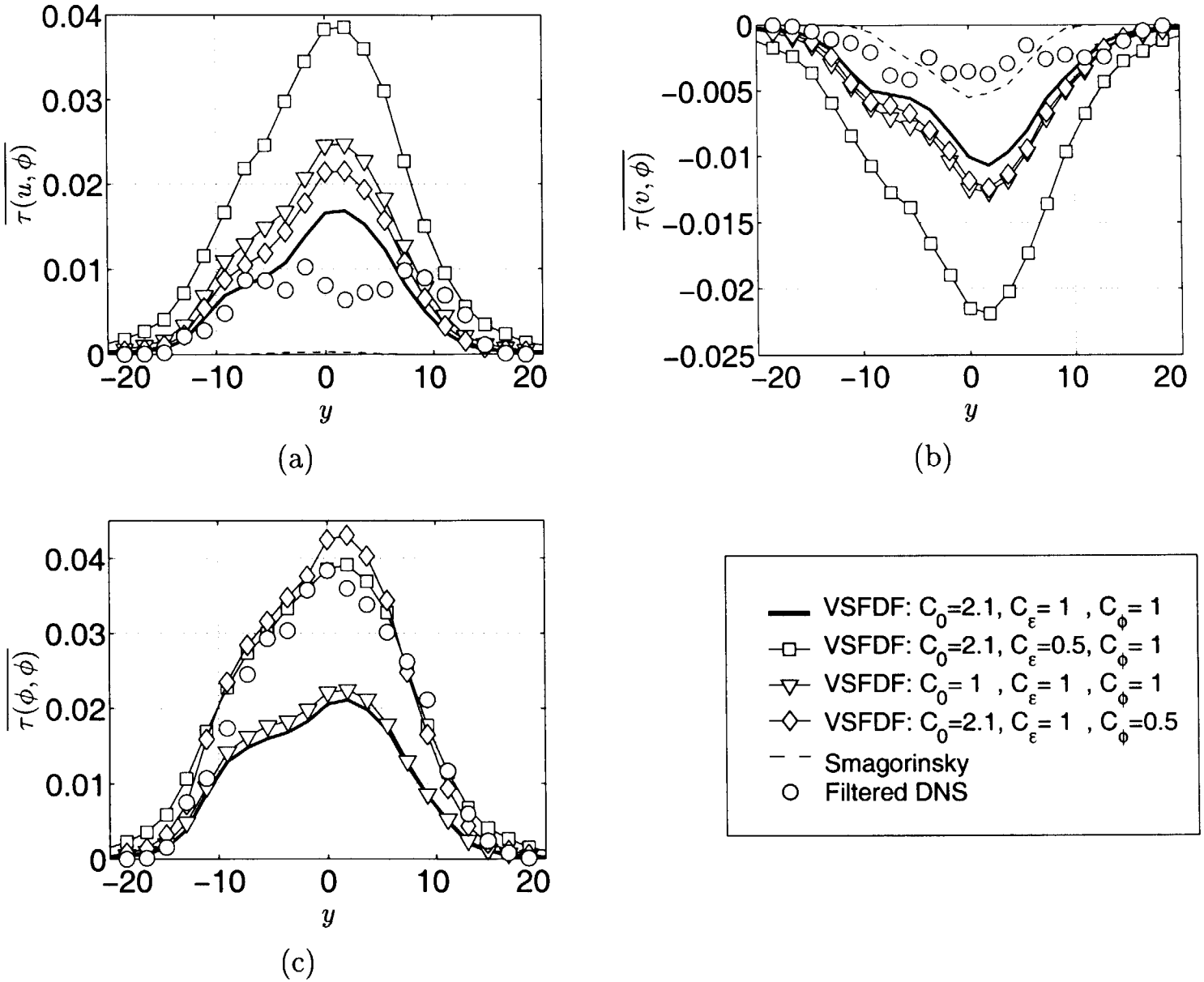
0.04
0.03
0.02
0.01
0
$\overline{\tau(u,\phi)}$
−20
−10
0
10
20
y
(a)
0
−0.005
−0.01
−0.015
−0.02
−0.025
$\overline{\tau(v,\phi)}$
−20
−10
0
10
20
y
(b)
0.04
0.03
0.02
0.01
0
$\overline{\tau(\phi,\phi)}$
−20
−10
0
10
20
y
(c)
VSFDF: C_0=2.1, C_ε= 1 , C_ϕ= 1
VSFDF: C_0=2.1, C_ε=0.5, C_ϕ= 1
VSFDF: C_0= 1 , C_ε= 1 , C_ϕ= 1
VSFDF: C_0=2.1, C_ε= 1 , C_ϕ=0.5
Smagorinsky
Filtered DNS

Figure 14

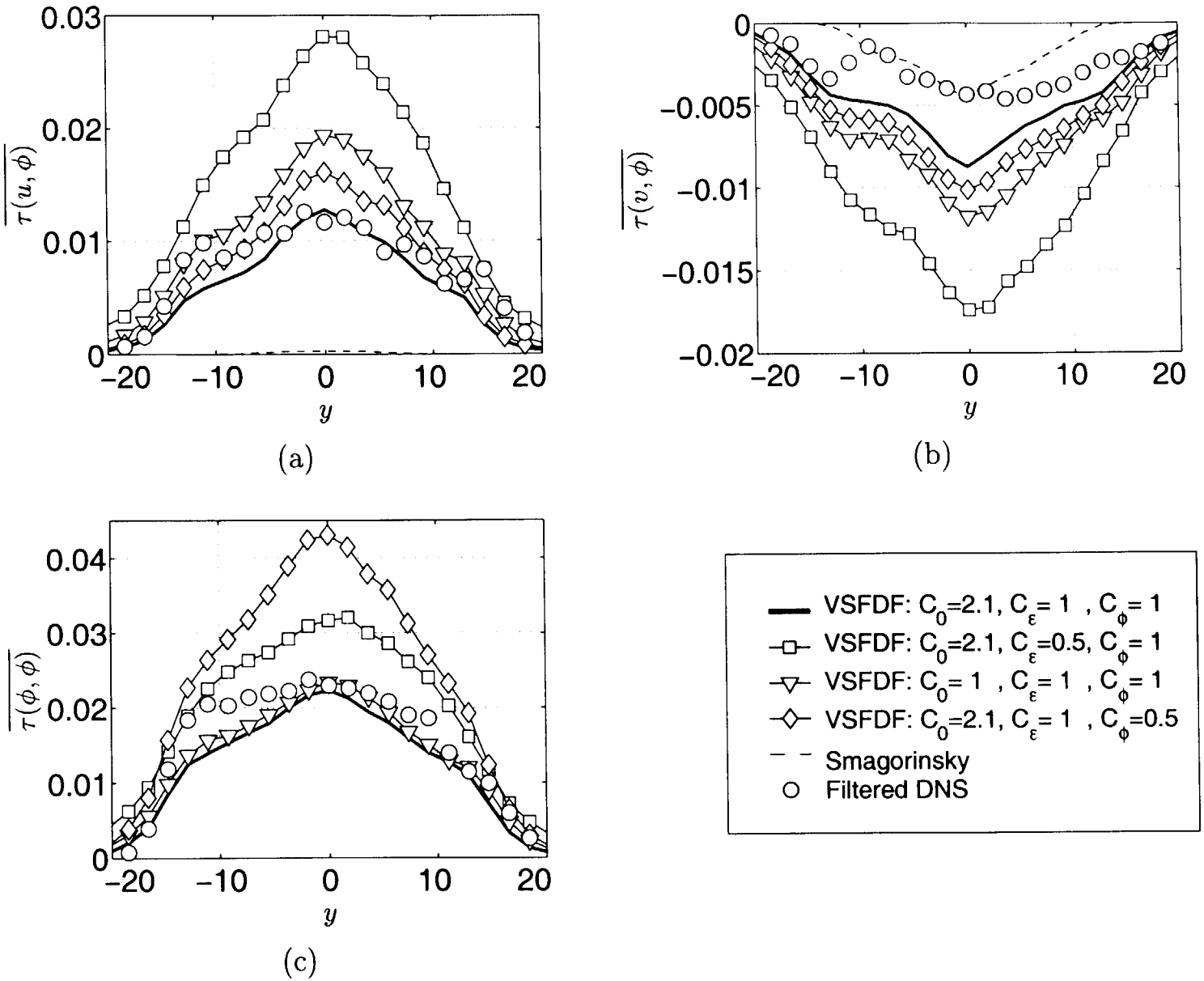
0.03
0.02
0.01
0
$\overline{\tau(u,\phi)}$
−20
−10
0
10
20
y
(a)
0
−0.005
−0.01
−0.015
−0.02
$\overline{\tau(v,\phi)}$
−20
−10
0
10
20
y
(b)
0.04
0.03
0.02
0.01
0
$\overline{\tau(\phi,\phi)}$
−20
−10
0
10
20
y
(c)
VSFDF: C_0=2.1, C_ε= 1 , C_ϕ= 1
VSFDF: C_0=2.1, C_ε=0.5, C_ϕ= 1
VSFDF: C_0= 1 , C_ε= 1 , C_ϕ= 1
VSFDF: C_0=2.1, C_ε= 1 , C_ϕ=0.5
Smagorinsky
Filtered DNS

Figure 15

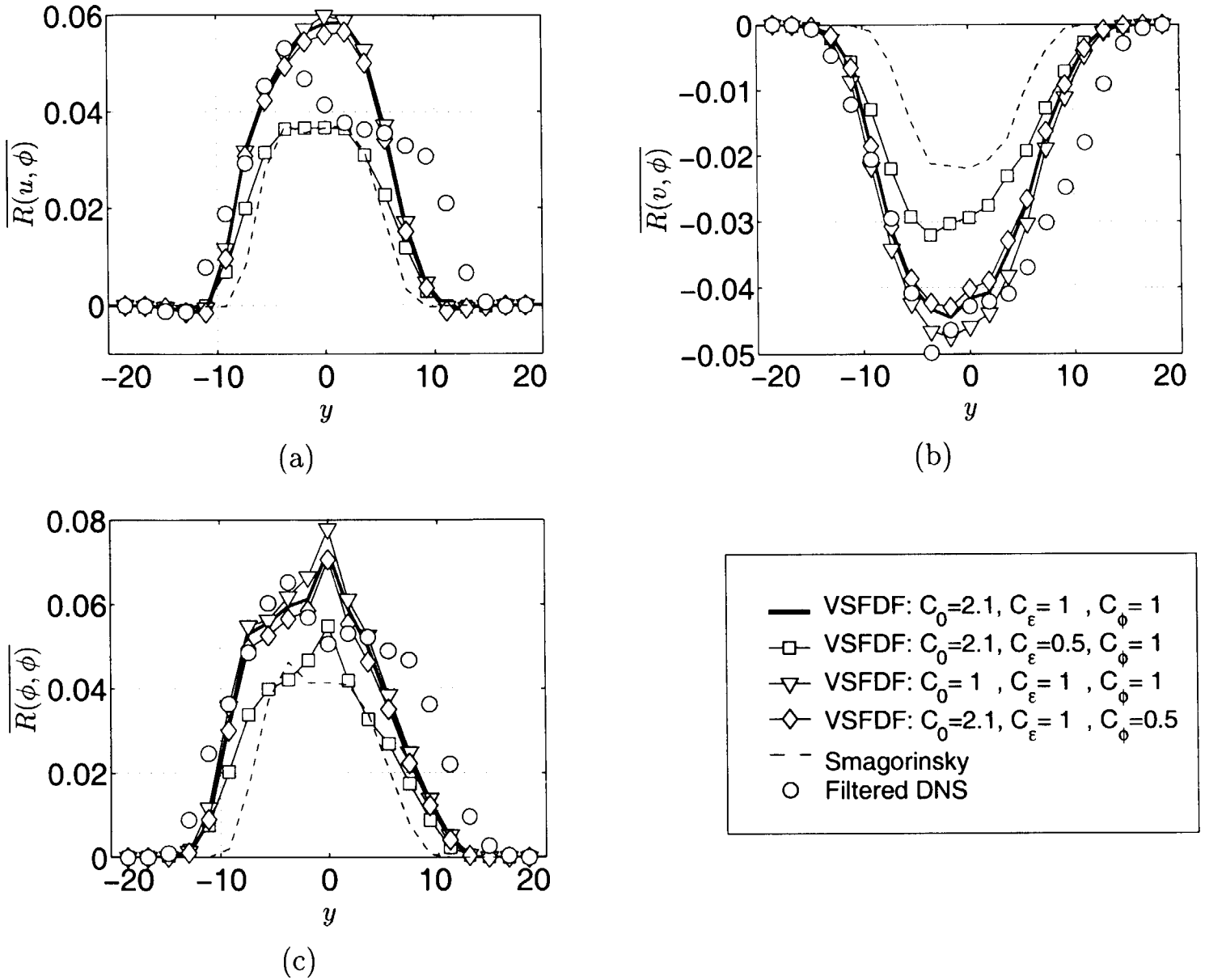
0.06
0.04
0.02
0
$\overline{R(u,\phi)}$
−20
−10
0
10
20
y
(a)
0
−0.01
−0.02
−0.03
−0.04
−0.05
$\overline{R(v,\phi)}$
−20
−10
0
10
20
y
(b)
0.08
0.06
0.04
0.02
0
$\overline{R(\phi,\phi)}$
−20
−10
0
10
20
y
(c)
VSFDF: C_0=2.1, C_ε= 1 , C_ϕ= 1
VSFDF: C_0=2.1, C_ε=0.5, C_ϕ= 1
VSFDF: C_0= 1 , C_ε= 1 , C_ϕ= 1
VSFDF: C_0=2.1, C_ε= 1 , C_ϕ=0.5
Smagorinsky
Filtered DNS

Figure 16

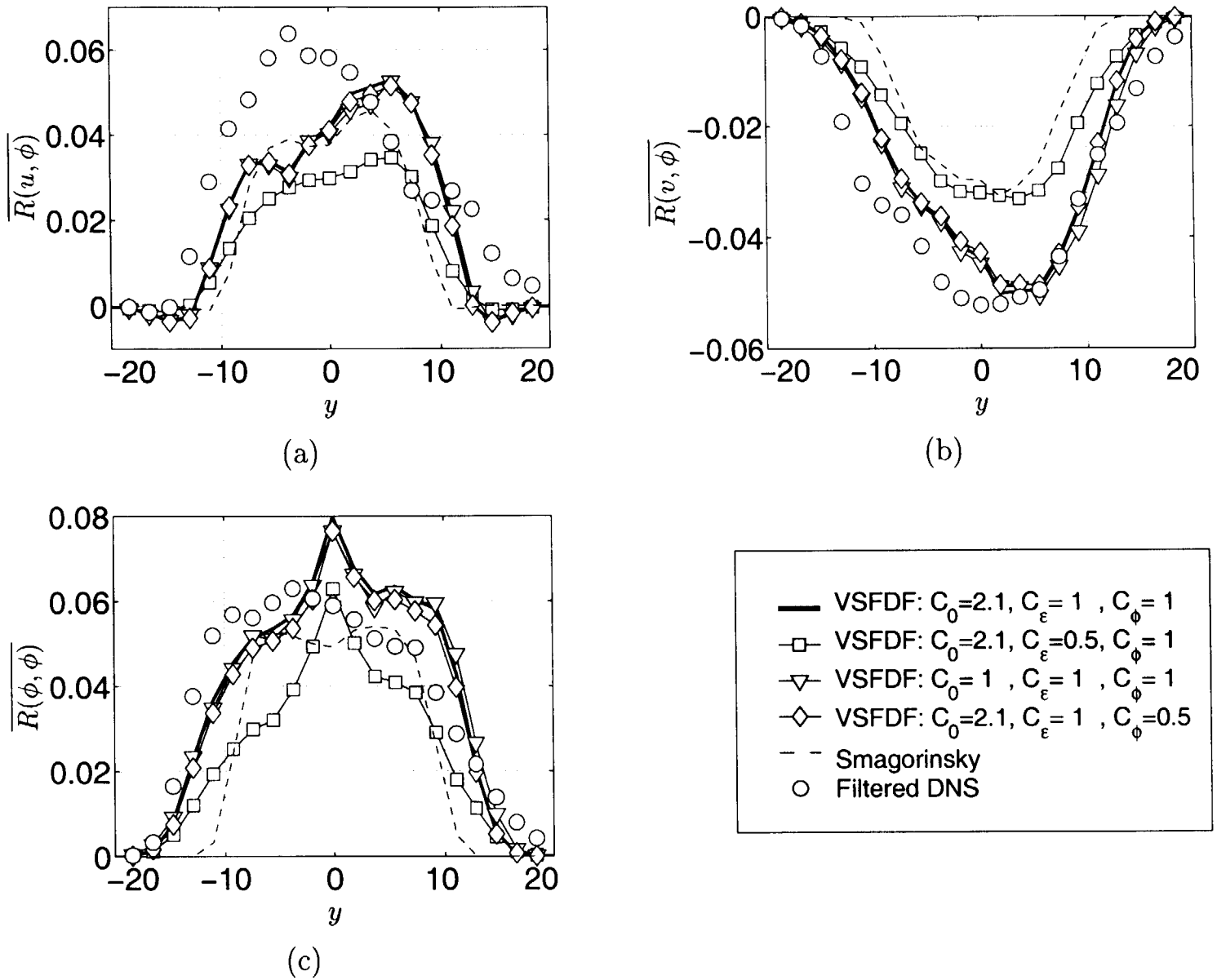
0.06
0.04
0.02
0
$\overline{R(u,\phi)}$
−20
−10
0
10
20
y
(a)
0
−0.02
−0.04
−0.06
$\overline{R(v,\phi)}$
−20
−10
0
10
20
y
(b)
0.08
0.06
0.04
0.02
0
$\overline{R(\phi,\phi)}$
−20
−10
0
10
20
y
(c)
VSFDF: C_0=2.1, C_ε= 1 , C_ϕ= 1
VSFDF: C_0=2.1, C_ε=0.5, C_ϕ= 1
VSFDF: C_0= 1 , C_ε= 1 , C_ϕ= 1
VSFDF: C_0=2.1, C_ε= 1 , C_ϕ=0.5
Smagorinsky
Filtered DNS

Figure 17

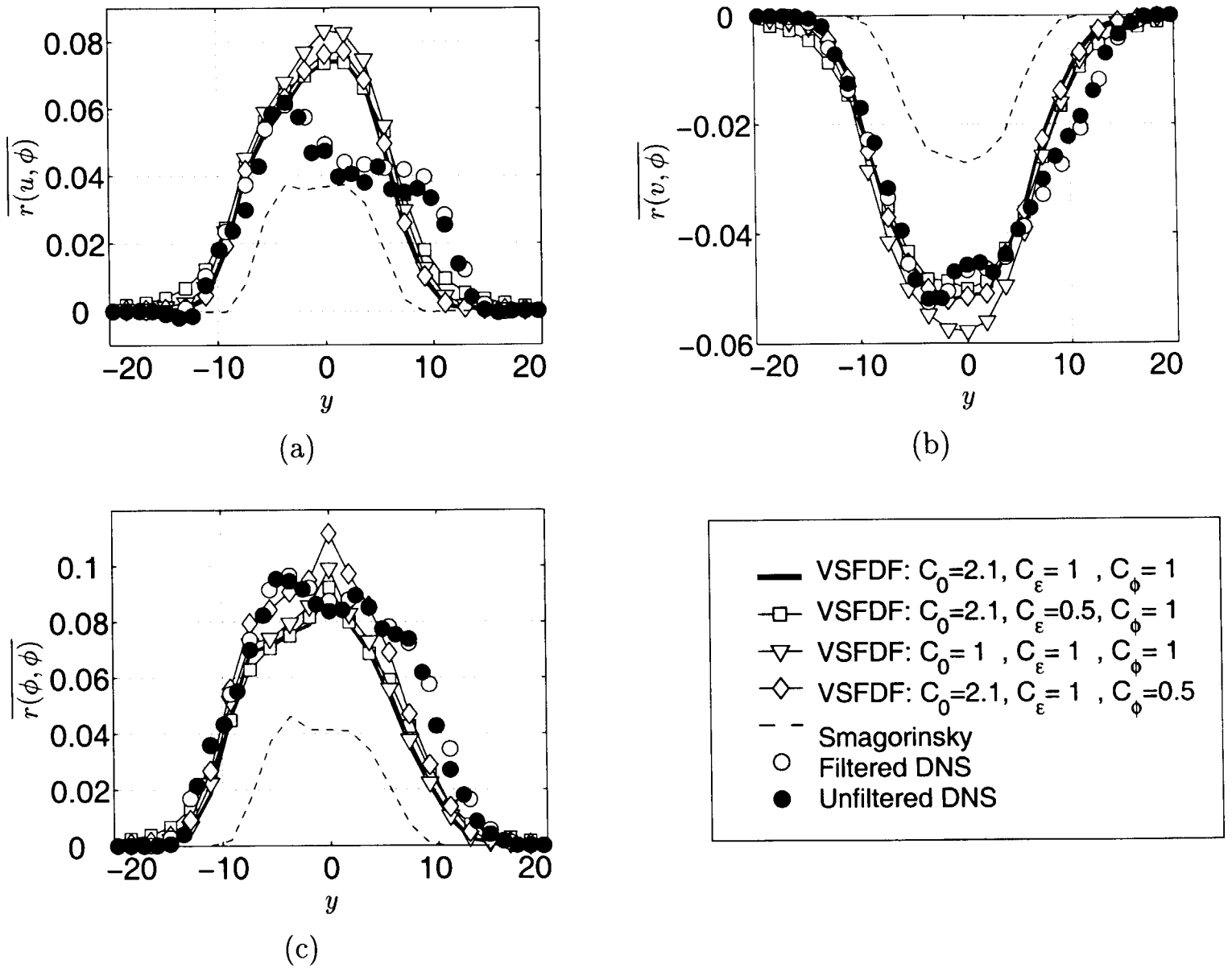
0.08
0.06
0.04
0.02
0
$\overline{r(u,\phi)}$
−20
−10
0
10
20
y
(a)
0
−0.02
−0.04
−0.06
$\overline{r(v,\phi)}$
−20
−10
0
10
20
y
(b)
0.1
0.08
0.06
0.04
0.02
0
$\overline{r(\phi,\phi)}$
−20
−10
0
10
20
y
(c)
VSFDF: C_0=2.1, C_ε= 1 , C_ϕ= 1
VSFDF: C_0=2.1, C_ε=0.5, C_ϕ= 1
VSFDF: C_0= 1 , C_ε= 1 , C_ϕ= 1
VSFDF: C_0=2.1, C_ε= 1 , C_ϕ=0.5
Smagorinsky
Filtered DNS
Unfiltered DNS

Figure 18

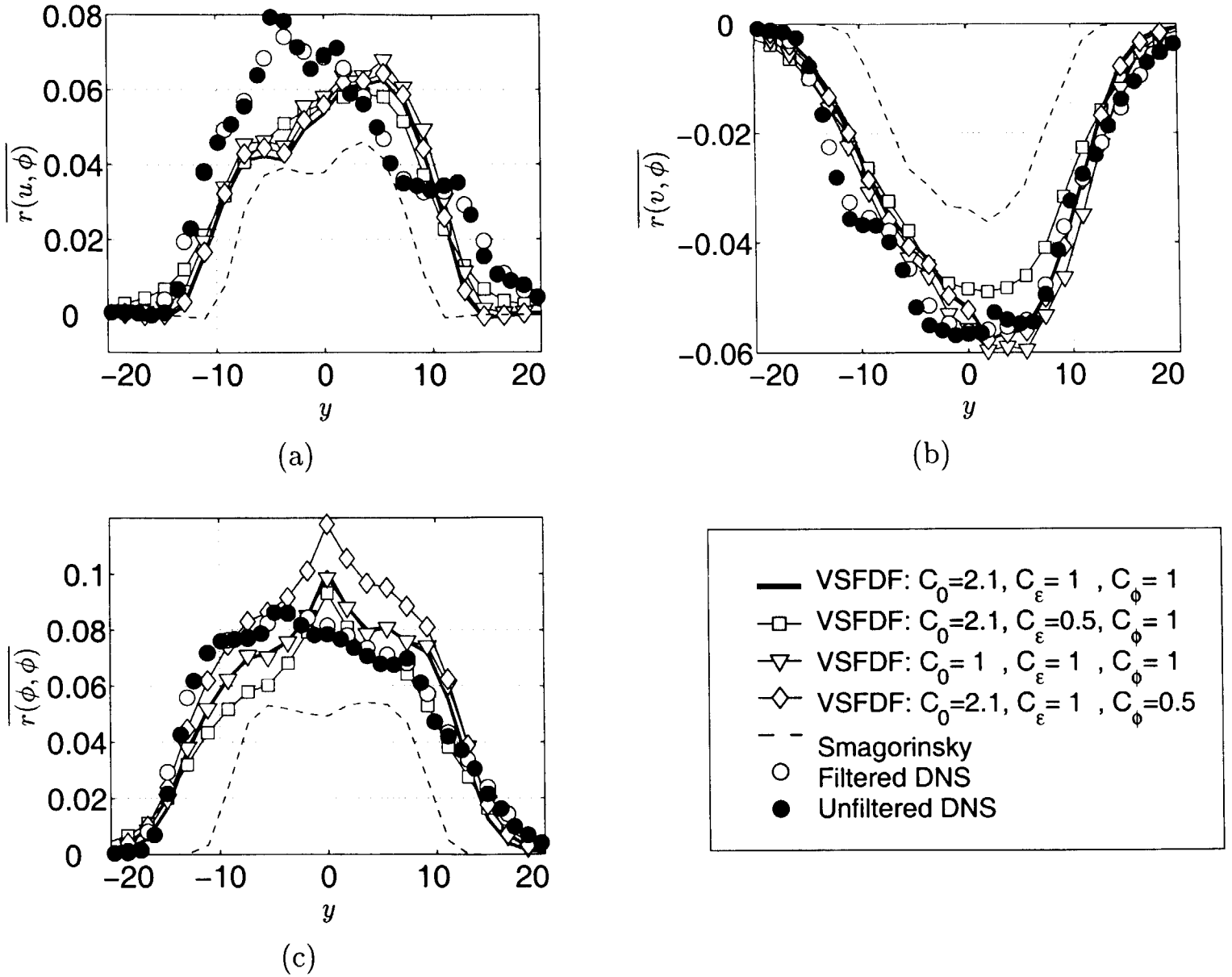
0.08
0.06
0.04
0.02
0
$\overline{r(u,\phi)}$
−20
−10
0
10
20
y
(a)
0
−0.02
−0.04
−0.06
$\overline{r(v,\phi)}$
y
(b)
0.1
0.08
0.06
0.04
0.02
0
$\overline{r(\phi,\phi)}$
y
(c)
VSFDF: C_0=2.1, C_ε= 1 , C_ϕ= 1
VSFDF: C_0=2.1, C_ε=0.5, C_ϕ= 1
VSFDF: C_0= 1 , C_ε= 1 , C_ϕ= 1
VSFDF: C_0=2.1, C_ε= 1 , C_ϕ=0.5
Smagorinsky
Filtered DNS
Unfiltered DNS

Figure 19

Appendix III

This Appendix is published as Ref. [48].

A C.I.P. Catalogue record for this book is available from the library of Congress

DNS/LES – Progress and Challenges

Proceedings of the Third AFOSR International Conference on DNS/LES

Editors:

Chaoqun Liu, UTA
Leonidas Sakell, AFOSR
Thomas Beutner, AFOSR

Publisher:

Greyden Press
2020 Builders Place
Columbus, Ohio 43204, USA

October 2001

ISBN 1-57074-488-2

A REVIEW OF MODERN DEVELOPMENTS IN LARGE EDDY SIMULATION OF TURBULENT REACTIVE FLOWS

PEYMAN GIVI
Department of Mechanical and Aerospace Engineering
University at Buffalo, SUNY
Buffalo, NY 14260-4400

Abstract. An overview is presented of recent developments and contributions in large eddy simulation (LES) of turbulent reactive flows. The foundation of some of the recently proposed subgrid scale (SGS) closures for such simulations is presented, along with a discussion of their capabilities and limitations. The scope of the review is limited to physical modeling. In doing so, only issues pertaining to additional complexities caused by chemical reactions are discussed. That is, the challenges associated with "general" LES of non-reactive flows are not considered, even though all of these challenges are indeed present (and in most cases are a lot more complex) in reactive flows. It is recognized that numerical algorithms and computational procedures play a significant role in (any) LES. However, this review does not deal with these issues except for cases wherein the actual numerical-computational methodology is directly coupled with the procedure by which LES is conducted. The SGS closure based on the recently developed "filtered density function" (FDF) method is described in a greater detail. This is due to more familiarity of this reviewer with this closure; it does not imply that other closures are less effective.

1. Introduction

In the late 1980's, I was preparing a review article on large scale numerical simulations of turbulent reactive flows. The intent was to provide a survey of the contributions made to both direct numerical simulation (DNS) and large eddy simulation (LES). However, when that article was finally published (Givi, 1989), its content was heavily biased towards DNS. This was not intentional, it just reflected the state of progress on LES of turbu-

lent combustion at that time. But with all of the enthusiasm for DNS in the combustion community, the limitations of such simulations were well recognized (even with the most optimistic predictions of growth in supercomputer technology). It was also clear that the future of large scale simulations of practical turbulent reacting flows would heavily depend on the development of LES. Therefore, it was quite easy to predict that LES would receive significant attention in computational predictions of turbulent reacting flows in the 1990's and into the next (present) century.

Now, at the time of writing this article (Summer 2001), while struggling to meet the deadline for its submission(!) I am not surprised by the extent of the contributions in developing subgrid scale (SGS) models or by the magnificent work on LES of a variety of turbulent reacting flow systems. In fact, I admit that the rate of these developments has been a lot faster than my capability to absorb, or in some cases even follow, the details of the proposed methodologies. In addition, the page-limit restrictions under which this is being prepared, preclude describing the details of the wide variety of currently available closures; similarly, citation of the relevant references cannot even be done exhaustively. Fortunately, many aspects of SGS closures and LES of reacting turbulence have recently been discussed in several excellent tutorial and review articles (Cook and Riley, 1998a; Candel *et al.*, 1999; Bilger, 2000; Branley and Jones, 2000; Menon, 2000; Peters, 2000; Pope, 2000; Luo, 2001; Poinsot and Veynante, 2001). Therefore, in the present review I concentrate on some of the major issues related to my area of research within this field.

2. Starting Equations

Large eddy simulation involves the use of the spatial filtering operation (Sagaut, 2001)

$$\langle Q(\mathbf{x},t)\rangle_\ell = \int_{-\infty}^{+\infty} Q(\mathbf{x}',t)\mathcal{G}(\mathbf{x}',\mathbf{x})d\mathbf{x}', \tag{1}$$

where $\mathcal{G}$ denotes the filter function of width Δ_G, and $\langle Q(\mathbf{x},t)\rangle_\ell$ represents the filtered value of the transport variable $Q(\mathbf{x},t)$. In variable density flows it is convenient to consider the Favré filtered quantity,

$$\langle Q(\mathbf{x},t)\rangle_L = \langle \rho Q\rangle_\ell / \langle \rho\rangle_\ell. \tag{2}$$

We consider spatially & temporally invariant and localized filter functions, $\mathcal{G}(\mathbf{x}',\mathbf{x}) \equiv G(\mathbf{x}'-\mathbf{x})$ with the properties $G(\mathbf{x}) = G(-\mathbf{x})$, and $\int_{-\infty}^{\infty} G(\mathbf{x})d\mathbf{x} = 1$. Moreover, we only consider "positive" filter functions for which all the moments $\int_{-\infty}^{\infty} x^m G(x)dx$ exist for $m \geq 0$.

To set the framework, we consider the transport equations of chemically reacting flows. To isolate the effects of chemical reaction in the simplest way, we consider single-phase (gaseous) combustion in a low Mach number flow with negligible radiative heat transfer and viscous dissipation. We also assume that Newton's law of viscosity, Fourier's law of heat conduction and Fick's law of mass diffusion are applicable. Therefore, the primary transport variables are the density ρ, the velocity vector u_i, $i = 1, 2, 3$ along the x_i direction, the pressure p, the species' mass fractions Y_α, and the total specific enthalpy h. All of the mass fractions and the enthalpy are grouped into the scalar array $\phi(\mathbf{x}, t) \equiv [\phi_1, \phi_2, \ldots \phi_\sigma] \equiv [Y_1,\ Y_2, \ldots, Y_{N_s}, h]$ of size $\sigma = N_s + 1$ where N_s denotes the total number of species. Application of the filtering operation to the equations of continuity, momentum, enthalpy (energy) and species mass fraction equations gives

$$\frac{\partial \langle\rho\rangle_\ell}{\partial t} + \frac{\partial \langle\rho\rangle_\ell \langle u_i\rangle_L}{\partial x_i} = 0, \tag{3}$$

$$\frac{\partial \langle\rho\rangle_\ell \langle u_j\rangle_L}{\partial t} + \frac{\partial \langle\rho\rangle_\ell \langle u_i\rangle_L \langle u_j\rangle_L}{\partial x_i} = -\frac{\partial \langle p\rangle_\ell}{\partial x_j} + \frac{\partial \langle\tau_{ij}\rangle_\ell}{\partial x_i} - \frac{\partial T_{ij}}{\partial x_i}, \tag{4}$$

$$\frac{\partial \langle\rho\rangle_\ell \langle\phi_\alpha\rangle_L}{\partial t} + \frac{\partial \langle\rho\rangle_\ell \langle u_i\rangle_L \langle\phi_\alpha\rangle_L}{\partial x_i} = -\frac{\partial \langle J_i^\alpha\rangle_\ell}{\partial x_i} - \frac{\partial M_i^\alpha}{\partial x_i} + \langle\rho S_\alpha\rangle_\ell, \tag{5}$$

where t represents time, and the filtered reaction source terms are denoted by $\langle\rho S_\alpha\rangle_\ell = \langle\rho\rangle_\ell \langle S_\alpha\rangle_L$. The viscous stress tensor and the mass/heat fluxes are denoted by τ_{ij}, and J_i^α, respectively. At low Mach numbers and heat release rates, by neglecting the viscous dissipation and thermal radiation the source terms in the enthalpy equation can be assumed to be negligible. Thus, $S_\alpha = S_\alpha(\phi)$. The terms $T_{ij} = \langle\rho\rangle_\ell(\langle u_i u_j\rangle_L - \langle u_i\rangle_L \langle u_j\rangle_L)$ and $M_i^\alpha = \langle\rho\rangle_\ell(\langle u_i\phi_\alpha\rangle_L - \langle u_i\rangle_L \langle\phi_\alpha\rangle_L)$ denote the SGS stress and the SGS mass flux, respectively. Equations (3)-(5) are coupled through the equation of state.

3. Closure Methodologies

For non-reacting flows the SGS closure is associated with T_{ij} and M_i^α (Canuto, 1994; Ciofalo, 1994; Lesieur and Metais, 1996). In reacting flows, an additional model is required for the filtered reaction rate $\langle S_\alpha\rangle_L$. This modeling is the subject of primary concern in this review.

One of the first contributions in LES of reactive flows, similar to that in LES of non-reacting flows, was made in atmospheric sciences (Schumann, 1989). In this work, the effects of SGS scalar fluctuations (as appear in the chemical source term) are assumed negligible, *i.e.* $\langle\hat{S}_\alpha(\phi)\rangle_L \approx \hat{S}_\alpha(\langle\phi\rangle_L)$. This assumption is compatible with that made in some of the more recent contributions (Boris *et al.*, 1992; Fureby and Grinstein, 1999), in which it

is argued that all of the essential SGS contributions are included in the numerical discretization procedure.

Modeling of the scalar fluctuations has been the subject of broad investigations in Reynolds averaged simulations (RAS) for over five decades, resulting in a variety of closure strategies (Libby and Williams, 1980; Libby and Williams, 1994). Within the past 10 years or so, almost all of these closures have been considered for LES. Examples: the eddy-break up models (Fureby and Lofstrom, 1994; Candel *et al.*, 1999), moment methods (Frankel *et al.*, 1993), the flamelet concept (Cook *et al.*, 1997; Cook and Riley, 1998b; De Bruyn Kops *et al.*, 1998; DesJardin and Frankel, 1998; DesJardin and Frankel, 1999; Pitsch and Steiner, 2000; Ladeinde *et al.*, 2001), the linear eddy model (LEM) (McMurtry *et al.*, 1992; Menon and Calhoon, 1996; Kim *et al.*, 1999; Menon, 2000), the conditional moment method (CMM) (Bushe and Steiner, 1999; Steiner and Bushe, 2001), and many others (Sykes *et al.*, 1992; Galperin and Orszag, 1993; Smith and Menon, 1996; Im *et al.*, 1997; McGrattan *et al.*, 1998; Thibaut and Candel, 1998; Battaglia *et al.*, 2000; Collin *et al.*, 2000). In addition, several of the closures previously developed for LES of non-reacting flows, have been extended for use in reacting flow simulations (DesJardin and Frankel, 1998; Jaberi and James, 1998).

The probability density function (PDF) methods have proven particularly useful in RAS (O'Brien, 1980; Pope, 1985; Dopazo, 1994; Fox, 1996; Pope, 2000). The systematic approach for determining the PDF is by means of solving its transport equation. An alternative approach is based on *assumed* methods in which the shape of the PDF is specified *a priori*. This has been pursued in several studies in most of which it is assumed that the thermo-chemical variables depend only on the mixture fraction, *e.g.* infinitely fast reaction, equilibrium chemistry. Therefore, the PDF is univariate (Madnia and Givi, 1993; Cook and Riley, 1994; Réveillon and Vervisch, 1996; Branley and Jones, 1997; Jiménez *et al.*, 1997; Mathey and Chollet, 1997; DesJardin and Frankel, 1998; DesJardin and Frankel, 1999; Forkel and Janicka, 2000; Kempf *et al.*, 2000). For LES of non-equilibrium reactive flows, it is necessary to assume the joint PDF of multi-scalars (Frankel *et al.*, 1993). Consistent with popular methods of generating univariate (Leemis, 1986) and multivariate (Johnson and Kotz, 1972) distributions, all of the assumed SGS scalar PDFs in the contributions cited above are based on the first and the second order moments. The PDFs generated in this way offer sufficient flexibility and are affordable for large scale simulations. However, it is now well understood that the "true" PDF strongly depends on the actual physics of mixing in a given flow condition (Jaberi *et al.*, 1996). Therefore, there is a need to determine such PDFs in a more systematic manner.

The "filtered density function" (FDF) methodology introduced by Pope (1990) provides the framework for fundamental developments of the PDF based SGS closures. This method provides a means of determining the PDF from its own transport equation. For the scalars' array $\phi(\mathbf{x},t)$ the FDF, denoted by P_L, is defined as (Pope, 1990)

$$P_L(\psi;\mathbf{x},t) = \int_{-\infty}^{+\infty} \zeta\left[\psi,\phi(\mathbf{x}',t)\right] G(\mathbf{x}'-\mathbf{x})d\mathbf{x}', \tag{6}$$

$$\zeta\left[\psi,\phi(\mathbf{x},t)\right] = \prod_{\alpha=1}^{\sigma} \delta[\psi_\alpha - \phi_\alpha(\mathbf{x},t)], \tag{7}$$

where δ denotes the delta function and ψ denotes the composition domain of the scalar array. The term $\zeta[\phi-\psi(\mathbf{x},t)]$ is the "fine-grained" density (Lundgren, 1967; O'Brien, 1980; Pope, 1985; Dopazo, 1994). In variable density flows, it is convenient to consider the "filtered mass density function" (FMDF), denoted by F_L, as

$$F_L(\psi;\mathbf{x},t) \equiv \int_{-\infty}^{+\infty} \rho(\mathbf{x}',t)\zeta\left[\psi,\phi(\mathbf{x}',t)\right] G(\mathbf{x}'-\mathbf{x})d\mathbf{x}'. \tag{8}$$

The integral property of the FDF and FMDF is such that

$$\int_{-\infty}^{+\infty} P_L(\psi;\mathbf{x},t)d\psi = 1, \quad \int_{-\infty}^{+\infty} F_L(\psi;\mathbf{x},t)d\psi = \langle\rho(\mathbf{x},t)\rangle_\ell. \tag{9}$$

For further discussions, it is useful to define the mass weighted conditional filtered mean of the variable $Q(\mathbf{x},t)$,

$$\langle Q(\mathbf{x},t)|\psi\rangle_\ell \equiv \frac{\int_{-\infty}^{+\infty} \rho(\mathbf{x}',t)Q(\mathbf{x}',t)\zeta\left[\psi,\phi(\mathbf{x}',t)\right] G(\mathbf{x}'-\mathbf{x})d\mathbf{x}'}{F_L(\psi;\mathbf{x},t)}. \tag{10}$$

Therefore, when Q can be completely described by the compositional variable, *i.e.* $Q(\mathbf{x},t) \equiv \hat{Q}(\phi(\mathbf{x},t))$, we have $\langle Q(\mathbf{x},t)|\psi\rangle_\ell = \hat{Q}(\psi)$. Also,

$$\int_{-\infty}^{+\infty} \langle Q(\mathbf{x},t)|\psi\rangle_\ell F_L(\psi;\mathbf{x},t)d\psi = \langle\rho(\mathbf{x},t)\rangle_\ell\langle Q(\mathbf{x},t)\rangle_L. \tag{11}$$

The transport equation for $F_L(\psi;\mathbf{x},t)$ is obtained by multiplying the transport equation for the fine grained density by the filter function $G(\mathbf{x}'-\mathbf{x})$ and integrating over $\mathbf{x}'$ space (Gao and O'Brien, 1993; Colucci *et al.*, 1998; Réveillon and Vervisch, 1998; Jaberi *et al.*, 1999; Jaberi, 1999; Zhou and Pereira, 2000; Tong, 2001),

$$\frac{\partial F_L(\psi;\mathbf{x},t)}{\partial t}+\frac{\partial[\langle u_i(\mathbf{x},t)|\psi\rangle_\ell F_L(\psi;\mathbf{x},t)]}{\partial x_i}=-\frac{\partial[\hat{S}_\alpha(\psi)F_L(\psi;\mathbf{x},t)]}{\partial\psi_\alpha}$$
$$+\frac{\partial}{\partial\psi_\alpha}\left[\left\langle\frac{1}{\hat{\rho}(\phi)}\frac{\partial J_i^\alpha}{\partial x_i}|\psi\right\rangle_\ell F_L(\psi;\mathbf{x},t)\right]. \quad (12)$$

The first term on the RHS is due to chemical reaction and is in a closed form. This demonstrates the primary advantage of the FDF methodology. However, the SGS convection (the second term on the LHS) and SGS mixing (the second term on the RHS) must be modeled. One of the most challenging issues in FDF is associated with closure of the mixing term. This has been the subject of broad investigations in PDF modeling (Pope, 1985; Pope, 2000). In Eq. (12) the effects of mixing are displayed through the "conditional expected diffusion" of the scalars, but can also be represented in the form of the "conditional expected dissipation" (O'Brien, 1980; Pope, 1985). The closure for this can be via any of the ones currently in use in PDF methods (Pope, 2000). In the absence of a clearly superior model, the linear mean square estimation (LMSE) model (O'Brien, 1980) has been used in almost all of previous LES based on FDF (Colucci *et al.*, 1998; Jaberi *et al.*, 1999; Garrick *et al.*, 1999; James and Jaberi, 2000; Zhou and Pereira, 2000). With $J_i^\alpha=-\gamma\frac{\partial\phi_\alpha}{\partial x_i}$, this model is

$$\frac{\partial}{\partial\psi_\alpha}\left[\left\langle-\frac{1}{\hat{\rho}}\frac{\partial}{\partial x_i}\left(\gamma\frac{\partial\phi_\alpha}{\partial x_i}\right)|\psi\right\rangle_\ell F_L\right] = \frac{\partial}{\partial x_i}\left[\gamma\frac{\partial(F_L/\langle\rho\rangle_\ell)}{\partial x_i}\right]$$
$$+\frac{\partial}{\partial\psi_\alpha}\left[\Omega_m(\psi_\alpha-\langle\phi_\alpha\rangle_L)F_L\right], \quad (13)$$

where $\Omega_m(\mathbf{x},t)$ is the "frequency" of mixing within the subgrid and must be modeled. The convective term can be modeled as

$$\langle u_i|\psi\rangle_\ell F_L=\langle u_i\rangle_L F_L-\gamma_t\frac{\partial(F_L/\langle\rho\rangle_\ell)}{\partial x_i}, \quad (14)$$

where γ_t is the SGS diffusion coefficient and must be specified. Equation (14) is in accord with that often used in conventional LES (Moin *et al.*, 1991; Canuto, 1994; Ciofalo, 1994; Lesieur and Metais, 1996). With this formulation, obviously the resolved hydrodynamic field must be determined by other means. This problem can be circumvented by considering the joint velocity-scalar FMDF,

$$\mathcal{F}_L(\mathbf{v},\psi,\mathbf{x};t)\equiv\int_{-\infty}^{+\infty}\rho(\mathbf{x}',t)\xi\left[\mathbf{v},\mathbf{u}(\mathbf{x}',t),\psi,\phi(\mathbf{x}',t)\right]G(\mathbf{x}'-\mathbf{x})d\mathbf{x}', \quad (15)$$

$$\xi\left[\mathbf{v}, \mathbf{u}(\mathbf{x},t), \psi, \phi(\mathbf{x},t)\right] = \prod_{k=1}^{3} \delta[v_k - u_k(\mathbf{x},t)] \prod_{\alpha=1}^{\sigma} \delta[\psi_\alpha - \phi_\alpha(\mathbf{x},t)], \quad (16)$$

where $\mathbf{v}$ denotes the composition domain of the random velocity vector, and $\xi[\mathbf{v}, \mathbf{u}(\mathbf{x},t), \psi, \phi(\mathbf{x},t)]$ is the fine-grained velocity-scalar density. Most recent work in this regard consider the transport of the velocity FDF (VFDF) (Gicquel, 2001) and the joint velocity-scalar FDF (VSFDF) (Drozda, 2001). The operational procedure is similar to that developed previously for PDF methods (Pope, 1985; Pope, 1994; Pope, 2000).

The closure problems as noted above are not particular to the FDF; all of the other schemes require similar modelings. For example, in the limit of equilibrium chemistry all of the statistics of the reacting fields are related to those of the mixture fraction. The FMDF of the mixture fraction can be obtained from the solution of Eq. (12) with $S = 0$. So, there is still a need for modeling of the mixing term. Even in cases where the FMDF is assumed, its distribution is parameterized with the low order moments of the mixture fraction. As indicated above, the first two moments are typically used for this parameterization. Therefore, there is a need for closure of the "total SGS dissipation" as appears in the second moment (SGS variance) equation. Several means of dealing with this closure problem are available (Girimaji and Zhou, 1996; Pierce and Moin, 1998; Cook and Bushe, 1999; Jiménez *et al.*, 2001; De Bruyn Kops and Riley, 2001).

The above problem is a bit more complex when the SGS chemical reaction is assumed to be in the "flamelet" regime (Peters, 2000). In this case, even with the one-dimensional flamelet model, the thermo-chemical variables are parameterized by the mixture fraction and its rate of dissipation (Cook *et al.*, 1997; Cook and Riley, 1998b; De Bruyn Kops *et al.*, 1998; DesJardin and Frankel, 1998; Cook and Riley, 1998b). Therefore, there is a need for *a priori* specification of the joint FDF of the mixture fraction and its dissipation. A review of different methods of dealing with this issue is available (Cook and Riley, 1998a). Equation (12) with $S = 0$ indicates that there is a dependence between the FDF of the mixture fractions and the conditional expected diffusion (and the conditional expected dissipation). This dependency is not considered in most previous contributions, but is the subject of current investigations (DesJardin *et al.*, 2001).

Modeling of the conditional expected dissipation is also required in the conditional moment method (Bushe and Steiner, 1999; Steiner and Bushe, 2001). This issue has been recognized at the early stages of developments of CMM in RAS (Bilger, 2000). With this model, the conditional filtered mean values of the thermo-chemical variables (LHS of Eq. (10)) are obtained by their modeled transport equation. This is obviously computationally less demanding that solving the FDF transport equation. But in order to

determine the actual filtered quantities, the distribution of the mixture fraction FDF must be specified.

An important issue in regard to FDF is associated with the numerical solution of its transport equation. The Lagrangian Monte Carlo scheme (Pope, 1985) has proven particularly useful for this purpose. In this scheme, the FDF is represented via an ensemble of computational elements or particles. Transport of these particles and the change in their properties are modeled by a set of stochastic differential equations (SDEs) (Soong, 1973). The diffusion process (Gardiner, 1990) has proven effective for this purpose. The coefficients in the Langevin equation governing this process are set in such a way that the resulting Fokker-Planck equation (Risken, 1989) is equivalent to the FDF transport equation. Therefore, the Monte Carlo solution of the SDEs represent the solution of the FDF in the probabilistic sense. This procedure has proven successful for simulating PDF in a variety of systems (Grigoriu, 1995). However, one must be careful in performing stochastic simulations in conjunction with modern CFD solvers. Many of the advanced discretization routines developed for solving deterministic differential equations may not be applicable, or may have to be significantly modified to be suitable for solving SDEs (Kloeden and Platen, 1995).

Implementation of LEM is also based on stochastic representation of the flow. In its original development in RAS (Kerstein, 1988), the processes of molecular diffusion, chemical reaction and turbulent convection are considered separately. This is achieved by a reduced one-dimensional (linear) description of the scalar field, which makes it possible to resolve the flow scales even for flows with relatively high Reynolds, Schmidt and Damköhler numbers. The interpretation of the one-dimensional domain is dependent on the particular flow under consideration. In this way, the processes of molecular diffusion and chemical reaction are taken into account exactly, but the effects of convection are modeled. This is achieved by "random rearrangement" (or stirring) events in such a way that the displacements of fluid elements result in a diffusivity equal to the "turbulent diffusivity." For LES, this procedure is followed within each of the computational cells, and stirring is performed to yield the desired SGS diffusivity. Menon and colleagues have made extensive use of LEM for LES of a wide variety of reacting flows. A recent review is available (Menon, 2000).

4. Acknowledgment

I am honored to have the opportunity to collaborate with Professor Stephen B. Pope (Cornell University) on FDF and PDF methods, and I am grateful to him and Professor Larry T.T. Soong (SUNY-Buffalo) for teaching me most of what I know about stochastic processes. I am indebted to my

current Ph.D. students, Mr. Tomasz G. Drozda, Mr. Reza Haji-Sheikhi and my former students and collaborators, Dr. Virgil Adumitroaie (Currently at CFD Research Inc.), Dr. Paul J. Colucci (Fluent Inc.), Professor Steve H. Frankel (Purdue University), Professor Sean C. Garrick (University of Minnesota), Dr. Laurent Y.M. Gicquel (CERFACS, Toulouse), Professor Farhad A. Jaberi (Michigan State University), Dr. Sunil James (Rolls-Royce Co.) and Professor Cyrus K. Madnia (SUNY-Buffalo) for their leaderships in all of our previous/ongoing LES work. Our current research in LES/FDF is being sponsored by the U.S. Air Force Office of Scientific Research under Grant F49620-00-1-0035 (Program Manager: Dr. Julian M. Tishkoff), the NASA Langley Research Center under Grant NAG-1-2238 (Technical Monitor: Dr. J. Philip Drummond), and the NASA Glenn Research Center under Grant NAG-3-2225 (Technical Monitor: Dr. Uday Hegde). Acknowledgment is also made to the Donors of the Petroleum Research Funds administrated by the American Chemical Society for their support under Grant ACS-PRF 36981-AC9. Computational resources are provided by the NCSA at the University of Illinois at Urbana, and by the CCR at SUNY-Buffalo.

References

Battaglia, F., McGrattan, K. B., Rehm, R. G., and Baum, H. R. (2000). Simulating fire whirls. *Combustion, Theory, and Modelling* **4**, 123–138.

Bilger, R. W. (2000). Future progress in turbulent combustion research. *Prog. Energy Combust. Sci.* **26**, 367–380.

Boris, J. P., Grinstein, F. F., Oran, E. S., and Kolbe, R. L. (1992). New insights into large eddy simulations. *Fluid Dyn. Res.* **10**, 199–238.

Branley, N. and Jones, W. P. (1997). Large eddy simulation of a turbulent non-premixed flame. In *Proceedings of the Eleventh Symposium on Turbulent Shear Flows*, pages 21.1–21.6, Grenoble, France.

Branley, N. and Jones, W. P. (2000). Large eddy simulation of turbulent flames. In *European Congress on Computational Methods in Applied Science and Engineering*, pages 1–23. Barcelona, Spain.

Bushe, W. K. and Steiner, H. (1999). Conditional moment closure for large eddy simulation of nonpremixed turbulent reacting flows. *Phys. Fluids* **11**, 1896–1906.

Candel, S., Thevenin, D., Darabiha, N., and Veynante, D. (1999). Progress in numerical combustion. *Combust. Sci. and Tech.* **149**, 297–337.

Canuto, V. M. (1994). Large eddy simulation of turbulence : A subgrid scale model including shear, vorticity, rotation, and buoyancy. *The Astro. Phys. Journal* **428**, 729–752.

Ciofalo, M. (1994). Large eddy simulation : A critical survey of models and applications. In *Advances in Heat Transfer*, pages 321–419. Academic Press, New York, NY. Vol 25.

Collin, O., Ducros, F., Veynate, D., and Poinsot, T. (2000). A thickened flame model for large eddy simulation of turbulent premixed combustion. *Phys Fluids* **12**, 1843–1863.

Colucci, P. J., Jaberi, F. A., Givi, P., and Pope, S. B. (1998). Filtered density function for large eddy simulation of turbulent reacting flows. *Phys. Fluids* **10**, 499–515.

Cook, A. W. and Bushe, W. K. (1999). A subgrid-scale model for the scalar dissipation rate in nonpremixed combustion. *Phys. Fluids* **11**, 746–749.

Cook, A. W. and Riley, J. J. (1994). A subgrid model for equilibrium chemistry in turbulent flows. *Phys. Fluids* **6**, 2868–2870.

Cook, A. W. and Riley, J. J. (1998a). Progress in subgrid-scale combustion modeling. In Hafez, M. and Oshima, K., editors, *Computational Fluid Dynamics Review 1998*, pages 914–931. World Scientific, Singapore.

Cook, A. W. and Riley, J. J. (1998b). Subgrid scale modeling for turbulent reacting flows. *Combust. Flame* **112**, 593–606.

Cook, A. W., Riley, J. J., and Kosály, G. (1997). A laminar flamelet approach to subgrid-scale chemistry in turbulent flows. *Combust. Flame* **109**, 332–341.

De Bruyn Kops, S. M. and Riley, J. J. (2001). Mixing models for large-eddy simulation of nonpremixed turbulent combustion. *ASME Journal of Fluids Engineering* **123**, 1–6.

De Bruyn Kops, S. M., Riley, J. J., Kosály, G., and Cook, A. W. (1998). Investigation of modeling for non-premixed turbulent combustion. *Combust. Flame* **60**, 105–122.

DesJardin, P. E. and Frankel, S. H. (1998). Large eddy simulation of a turbulent nonpremixed reacting jet: Application and assessment of subgrid-scale combustion models. *Phys. Fluids* **10**, 2298–2314.

DesJardin, P. E. and Frankel, S. H. (1999). Two-dimensional large eddy simulation of soot formation in the near-field of a strongly radiating nonpremixed acetylene-air turbulent jet flame. *Combust. Flame* **119**, 121–132.

DesJardin, P. E., Smith, T. M., and Roy, C. J. (2001). Numerical simulations of a methanol pool fire. AIAA Paper AIAA-01-0636.

Dopazo, C. (1994). Recent developments in PDF methods. In Libby and Williams (1994), chapter 7, pages 375–474.

Drozda, T. G. (2001), Consistency assessment of velocity-scalar filtered density function for large-eddy simulation of turbulent flows. M.S. Thesis, Department of Mechanical and Aerospace Engineering, State University of New York at Buffalo, Buffalo, NY.

Forkel, H. and Janicka, J. (2000). Large-eddy simulation of a turbulent hydrogen diffusion flame. *Flow, Turbulence and Combustion* **65**, 163–175.

Fox, R. O. (1996). Computational methods for turbulent reacting flows in chemical process industry. *Revue De L'Institut Francais Du Petrole* **51**, 215–246.

Frankel, S. H., Adumitroaie, V., Madnia, C. K., and Givi, P. (1993). Large eddy simulations of turbulent reacting flows by assumed PDF methods. In Ragab, S. A. and Piomelli, U., editors, *Engineering Applications of Large Eddy Simulations*, pages 81–101. ASME, FED-Vol. 162, New York, NY.

Fureby, C. and Grinstein, F. F. (1999). Monotonically integrated large eddy simulation of free shear flows. *AIAA J.* **37**, 544.

Fureby, C. and Lofstrom, C. (1994). Large-eddy simulations of bluff body stabilized flames. In *Proceedings of 25th Symp. (Int.) on Combustion*, pages 1257–1264. The Combustion Institute, Pittsburgh, PA.

Galperin, B. and Orszag, S. A., editors. (1993). *Large Eddy Simulations of Complex Engineering and Geophysical Flows*. Cambridge University Press, Cambridge, England.

Gao, F. and O'Brien, E. E. (1993). A large-eddy simulation scheme for turbulent reacting flows. *Phys. Fluids A* **5**, 1282–1284.

Gardiner, C. W. (1990). *Handbook of Stochastic Methods*. Springer-Verlag, New York, NY.

Garrick, S. C., Jaberi, F. A., and Givi, P. (1999). Large eddy simulation of scalar transport in a turbulent jet flow. In Knight, D. and Sakell, L., editors, *Recent Advances in DNS and LES*, volume 54 of *Fluid Mechanics and its Applications*, pages 155–166. Kluwer Academic Publishers, The Netherlands.

Gicquel, L. Y. M. (2001), *Velocity Filtered Density Function for Large Eddy Simulation of Turbulent Flows*. Ph.D. Dissertation, Department of Mechanical and Aerospace Engineering, State University of New York at Buffalo, Buffalo, NY.

Girimaji, S. S. and Zhou, Y. (1996). Analysis and modeling of subgrid scalar mixing using numerical data. *Phys. Fluids* **8**, 1224–1236.

Givi, P. (1989). Model free simulations of turbulent reactive flows. *Prog. Energy Combust. Sci.* **15**, 1–107.

Grigoriu, M. (1995). *Applied Non-Gaussian Processes.* Prentice-Hall, Englewood Cliffs, NJ.

Im, H. G., Lund, T. S., and Ferziger, J. H. (1997). Large eddy simulation of turbulent front propagation with dynamic subgrid models. *Phys. Fluids* **9**.

Jaberi, F. A. and James, S. (1998). A dynamic similarity model for large eddy simulation of turbulent combustion. *Phys. Fluids* **10**, 1775–1777.

Jaberi, F. A., Miller, R. S., Madnia, C. K., and Givi, P. (1996). Non-Gaussian scalar statistics in homogeneous turbulence. *J. Fluid Mech.* **313**, 241–282.

Jaberi, F. A., Colucci, P. J., James, S., Givi, P., and Pope, S. B. (1999). Filtered mass density function for large eddy simulation of turbulent reacting flows. *J. Fluid Mech.* **401**, 85–121.

Jaberi, F. A. (1999). Large eddy simulation of turbulent premixed flames via filtered mass density function. AIAA Paper 99-0199.

James, S. and Jaberi, F. A. (2000). Large scale simulations of two-dimensional non-premixed methane jet flames. *Combust. Flame* **123**, 465–487.

Jiménez, J., Liñán, A., Rogers, M. M., and Higuera, F. J. (1997). *A Priori* testing of subgrid models for chemically reacting non-premixed turbulent flows. *J. Fluid Mech.* **349**, 149–171.

Jiménez, J., Ducros, F., Cuenot, B., and Bédat, B. (2001). Subgrid scale variance and dissipation of a scalar field in large eddy simulations. *Phys. Fluids* **13**, 1748–1754.

Johnson, N. L. and Kotz, S. (1972). *Distributions in Statistics: Continious Multivariate Distributions.* John Wiley and Sons, New York, NY.

Kempf, A., Forkel, H., Chen, J. Y., Sadiki, A., and Janicka, J. (2000). Large-eddy simulation of a counterflow configuration with and without combustion. *Proceedings of the Combustion Institute* **28**, 35–40.

Kerstein, A. R. (1988). A linear eddy model of turbulent scalar transport and mixing. *Combust. Sci. and Tech.* **60**, 391–421.

Kim, W.-W., Menon, S., and Mongia, H. C. (1999). Large-eddy simulation of a gas turbine combustor flow. *Combust. Sci. and Tech.* **143**, 25–62.

Kloeden, P. E. and Platen, E. (1995). *Numerical Solution of Stochastic Differential Equations*, volume 23 of *Applications of Mathematics, Stochastic Modelling and Applied Probability.* Springer-Verlag, New York, NY.

Ladeinde, F., Cai, X., Sekar, B., and Kiel, B. (2001). Application of combined LES and flamelet modeling to methane, propane, and jet-A combustion. AIAA Paper 2001-0634.

Leemis, L. M. (1986). Relations among common univariate distributions. *American Statistician* **40**, 143–146.

Lesieur, M. and Metais, O. (1996). New trends in large eddy simulations of turbulence. *Ann. Rev. Fluid Mech.* **28**, 45–82.

Libby, P. A. and Williams, F. A., editors. (1980). *Turbulent Reacting Flows*, volume 44 of *Topics in Applied Physics.* Springer-Verlag, Heidelberg.

Libby, P. A. and Williams, F. A., editors. (1994). *Turbulent Reacting Flows.* Academic Press, London, England.

Lundgren, T. S. (1967). Distribution functions in the statistical theory of turbulence. *Phys. Fluids* **10**, 969–975.

Luo, K. H. (2001). DNS and LES of turbulence-combustion interactions. In Geurts, B. J., editor, *Modern Simulation Strategies for Turbulent Flow*, chapter 14, pages 263–293. R. T. Edwards, Inc., Philadelphia, PA.

Madnia, C. K. and Givi, P. (1993). Direct numerical simulation and large eddy simulation of reacting homogeneous turbulence. In Galperin and Orszag (1993), chapter 15, pages 315–346.

Mathey, F. and Chollet, J. P. (1997). Large eddy simulation of turbulent reactive flows. In *Proceedings of the Eleventh Symposium on Turbulent Shear Flows*, pages 16.19–16.24,

Grenoble, France.

McGrattan, K. B., Baum, H. R., and Rehm, R. G. (1998). Large eddy simulation of smoke movement. *Fire Safety Journal* **30**, 161–178.

McMurtry, P. A., Menon, S., and Kerstein, A. R. (1992). A linear eddy sub-grid model for turbulent reacting flows: Application to hydrogen-air combustion. In *Proceedings of 24th Symp. (Int.) on Combustion*, pages 271–278. The Combustion Institute, Pittsburgh, PA.

Menon, S. and Calhoon, W. H. (1996). Subgrid mixing and molecular transport modeling in a reacting shear layer. In *Proceedings of 26th Symp. (Int.) on Combustion*, pages 59–66. The Combustion Institute, Pittsburgh, PA.

Menon, S. (2000). Subgrid combustion modelling for large-eddy simulations. *Int. J. Engine Research* **1**, 209–227.

Moin, P., Squires, W., Cabot, W. H., and Lee, S. (1991). A dynamic subgrid-scale model for compressible turbulence and scalar transport. *Phys. Fluids A* **3**, 2746–2757.

O'Brien, E. E. (1980). The probability density function (PDF) approach to reacting turbulent flows. In Libby and Williams (1980), chapter 5, pages 185–218.

Peters, N. (2000). *Turbulent Combustion*. Cambridge University Press, Cambridge, UK.

Pierce, C. D. and Moin, P. (1998). A dynamic model for subgrid-scale variance and dissipation rate of a conserved scalar. *Phys. Fluids* **10**, 3041–3044.

Pitsch, H. and Steiner, H. (2000). Large eddy simulation of a turbulent piloted methane/air diffusion flame (Sandia flame D). *Phys. Fluids* **12**, 2541–2554.

Poinsot, T. and Veynante, D. (2001). *Theoretical and Numerical Combustion*. R. T. Edwards, Inc., Philadelphia, PA.

Pope, S. B. (1985). PDF methods for turbulent reactive flows. *Prog. Energy Combust. Sci.* **11**, 119–192.

Pope, S. B. (1990). Computations of turbulent combustion: Progress and challenges. In *Proceedings of 23rd Symp. (Int.) on Combustion*, pages 591–612. The Combustion Institute, Pittsburgh, PA.

Pope, S. B. (1994). Lagrangian PDF methods for turbulent flows. *Ann. Rev. Fluid Mech.* **26**, 23–63.

Pope, S. B. (2000). *Turbulent Flows*. Cambridge University Press, Cambridge, UK.

Réveillon, J. and Vervisch, L. (1996). Response of the dynamic LES model to heat release. *Phys. Fluids* **8**, 2248–2250.

Réveillon, J. and Vervisch, L. (1998). Subgrid-scale turbulent micromixing: Dynamic approach. *AIAA J.* **36**, 336–341.

Risken, H. (1989). *The Fokker-Planck Equation, Methods of Solution and Applications*. Springer-Verlag, New York, NY.

Sagaut, P. (2001). *Large Eddy Simulation for Incompressible Flows*. Springer, New York.

Schumann, U. (1989). Large eddy simulation of turbulent diffusion with chemical reactions in the convective boundary layer. *Atmospheric Environment* **23**, 1713–1726.

Smith, T. M. and Menon, S. (1996). The structure of premixed flames in a spatially evolving turbulent flow. *Combust. Sci. and Tech.* **119**, 77–106.

Soong, T. T. (1973). *Random Differential Equations in Science and Engineering*. Academic Press, New York, NY.

Steiner, H. and Bushe, W. K. (2001). Large eddy simulation of a turbulent reacting jet with conditional source-term estimation. *Phys. Fluids* **13**, 754–759.

Sykes, R. I., Henn, D. S., Parker, S. F., and Lewellen, W. S. (1992). Large-eddy simulation of a turbulent reacting plume. *Atmospheric Environment* **26**, 1713–1726.

Thibaut, D. and Candel, S. (1998). Numerical study of unsteady turbulent premixed combustion: Application to flashback simulation. *Combustion and Flame* **113**, 53–65.

Tong, C. (2001). Measurements of conserved scalar filtered density function in a turbulent jet. *Phys. Fluids* **13**, 2923–2937.

Zhou, X. Y. and Pereira, J. C. F. (2000). Large eddy simulation (2D) of a reacting plan mixing layer using filtered density function. *Flow, Turbulence and Combustion* **64**, 279–300.